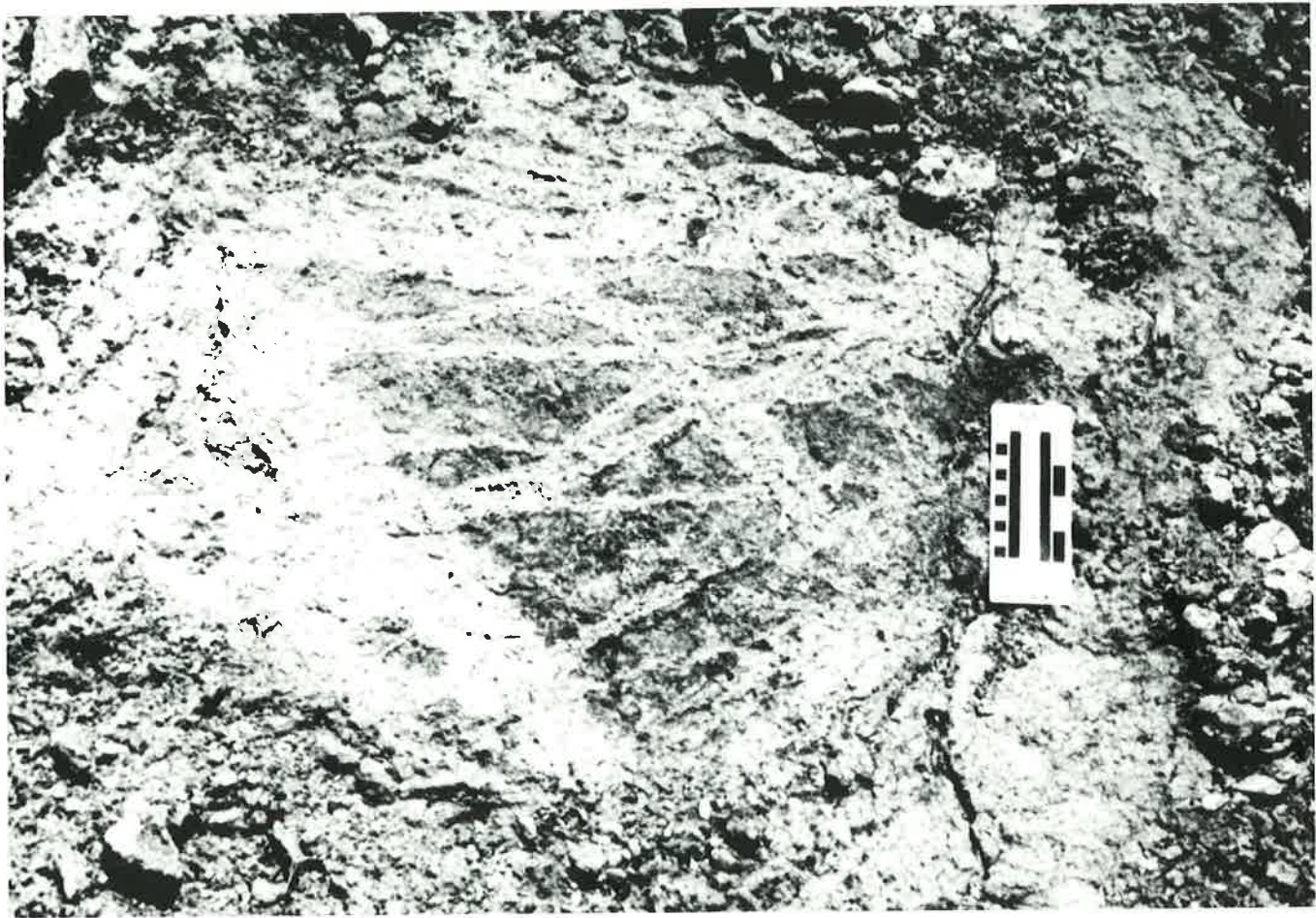# GEOLOGY AND GEOCHEMISTRY OF ALTERED SERPENTINITES IN THE BURKS MOUNTAIN COMPLEX, COLUMBIA COUNTY, GEORGIA

Mark D. Cocker

GEORGIA DEPARTMENT OF NATURAL RESOURCES
ENVIRONMENTAL PROTECTION DIVISION
GEORGIA GEOLOGIC SURVEY

BULLETIN 124

Cover Photo: Fractured clast of serpentinite, altered to talc along fractures and rim of clast. Small divisions on scale are centimeters. Outcrop along Old Petersburg Road.

GEOLOGY AND GEOCHEMISTRY OF ALTERED SERPENTINITES IN THE BURKS MOUNTAIN COMPLEX, COLUMBIA COUNTY, GEORGIA

Mark D. Cocker

Bulletin 124

TABLE OF CONTENTS

LIST OF ILLUSTRATIONS

LIST OF TABLES

GEOLOGY AND GEOCHEMISTRY OF ALTERED SERPENTINITES IN THE BURKS MOUNTAIN COMPLEX, COLUMBIA COUNTY, GEORGIA

by

Mark D. Cocker

ABSTRACT

Ultramafite bodies, hosting potentially economic talc, nickel, chromium, vanadium, titanium, and rare earth element mineralization, occur within metamorphic rocks of the Kiokee belt in Columbia County, Georgia. The ultramafites are fragments of the elongate Burks Mountain igneous complex. This complex is conformably enclosed within gently to moderately dipping, middle to upper amphibolite facies gneisses and schists.

The Burks Mountain complex near Pollards Corner, Georgia consists principally of serpentinites derived from differentiated, layered cumulate metaharzburgites. The serpentinite is vertically zoned from olivine-normative rich at the base to enstatite-normative rich at the top. Rhythmic, fine-scale silicate banding is developed near the upper part of the exposed complex. Associated with the silicate banding are layers of massive magnetite and ilmeno-hematite, enriched in V, P, TiO_2 and rare earth elements. Textures suggest separation of an immiscible Fe-rich melt from the silicate melt, perhaps related to an injection of new magma, and slow cooling at deep crustal levels.

Remnants of an olivine +/-enstatite +/- tremolite +/- anthophyllite + chlorite assemblage, preserved in the metaharzburgite is indicative of upper amphibolite facies metamorphism and peak metamorphic conditions near 700°C and 3-5 kb. Later, retrograde greenschist facies metamorphism of the metaharzburgite to a lizardite serpentinite indicates that conditions during serpentinization were probably below 250°C and 500 bars pressure with less than 300 bars fluid pressure.

Subsequent fracturing of the serpentinites opened channelways for hydrous, siliceous, and CO_2-bearing fluids to form talc selvages around serpentinite clasts and along fractures in the serpentinite. In one of the serpentinites, which was studied in detail, extensive fracturing occurred along its upper contact. The resulting multilithic breccia consists mainly of talc clasts with minor amounts of Kiokee gneiss and kaolinized granite clasts in a matrix of chlorite. Chlorite formed at the expense of lizardite and talc during the influx of alumina-bearing solutions. Also at that time, chloritization of the adjacent country rock led to development of secondary albite and biotite, and remobilized CaO and TiO_2 to form titanite and ilmenite. Widespread quartz veining and silicification affected large portions of some of the other serpentinite bodies.

It is suggested that the mafic-ultramafic Burks Mountain complex was intruded at deep crustal levels into the Kiokee belt rocks that may represent a continental margin or a transitional continental-island arc setting. During the Alleghanian orogeny, this complex was dismembered and emplaced into its present structural position. The metamorphism, fracturing and alteration of the ultramafites is probably related to the Alleghanian orogeny and events during or immediately following its waning stages. Peak metamorphism and deformation in the Kiokee belt is dated at 315 to 268 Ma (Dallmeyer and others, 1986).

INTRODUCTION

PURPOSE

The geology and geochemistry of talc-bearing ultramafites and of the enclosing country rocks located approximately 3.5 km ESE of Pollards Corner in Columbia County, Georgia is described and interpreted in this report. A description of the talc mineralization, its origin, and its economic significance is documented in an accompanying publication (Cocker, in press (b)). The economic potential for nickel, chromium, titanium, vanadium and rare earth elements are also discussed in the accompanying publication.

LOCATION

The area covered by the current investigation is located 3.5 km ESE of Pollards Corner in Columbia

1

County, Georgia (Fig. 1). The northwestern corner of the project area is approximately 82°15'W and 33°37'30"N in the northwestern corner of the Evans 7.5' quadrangle. Reconnaissance studies to the west overlapped into the northeast corner of the Appling 7.5' quadrangle.

Access to the area is via Georgia Highway #304/ U.S. Highway #221 or Georgia Highway #104 to Pollards Corner and via the paved Old Petersburg Road or the graded dirt Old Middleton Road to the village of Rosemont at the western end of Burks Mountain.

TOPOGRAPHY

Elevation of the project area generally ranges from 250 to 350 feet (76 to 108 m). The surface is gently rolling to flat and is cut by a few steep-sided gullies, 3 to 7 feet (1 to 2 m) deep. Along the northern edge of the project area, the western end of Burks Mountain rises 180 feet (55 m) above the surrounding area to a maximum elevation of 535 feet (163 m). This east-west trending ridge consists of a series of elongate hills, which gradually decrease in altitude to the east, and terminates at the Savannah River. Pervasively silicified serpentinites underlying Burks Mountain are significantly more resistant to weathering than surrounding lithologies.

Earlier studies (Hopkins, 1914; LeGrand and Furcron, 1956; McLemore, 1965; Worthington, 1964; and Hurst and others, 1966) refer to the western end of Burks Mountain as Burte (or Burt) Mountain and to the eastern end as Dixie Mountain. Recent studies (Secor, 1987; Sacks and others, 1987; Sacks and others, 1989; Vincent, and others, 1990) refer to the ridge as Burks Mountain because it is named as such on the Evans 7.5' topographic quadrangle. In this report, this ridge will be referred to as Burks Mountain, with references to Dixie and Burte Mountain as used in earlier studies.

EXPOSURE

Rocks in the project area are exposed along: three major roadcuts on Old Petersburg Road; steep-sided gullies and creeks; and on the upper slopes of Burks Mountain. In addition, outcrops of resistant rocks are scattered in fields and forested areas. The high annual rainfall averaging 48.5 inches (LeGrand and Furcron, 1956) and warm temperatures are typical of subtropical conditions leading to extensive weathering of bedrock.

VEGETATION

Forests of pine and mixed hardwood, the South-

ern Pinelands, cover approximately 50 percent of the project area with the remainder of this area consisting of open pasture. The vegetation patterns reflect, to a certain extent, the character of the underlying lithologies.

Serpentinite, talc and silicified serpentinite tend to form poor soils, which are generally rocky and well drained. Such soils are drier than the more deeply weathered soil and saprolite developed over the surrounding rocks. Soils developed from serpentinites are generally enriched in Mg and Fe, but very low in vital nutrients such as K, Na, P, Al and various trace elements associated with less basic rocks. This unusual soil composition is commonly reflected in unusual vegetation communities. Within this study area, oaks, sweetgum and hickory are prevalent in areas with outcrop or float from the serpentinite.

Deeply weathered gneisses, granites and schists or coastal plain sandstones tend to form the better soils. Pastures or pines are more prevalent in these areas of more felsic substrate.

PREVIOUS STUDIES

The earliest geologic studies of the Pollards Corner area were generally regional in scope (Hopkins, 1914; Crickmay, 1952; LeGrand and Furcron, 1956). These studies first noted the occurrence of mafic and ultramafic rocks in this part of the Piedmont.

During the 1960's a number of studies were concerned with the economic evaluation of the Pollard's Corner area (Worthington, 1964; McLemore, 1965; Hurst and others, 1966). In the early 1960's, the J.M. Huber Corporation tested the nickel and chrome potential in four core holes in the vicinity of Dixie Mountain and in one core hole approximately 1/2 mile southeast of Pollard's Corner.

More recent studies include a brief description of the "Burks Mountain suite" of ultramafic rocks (Vincent and others, 1990) and regional studies of stratigraphy, petrology, structure and tectonic evolution of the southeasternmost Piedmont in Georgia and South Carolina (Maher, 1978; Secor and others, 1986a and 1986b; Sacks and others, 1987; Sacks and others, 1989). A regional synthesis of the stratigraphy, structure, and tectonostratigraphy of the southernmost part of the Appalachian orogen has also been recently compiled (Higgins and others, 1988).

"BURKS MOUNTAIN COMPLEX"

The mafic/ultramafic bodies in the vicinity of Pollards Corner remained unnamed (Hopkins, 1914; LeGrand and Furcron, 1956; McLemore, 1965) until
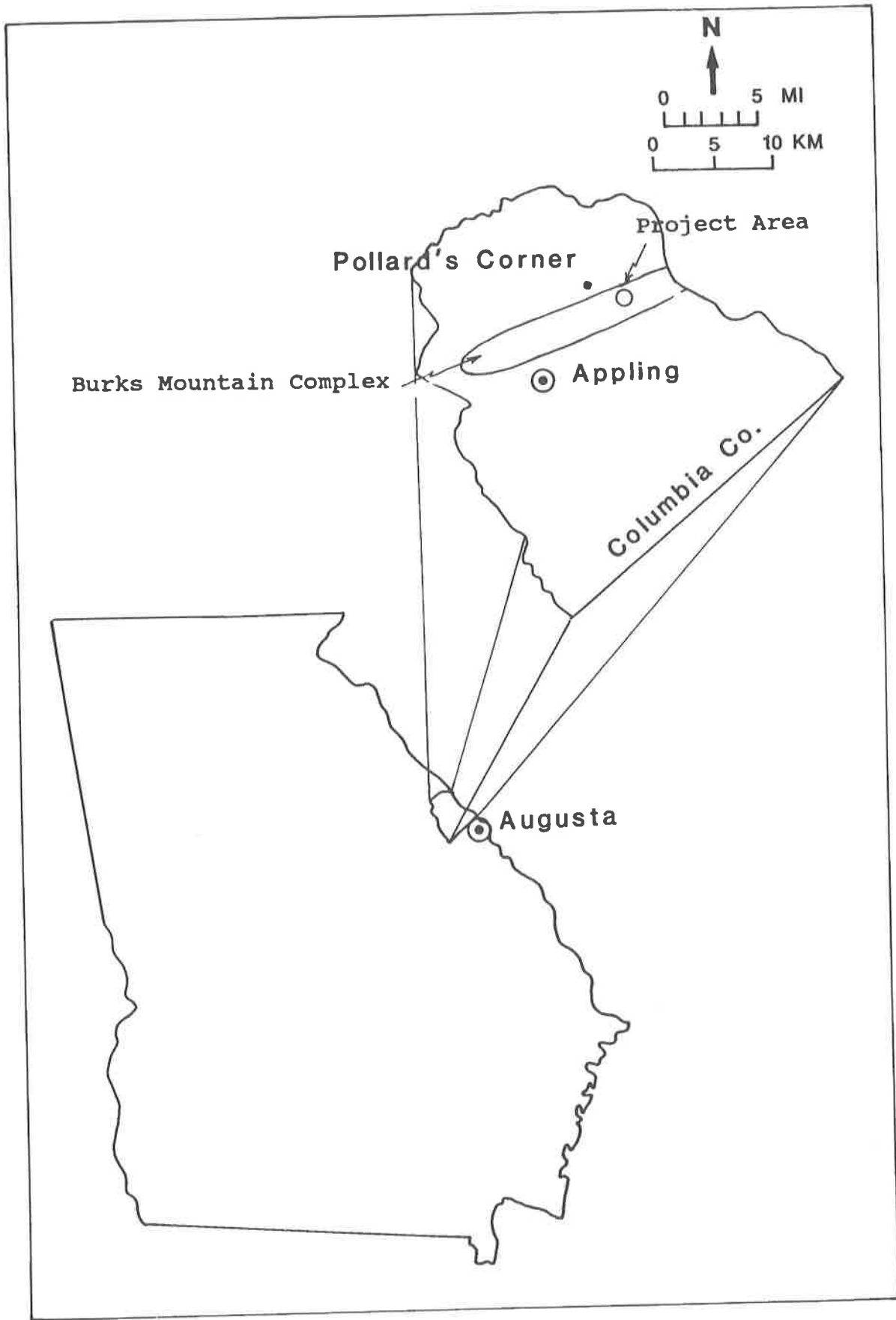
Figure 1. Location map of the Burks Mountain complex and project area.

they were defined as the Burks Mountain complex by Sacks and others (1987) and the Burks Mountain suite by Vincent and others (1990). In order to establish some consistency and simplicity in terminology, this report will refer to the mafic/ultramafic bodies as the Burks Mountain complex. The Burks Mountain suite of lithologies as described by Vincent and others (1990) are actually alteration phases of the same protolith (Cocker, 1989a).

FIELD AND LABORATORY TECHNIQUES

The present investigation focussed on a small area which was mapped in detail on a scale of 1"=200 feet (1:2400) using an enlarged topographic base. Roadcuts containing exposures of the serpentinite or important metamorphic, intrusive and structural relations were mapped in greater detail at a scale of 1"=50 feet (1:600). As an aid in 1:2400 scale mapping and to establish stations for a detailed ground magnetic survey, a grid was established using tape and Brunton compass. A baseline (the 0N line in Fig. 10) was established along a N73°E line with stations every 200 feet along that line. From those baseline stations, secondary lines were run perpendicular to the baseline with additional stations established every 100 feet along these secondary lines. An initial ground magnetic survey orientation line (the 00E line in Fig. 10) was run along the Old Petersburg Road with stations every 50 feet. The grid was oriented parallel to the Old Petersburg Road so as to avoid barbed wire fences and power lines and to be perpendicular to the anticipated strike of the serpentinites and local structure. These procedures were designed to maximize anticipated geologic effects and to minimize cultural effects on the ground magnetic survey.

Ten drill holes were cored in 1987 and 1988 to obtain subsurface lithologic, structural, alteration, and veining data. Drill core was logged in detail (1"=10 feet) and then sampled for geochemical analysis, thin section and x-ray diffraction studies.

Rock-chip geochemical samples were collected during the field mapping phase from selected outcrops and float. Float was sampled when outcrops were lacking and after it was determined by field relations that the float was essentially in place. Rock-chip samples were collected by taking 20 to 30 1/2 inch chips from an area of approximately 5 to 10 feet in diameter to minimize single sample variations. Channel samples were taken to obtain an average composition of certain lithologies. Occasionally, the sampling area was restricted to a particular portion of an outcrop, or single samples were taken because of sample availability.

Whole-rock analyses of core and surface samples included analysis for SiO_2, Al_2O_3, Fe_2O_3, FeO, MgO, CaO, Na_2O, K_2O, LOI, TiO_2, P_2O_5, and MnO. Selected samples were analyzed for Au, Ag, Cu, Pb, Zn, As, Hg, Pt, Pd, Co, Ni, Cr, Sr, V and Ba. Induced coupled argon plasma (ICAP) techniques were used for SiO_2, Al_2O_3, MgO, CaO, Na_2O, K_2O, TiO_2, P_2O_5, and MnO, Sr, V and Ba. Dichromatic titration was used for Fe^{+2} and Fe^{+3}. Loss-on-ignition (LOI) was determined by gravimetric analysis. Ni, Cr, Co, Rb, Cu, Pb, Zn, Ag, Au and As were determined by atomic absorption (AA). Fire assay and ICP were used for Pt and Pd analysis. Samples were sent to Skyline Labs., Inc.(Wheat Ridge, CO) for standard whole-rock analyses and for trace-element analyses. In addition, selected samples were analyzed for rare earth elements (REE) by instrumental neutron activation analysis (INAA) and by x-ray fluoresence (XRF) by Bondar-Clegg, Inc. (Lakewood, CO).

X-ray diffraction analysis (XRD) was used to determine the mineralogy of the serpentinite, because optical and chemical methods are not suitable for distinguishing the various serpentine minerals: antigorite, lizardite and chrysotile. Because the serpentine minerals have different structures, diffraction methods can distinguish the different types of serpentine. The 330 reflection at 1.56-1.57 Angstroms, which is unique to antigorite (Bailey, 1969; Wicks and O'Hanley, 1988), distinguishes antigorite from lizardite. The chrysotile structure is composed of two layers and is distinguished on the basis of 20l reflections. The one-layer nature of lizardite 1T (in contrast to the two-layer structure of chrysotile) is clearly indicated by the 11l series of reflections (Wicks and O'Hanley, 1988). Other minerals: talc, chlorite, calcite, dolomite and magnesite, were identified by XRD.

Petrographic studies consisted of optical mineral identification and textural relations descriptions using standard transmitted- and reflected-light microscopy. Twenty-three standard thin-sections and 6 polished thin-sections of fresh, unweathered drill core samples collected during this study plus 12 standard thin-sections of surface samples collected by Vincent and others (1990) were examined. These samples represent 11 separate serpentinite bodies which together extend over 12 km along strike. Modes of mineral abundances were determined from point counts of 300 to 350 grains per thin-section. For counts of 300-350 points, a two standard deviation error ranges from <1 to 5 percent with a 95 percent confidence level (Van der Plas and Tobi, 1965). The lower error level (<1) is for low percentage minerals, and the higher error level is for mineral percentages in the 25-75 percent range.

REGIONAL GEOLOGY

A series of serpentinite bodies occurring southeast of Pollards Corner in Columbia County, Georgia form part of an elongate group of mafic/ultramafic rocks defined as the Burks Mountain complex (Sacks and others, 1989). The Burks Mountain complex (Fig. 2) extends from Columbia County in Georgia into South Carolina for a total strike length of over 20 miles (33 km). A second belt of small pods and lenses of ultramafic rock and amphibolite, located 2.5-3 miles (4-5 km) north of and roughly parallel to the Burks Mountain complex, may be part of the Burks Mountain complex which was folded over on the northwest limb of the Kiokee antiform (Sacks and others, 1989). The Burks Mountain complex mainly consists of serpentinite, metagabbro, talc and several types of amphibolite interpreted as a suite of metamorphosed and locally altered harzburgite, cumulate wherlite or olivine clinopyroxenite, cumulate gabbro and anorthositic gabbro, rodingite and possibly mafic volcanic rocks (Sacks and others, 1989).

The Burks Mountain complex is roughly parallel to the regional strike (Fig. 2) and concordant with regional foliation of gently to moderately dipping, middle to upper amphibolite grade, migmatitic metamorphic rocks of the Kiokee belt (part of the Macon melange of Higgins and others, 1988) in the southeastern part of the Piedmont Province of Georgia. The Kiokee belt is a northeast-trending, lithostratigraphic belt extending from eastern Georgia into South Carolina. It consists of a sequence of migmatitic micaceous quartzo-feldspathic gneiss, locally interlayered with amphibole-biotite schist, and biotite-muscovite schist. Migmatitic gneiss and sillimanite schist indicate that middle to upper amphibolite facies metamorphism was attained in the Kiokee belt (Secor and others, 1986a; Secor, 1987; Maher, 1978 and 1987; Snoke and Frost, 1988; Sacks and others, 1989). The Kiokee belt is separated on the north (Fig. 2) from lower-grade, greenschist facies, metamorphic rocks of the Carolina slate belt by a 4-5 km wide zone of cataclastic rocks referred to as the Modoc fault zone (Secor and others, 1986a; Sacks and Dennis, 1987). On the south, the Kiokee belt is separated from similar, lower-grade, greenschist facies, metamorphic rocks of the Belair belt by the Augusta fault zone (O'Connor and Prowell, 1976; Maher, 1978 and 1987).

Metamorphism and emplacement of the Kiokee belt into its present position occurred during the Alleghanian orogeny, the last recognized major episode in the development of the Appalachian orogen (Secor and others, 1986a and 1986b; Dallmeyer and others, 1986; and Secor, 1987). In Georgia and South Carolina, the Alleghanian orogen is divided into three stages of deformation lasting from 315-268 Ma (Secor and others, 1986a and 1986b; Dallmeyer and others, 1986; and Secor, 1987). The Lake Murray deformation, accompanied by extensive felsic magmatic activity, produced amphibolite grade regional metamorphism in the Kiokee belt. Intense shearing along the Modoc fault zone juxtaposed migmatites of the Kiokee belt against lower-grade greenschist facies rocks of the Carolina slate belt. Regional-scale folding during the Clark Hill deformation produced the Kiokee antiform (Secor and others, 1986a, Maher, 1978). The northwest limb of the Kiokee antiform was steeply folded and then cut by the Modoc fault zone. Shearing along the Irmo shear zone, which lies within the Modoc fault zone in Georgia and South Carolina, occurred during the Irmo deformation.

Current evidence suggests that the Appalachian orogen is a tectonic collage of numerous lithotectonic blocks added to the North American craton by collision or by transform faulting throughout the Paleozoic Era (Cook and others, 1979; Williams and Hatcher, 1982; Higgins and others, 1988). The Kiokee belt and the adjacent Carolina slate belt to the north and Belair belt to the south may have accumulated in association with one or more subduction-related, Cambrian-age volcanic arcs (530-580 Ma) developed adjacent to the African continent (Whitney and others, 1978; Feiss, 1982; Rogers, 1982; Secor and others, 1983 and 1986b; Shelley and others, 1988; Higgins and others, 1988). These lithotectonic blocks were accreted to North America by the Late Ordovician (Kish and others, 1979; Vick and others, 1987; Sacks and others, 1989), and metamorphosed and emplaced into their present position during the Alleghanian orogeny (Secor and others, 1986a and 1986b; Dallmeyer and others, 1986; and Secor, 1987).

During northwestward translation of the crystalline thrust sheet above an Appalachian decollement over relatively unmetamorphosed strata (Cook and others, 1979), a ramp antiform developed with the Kiokee belt in its core (Secor, 1987). Fluids released
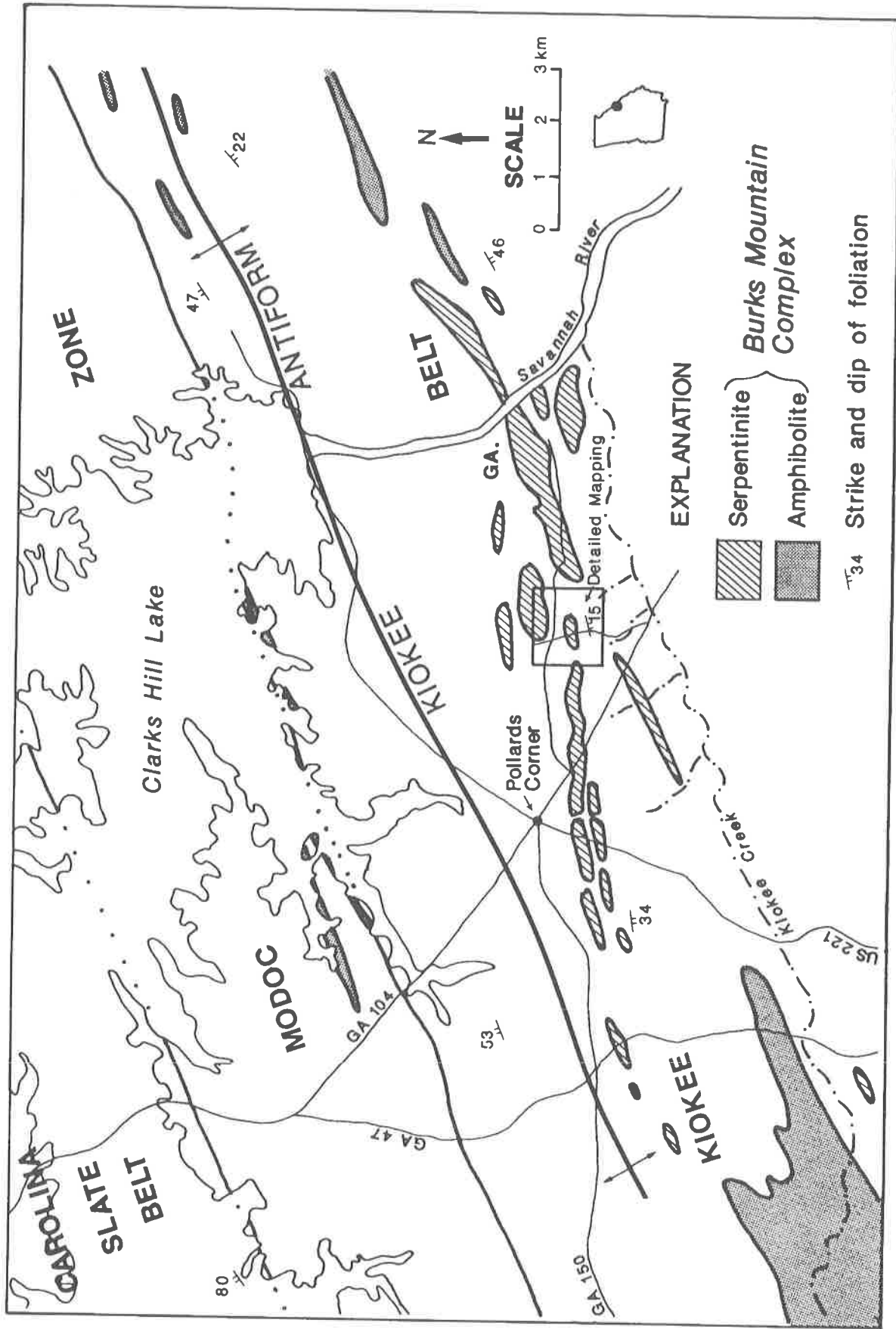
Figure 2. Generalized geologic map of the Polards Corner area. (Modified from Georgia Geologic Survey, 1976; Sacks and others, 1989).

6

from the overriden rocks probably helped lubricate the thrust faulting and may have produced retrograde metamorphism in the overthrust sheet (Armstrong and Dick, 1974; Tull, 1978; Frazier and Schwimmer, 1987).

Subsequent to the Alleghanian penetrative deformation and the accompanying regional metamorphism, brittle faulting developed in the eastern Piedmont. One fault set is composed of northeast-trending, steeply dipping, generally silicified faults. Geologic relations bracket the age of these faults between 268 Ma and 195 Ma (Secor and others, 1986a) suggesting that they may be related to Mesozoic rifting associated with the opening of the Atlantic Ocean. Two other sets, consisting of small vertical faults, commonly cross-cut the cataclastic textures of the Modoc fault zone and strike at about $N40^{\circ}W$ and $N20^{\circ}E$ (Howell and Pirkle, 1976). The latter fault set may be similar in age to that of the Cenozoic Belair fault located along the southeastern edge of the Kiokee belt near Augusta (O'Connor and Prowell, 1976; Howell and Pirkle, 1976).

LOCAL GEOLOGY

ROCK TYPES

General

In the Savannah River area, rocks of the Kiokee belt consist of a migmatitic, two-mica gneiss, with subordinate layers of amphibolite, schist and muscovite gneiss. The gneiss is fine- to medium-grained and contains biotite with lesser amounts of muscovite. Included within the two-mica gneiss are: homogeneous, muscovite gneiss; migmatitic, sillimanite-bearing, two-mica schist; metaquartzite; biotite gneiss; and leucocratic granite. These rocks are intruded by numerous concordant and discordant pegmatite and aplite dikes (Maher, 1978). A pronounced layering and foliation formed during the Lake Murray deformation event are characterized by: compositional banding, layers of different grain size, and preferred orientation of inequant minerals (Maher, 1978).

Within the area of investigation, the Kiokee belt rocks consist mainly of an interlayered sequence of migmatitic, micaceous quartzo-feldspathic gneiss plus hornblende-biotite gneiss and schist with minor metaquartzite (mg in Fig. 3). Additional lithologies include granitic gneiss, biotite-quartz-feldspar gneiss, granite, metagabbro, metabasalt and serpentinite. Layering and foliation strike northeast and dip between $10-30^{\circ}SE$ (Fig. 3). Abundant, medium-grained, quartz-feldspar granite dikes (Pmg in Fig. 3) intrude the metamorphic rocks and are cut in turn by numerous, generally narrow, quartz-feldspar pegmatites.

Felsic Lithologies

Quartzo-feldspathic or granitic gneiss consists of 23-33 percent quartz, 19-30 percent microcline, 29-45 percent plagioclase (An_{15-25}), 2-8 percent biotite, 0-2 percent muscovite, 0-1.6 percent blue-green hornblende, trace to 1 percent titanite, trace opaques, and 0-1 percent apatite. Myrmekite is common and is composed of quartz and plagioclase. Coarse-grained (0.4-4.5 mm), strained quartz and feldspar are elongated (Fig. 4) parallel to a foliation defined by thin layers of biotite and considerably smaller (0.02-1 mm) quartz and feldspar grains. Elongation of the quartz and feldspar grains is commonly up to a 4:1 length to width ratio. Rounded and embayed biotite suggests dissolution and remobilization of components during metamorphism. Muscovite occurs as well-formed grains that appear to replace feldspar and as patchy, non-aligned, embayed remnants. Anhedral to euhedral titanite appears to be secondary as it commonly rims an opaque mineral tentatively identified as ilmenite.

Biotite-quartz-feldspar gneiss is composed of alternating biotite and quartz + feldspar-rich layers. Overall, thin section-scale composition is 25 percent biotite, 30 percent quartz, 23 percent plagioclase, 21 percent orthoclase, <1 percent apatite, <1 percent titanite, <1 percent zircon, and a trace amount of opaques. Although the banding has been folded, biotite crystals are not bent or otherwise stressed, and a small number of biotites are oriented across the banding. This indicates recrystallization of biotite and growth of post-kinematic biotite. Grain size averages between 0.2-1 mm. Quartz commonly displays a mylonitic texture with coarse-grained, strained quartz and plagioclase (An_{22-31}) occurring in layers separated by fine-grained quartz and feldspar. Anhedral and elongate secondary(?) titanite (<1 percent) commonly is concentrated with zircon in biotite-rich layers, and commonly rims opaque minerals (ilmenite?).

Granitic rocks are exposed as numerous small outcrops aligned as a northeast trending dike, and they occur in the large roadcut south of the multilithic breccia (Fig. 3). Granitic dikes were intercepted in the drill core (Fig. 5). Granitic clasts occur in the multilithic breccia in the Old Petersburg Road roadcut and in drill core. A thin-section of sample PC 2-88, from DDH 87-2, reveals no penetrative texture and only minor strain visible in the silicates. Biotite occurs in random orientation in this thin-section. These relationships suggest that these granitic rocks are mainly post-kinematic. This rock consists of 36 percent quartz, 34 percent
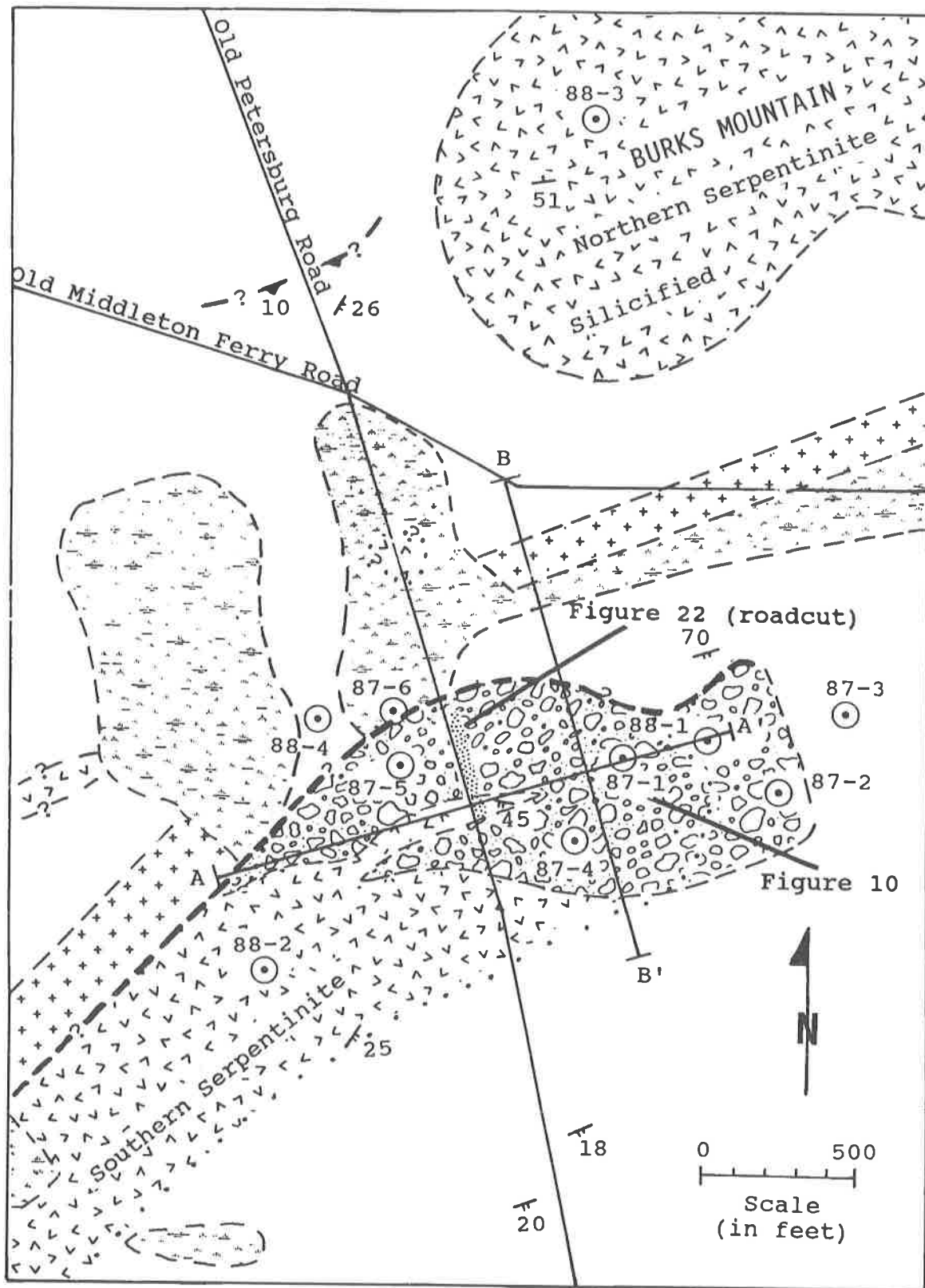
Figure 3. Geologic map of the talc prospect (Cocker, 1991b). Map shows the locations of drill holes and sections A-A′ and B-B′.

8

EXPLANATION

Cretaceous/Tertiary undifferentiated

Multilithic breccia

Serpentinite

Permo-Carboniferous granite

Migmatitic biotite amphibole gneiss

Contact (dashed where uncertain; dotted where concealed)

Fault (inferred from ground magnetic data and drill holes)

Low angle fault (thrust ?)

25 Strike and dip of foliation

10 Strike and dip of centimeter-scale igneous layering

87-1 Diamond drill hole

A—A Line of section

Roadcut
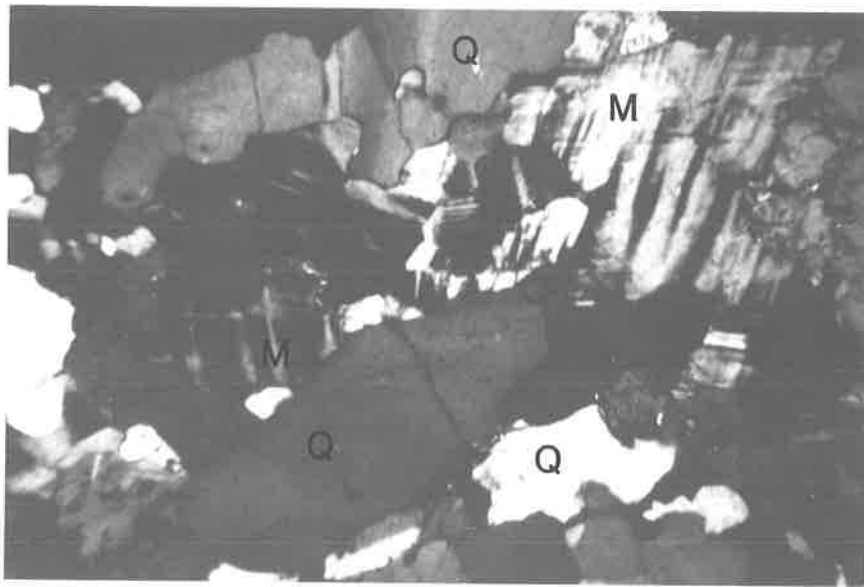
Figure 4. Photomicrograph of quartzo-feldspathic gneiss. Note the elongation of quartz (Q) and microcline (M). Sample is from DDH 87-1, 208 feet. Width of field of view is 2.65 mm.
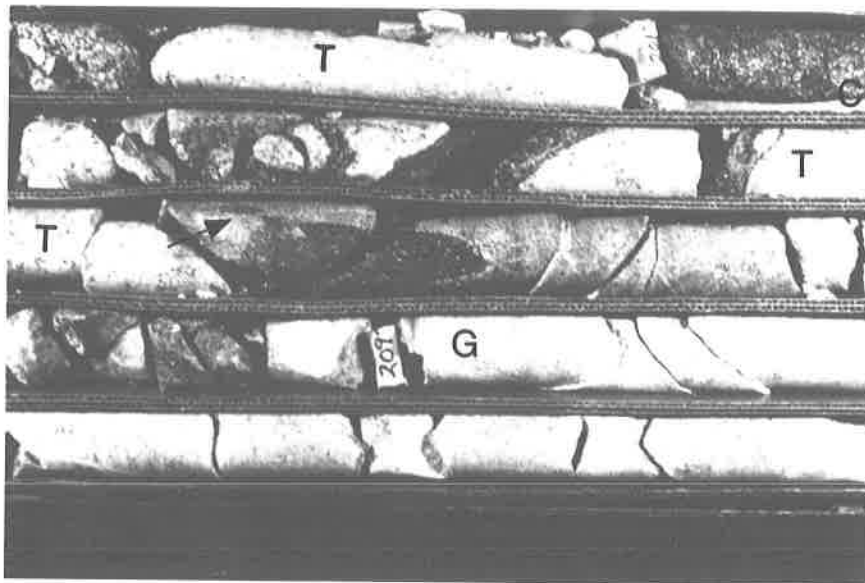
Figure 5. Granite in contact with talc and coarse-grained chlorite in drill core. Rocks include granite (G), talc (T), and chlorite (C). Contact is shown by arrow. DDH 88-2 from 200-212 feet. Top of core is in upper right and bottom is in lower left. Width of photo is approximately 2 feet.

microcline, 27 percent plagioclase, 3 percent biotite, <1 percent opaques, and a trace amount of zircon. Myrmekite, consisting of plagioclase and quartz, is abundant.

Mafic Lithologies

The mafic rocks of the Burks Mountain complex are dominantly amphibolite and epidote amphibolite with garnet amphibolite, garnet-epidote amphibolite, metagabbro and anorthositic gabbro also present (Sacks and others, 1989). Coarse-grained amphibolites with relict cumulate textures are interpreted as metagabbros. Two types of metagabbros in the Burks Mountain complex are distinguished on the basis of their mineralogy and geochemistry. Pyroxene metagabbros contain approximately equal amounts of plagioclase and hornblende, whereas the anorthositic metagabbros contain only minor interstitial hornblende and have higher CaO and Al_2O_3 contents (Sacks and others, 1989). Epidote-rich metagabbroic amphibolites, spatially associated with serpentinite, are interpreted to be rodingites because they are enriched in CaO (18-23 weight percent) and Sr (700-3500 ppm), relative to Al_2O_3 (12-18 weight percent) (Sacks and others, 1989). Rodingites are calc-silicate rocks formed from metasomatism of mafic to felsic rocks associated with serpentinized ultramafic rocks.

Amphibolites not associated with serpentinite in the Burks Mountain complex are relatively fine-grained and lack cumulate textures. They contain blue-green hornblende, plagioclase, and quartz with minor epidote, biotite, chlorite, garnet, titanite and opaques. Basaltic protoliths for these amphibolites are suggested by their chemistry: MgO + CaO <22 weight percent and TiO_2 = 0.8 to 2.0 weight percent (Sacks and others, 1989).

In the present study, two amphibolites were encountered: a metagabbro and a metabasalt. The metagabbro occurs as clasts in the multilithic breccia in DDH PC87-1 at a depth of approximately 43 feet. It consists of 50 percent blue-green hornblende, 18 percent plagioclase, 25 percent epidote, 5 percent opaque minerals (magnetite ?), 1 percent olivine, and trace amounts of titanite and apatite. Olivine is rare and occurs as remnants rimmed by hornblende. Epidote principally replaces plagioclase but also commonly replaces hornblende (Fig. 6). Titanite occasionally rims the magnetite(?). Average grain size of this amphibolite is 0.1-0.2 mm. This amphibolite is interpreted to be a metagabbro intermediate in composition (Fig. 7) to the rodingites and anorthositic gabbros noted by Sacks and others (1989). This amphibolite is similar in Al_2O_3 content (17.2 weight percent) but lower in CaO (14.5

weight percent) compared to the rodingite samples containing Al_2O_3 (12-18 weight percent) and CaO (18-23 weight percent) (Sacks and others, 1989).

The drill core intercepts (this study) into fresh Kiokee rocks suggest that the metabasalts are the most abundant amphibolites occurring the Kiokee belt rocks that host the Burks Mountain complex. They consist of 44-47 percent plagioclase, 33-43 percent hornblende, 6-8 percent biotite, 2-4 percent ilmenite(?) + magnetite(?), 0.3-1 percent apatite, 0-3 percent quartz, and trace amounts of titanite (Fig. 8). Plagioclase ranges from An_{24} to An_{36}. Average grain size of this amphibolite ranges from 0.4-2 mm. Hornblende occurs as small, euhedral grains up to large, anhedral masses. Quartz is anhedral and relatively fine-grained (about 0.2 mm). Opaques are anhedral to euhedral with no apparent concentration. The presence of secondary titanite as rims on some opaque minerals suggests these opaques may be ilmenite. Apatite is anhedral to euhedral. Preferred orientation of biotite ranges from none in sample PC 1-175 to strongly parallel layered concentrations defining foliation/banding as seen above the 96 foot mark in DDH 88-2 in Fig. 9.

Ultramafic Lithologies

Within the project area, two major serpentinite masses of the Burks Mountain complex are referred to as the northern and southern serpentinites (Fig. 3). The pervasively silicified northern serpentinite is relatively well-exposed as the western end of the Burks Mountain ridge. It is considerably more resistant to weathering than adjacent gneisses and granites. The southern serpentinite is not exposed but is overlain by a multilithic breccia, containing mainly ultramafic clasts. This breccia is exposed in a long roadcut on the Old Petersburg Road approximately 1400 feet south of the Old Middleton Ferry Road. Talc boulders derived by weathering of the multilithic breccia were used to define the areal extent of the multilithic breccia. Drill data and a ground magnetic survey (Fig. 10) define the subsurface aspect of the southern serpentinite which appears concordant or nearly concordant to the enclosing regional foliation. The magnetics indicate that the southern serpentinite strikes N 64°E.

Kiokee gneisses and amphibolites underlie the southern serpentinite in all drill holes and overlie this serpentinite in DDH PC 88-2 (Fig. 21 and 22). In the other drill holes, the serpentinite is overlain by the multilithic breccia. Most of the clasts in the multilithic breccia are ultramafites similar to the underlying serpentinite, suggesting that a large portion of this breccia was probably derived from the serpentinite. Drilled intercepts show the southern serpentinite to
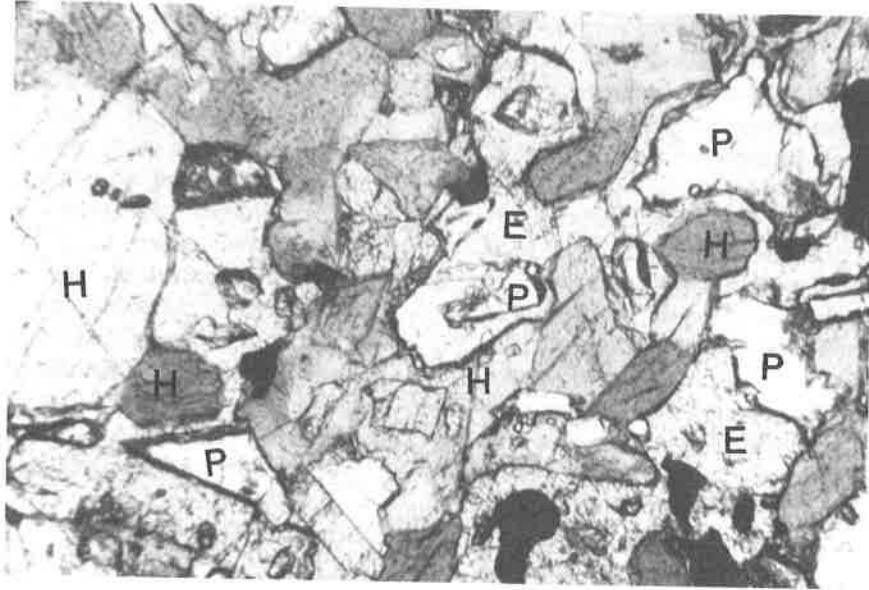
Figure 6. Photomicrograph of metagabbro (amphibolite). Minerals include hornblende (H), plagioclase (P) and epidote (E). The epidote has formed during a reaction between hornblende and plagioclase. Sample is from DDH 87-1, 43 feet. Width of field of view is 2.65 mm.
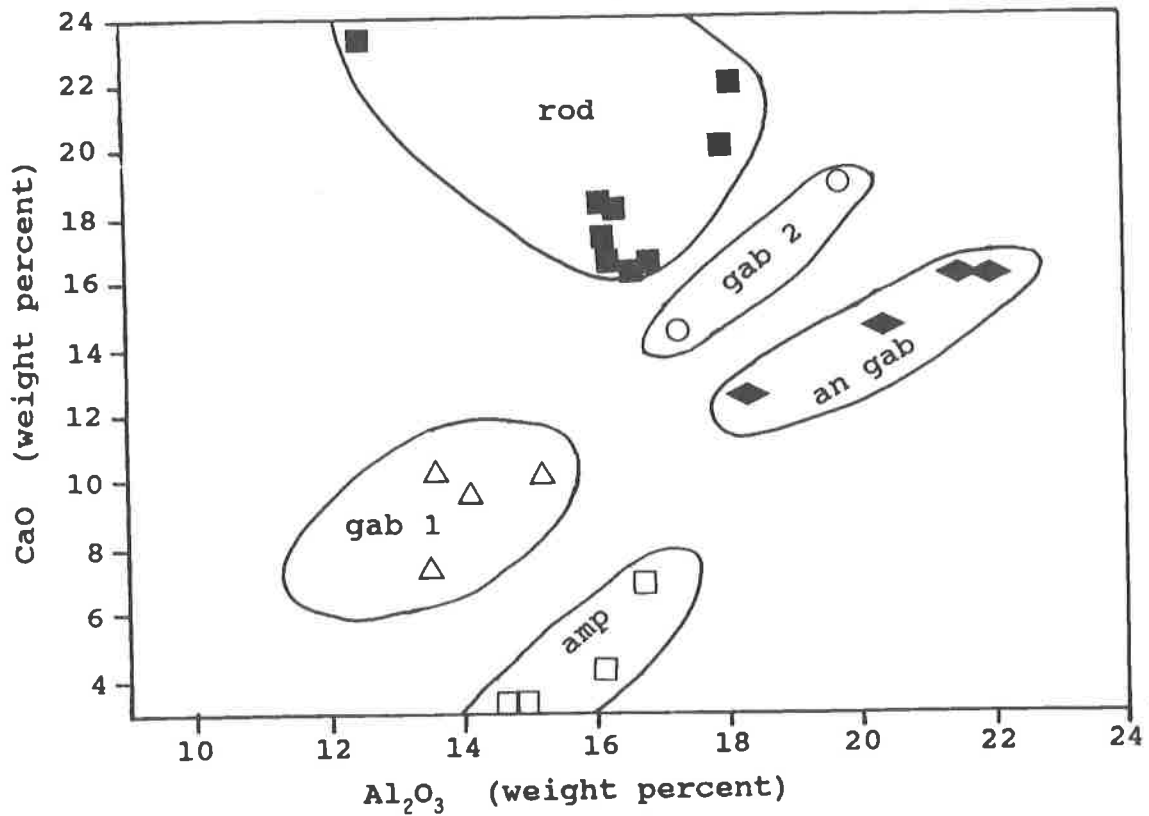
Explanation:

gab 1 = gabbro (1)
an gab = anorthositic gabbro (1)
rod = rodingite (1)
gab 2 = gabbro (2)
amp = amphibolite (2)

Sources:
(1). Sacks and others (1989)
(2). Cocker (this report)

Figure 7. CaO-Al$_2$O$_3$ diagram of mafic lithologies.
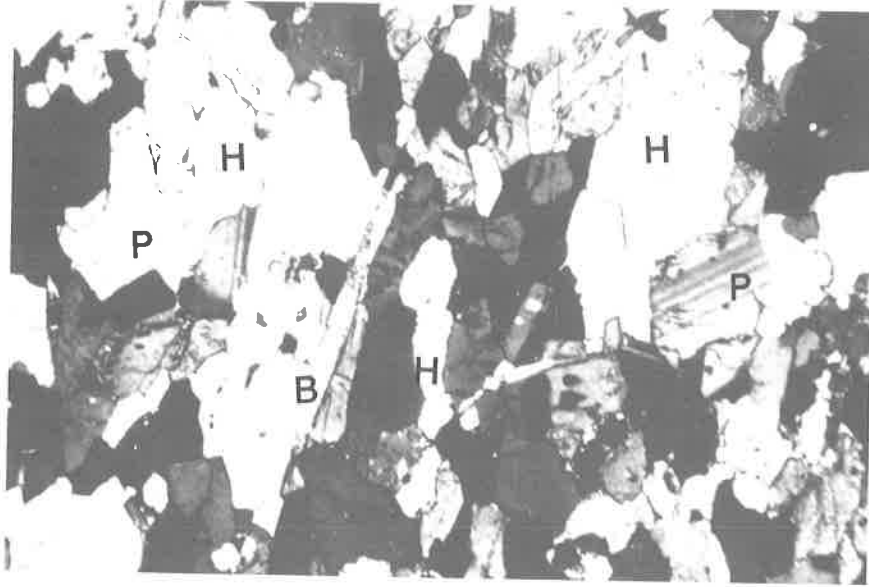
Figure 8. Photomicrograph of metabasalt (amphibolite). Minerals include hornblende (H), plagioclase (P), and biotite (B). Sample is from DDH 87-4, 225 feet. Width of field of view is 2.65 mm.

Figure 9. Banded amphibolite gneiss (metabasalt) in contact with talc and coarse-grained chlorite in drill core. Rocks include amphibolite (A), talc (T), and chlorite (C). DDH 88-2 from 94-112 feet. Contact is shown by arrow. Top of core is at upper right and bottom is at lower left. Width of photo is approximately 2 feet.
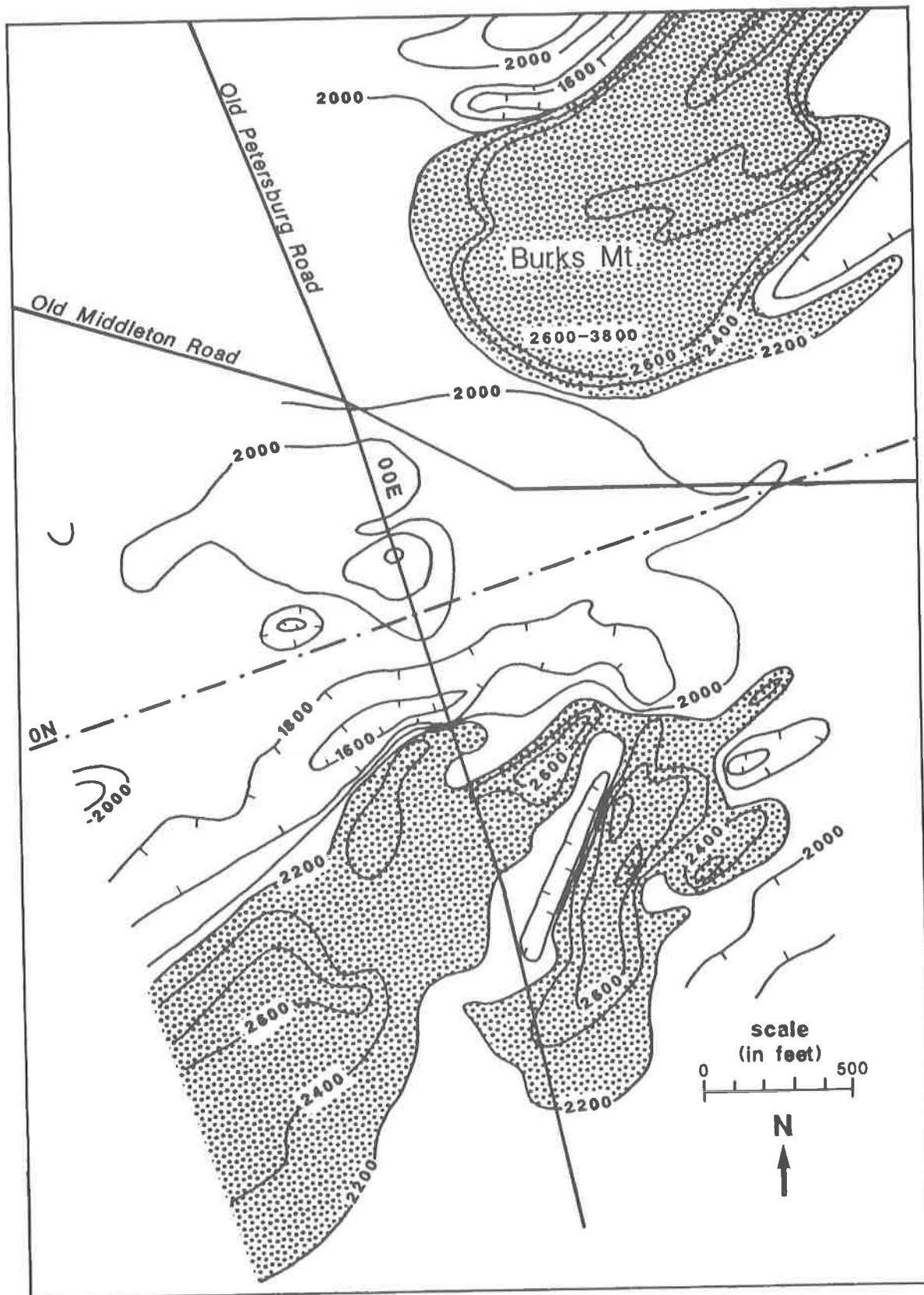
Figure 10. Ground magnetic map of the talc prospect. Contour interval is 200 gammas (Cocker, 1991 (b)). The ground magnetic readings greater than 2200 gammas are shaded. These areas are underlain at or near the surface by magnetite-bearing serpentinite.

range from 95-145 feet (29-44 m) thick with an average of 117 feet (36 m). Where the lower contact of the southern serpentinite was recovered, it consists of a relatively narrow zone of steatized serpentinite with local intervals of coarse-grained chlorite. The upper and lower contacts of the serpentinite in DDH PC 88-2 are similar.

The principal ultramafic lithology of the Burks Mountain complex is a dark green to black, homogeneously textured serpentinite. The typical, least altered serpentinite is composed of 65-85 percent, coarse (0.1-1 mm), mesh-textured, lizardite serpentine (Fig. 11). Disseminated, ubiquitous (1-5 percent), primary "chromite" occurs as large (0.5-6 mm), pitted, deeply embayed and corroded masses (Fig. 12 and 13) and smaller (0.05-0.1 mm), subhedral to euhedral grains. All chromite, except for one sample collected by Vincent and others (1990), is altered to ferritchromite and/or Cr-magnetite (see section on metamorphism). Local concentrations of disseminated to layered and massive Ti-magnetite and ilmeno-hematite occur in the northern serpentinite on the western end of Burks Mountain. Abundant (0-4 percent), very fine-grained (0.1-0.2 mm), secondary magnetite "dust" is concentrated along and commonly forms elongate masses around mesh-texture rims in lizardite (Fig. 11 and 14). This magnetite formed by the release of Fe during serpentinization of Fe-Mg silicates - principally olivine and pyroxene (Fig. 14). The least altered serpentinite commonly contains 5-25 percent secondary carbonate, talc, chlorite, and quartz. Secondary magnetite is absent in talc formed during alteration of the lizardite.

The mineralogy of the serpentinite is divided into three categories: 1) primary igneous minerals which are relicts from the original ultramafic body (Cr-spinels - altered to magnetite); 2) metamorphic minerals which formed during regional metamorphism (anthophyllite, tremolite, lizardite, enstatite (altered to talc or lizardite), olivine (altered to lizardite and magnetite), talc, chlorite, Fe-Cr spinel, and magnetite); and 3) secondary minerals which are alteration products, formed after regional metamorphism of primary and metamorphic minerals (talc, chlorite, magnetite, carbonates, and quartz).

The original composition of the serpentinite is inferred to be a peridotite/harzburgite based on preserved primary textures and whole-rock geochemistry of the least altered serpentinite. Mesh-textured lizardite (Fig. 11 and 14) pseudomorphic after olivine and orthopyroxene (bastite) indicate a harzburgite protolith (Sacks and others, 1989). Other, relatively uncommon, ultramafic rocks in the Burks Mountain complex are interpreted as having olivine-clinopyroxenite cumulates (wehrlites) as a protolith with possible relict igneous layering (Sacks and others, 1989).

From normative analyses of anhydrous serpentinite whole-rock chemical analyses, original compositions are inferred to range from 53 percent enstatite, 37 percent forsterite, and 0 percent diopside to 17 percent enstatite, 67 percent forsterite, and 3 percent diopside. (The CaO used to make diopside in the normative calculations occurs as carbonate in the serpentinite and may reflect influx of CaO-bearing solutions). A steady, progressive change in the abundance of normative mafic minerals with depth suggests an igneous differentiation trend in the serpentinized harzburgite (Fig. 15 and 16). Normative enstatite demonstrates a continual enrichment from 17 percent at the base to 53 percent near the top, normative forsterite declines from 67 percent to 37 percent, and normative diopside declines from 13 percent to 0 percent. Two analyses collected 10 feet above the base of the serpentinite are off of these trends and may represent the original composition of the ultramafic magma (a chilled average composition) or contamination from more siliceous fluids (metamorphic or alteration) near the lower contact. The clustering of normative forsterite and enstatite pairs from different drill holes at similar heights above the base strongly suggests that the basal contact of the serpentinite with the underlying gneiss is more or less intact and unchanged following its emplacement. If this serpentinite is a fault slice of a larger ultramafic body, then additional ultramafites may have existed stratigraphically below the present base.

Relict igneous layering occurs as: layered concentrations of Cr-magnetite; layered concentrations of high-TiO_2 magnetite; and fine to coarser scale silicate banding. Thick, >8 cm, layers containing coarse, vein-like segregations of high-TiO_2 magnetite, hematite and ilmenite (Fig. 17) are associated with the silicate banding on Burks Mountain (Cocker, 1989c). Concentrations of Cr-magnetite in layers dipping approximately at the same angle to local and regional gneissic banding are locally present in the drill core. Fine, millimeter-scale (Fig. 18) and coarser- (>10 cm) scale primary silicate banding is exposed on the western end of Burks Mountain. This layering dips at steep angles to the northwest (perhaps due to rotation following emplacement). The fine-scale layering displays warping which is similar to load cast deformation in sedimentary rocks. Similar warping is noted in the pyroxenites of a layered ophiolite complex in Papua New Guinea (Jaques, 1981). Despite extensive alteration, the millimeter-scale layers consisted of cyclic cumulate olivine + intercumulate enstatite (?), now altered to quartz and talc respectively, and cumulate enstatite (?) altered to talc (Fig. 19).
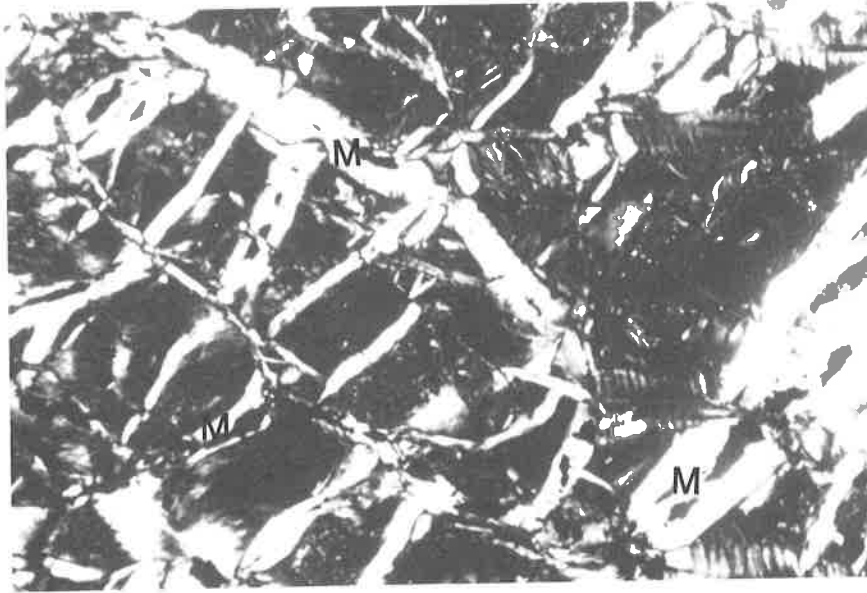
Figure 11. Photomicrograph of lizardite. Magnetite (M) released during serpentinization is concentrated along the mesh texture rims. Sample is from DDH 87-1, 88 feet. Width of field of view is 1.13 mm.
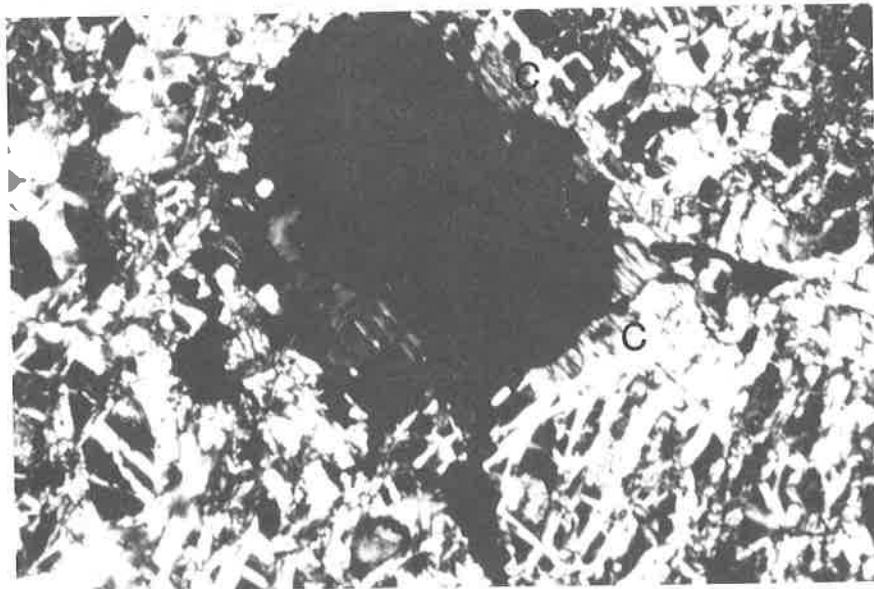
Figure 12. Photomicrograph of Fe-Cr spinel, lizardite and chlorite. Large, rectangular opague (black) grain is Fe-Cr spinel (magnetite) which is rimmed and slightly embayed with chlorite (C) and surrounded by mesh-textured lizardite. Sample is from DDH 87-4, 185 feet. Width of field of view is 2.65 mm.
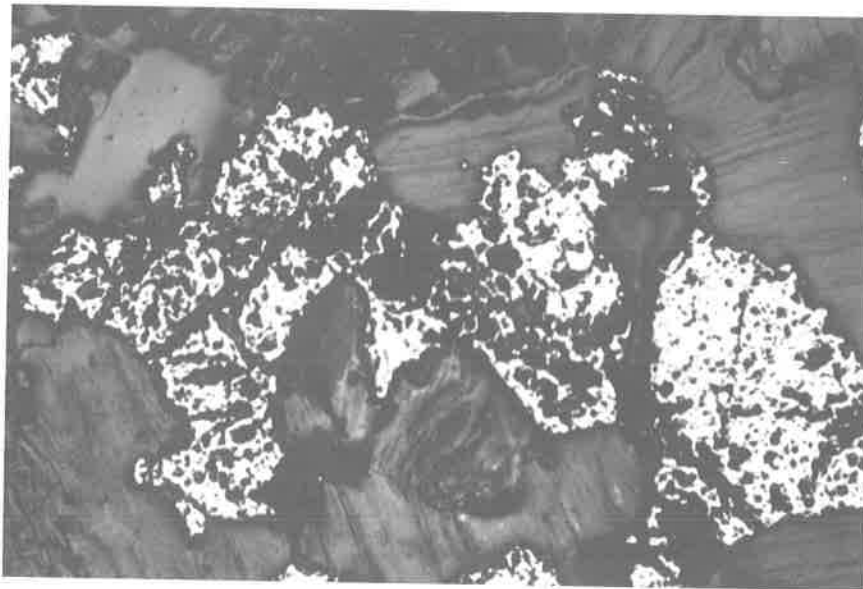
Figure 13. Photomicrograph of Fe-Cr spinel (reflected light). Surrounding mineral (gray) is chlorite. Sample is from DDH 87-4, 225 feet. Width of field of view is 1.13 mm.
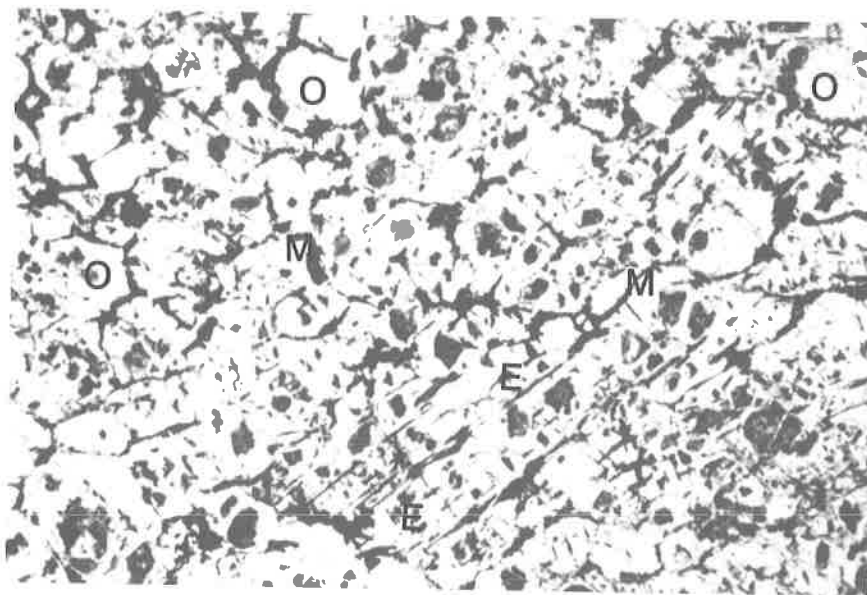
Figure 14. Photomicrograph of lizardite pseudomorphs after olivine and enstatite. Magnetite (M) is concentrated along rims of the mesh-texture and outlines lizardite pseudomorphs of olivine (O) and enstatite (E) and is also concentrated along cleavages in the enstatite. Areas of higher relief are magnesite which has partially replaced lizardite in the core of the mesh-texture. Sample is from DDH 87-4, 140 feet. Width of field of view is 2.65 mm.
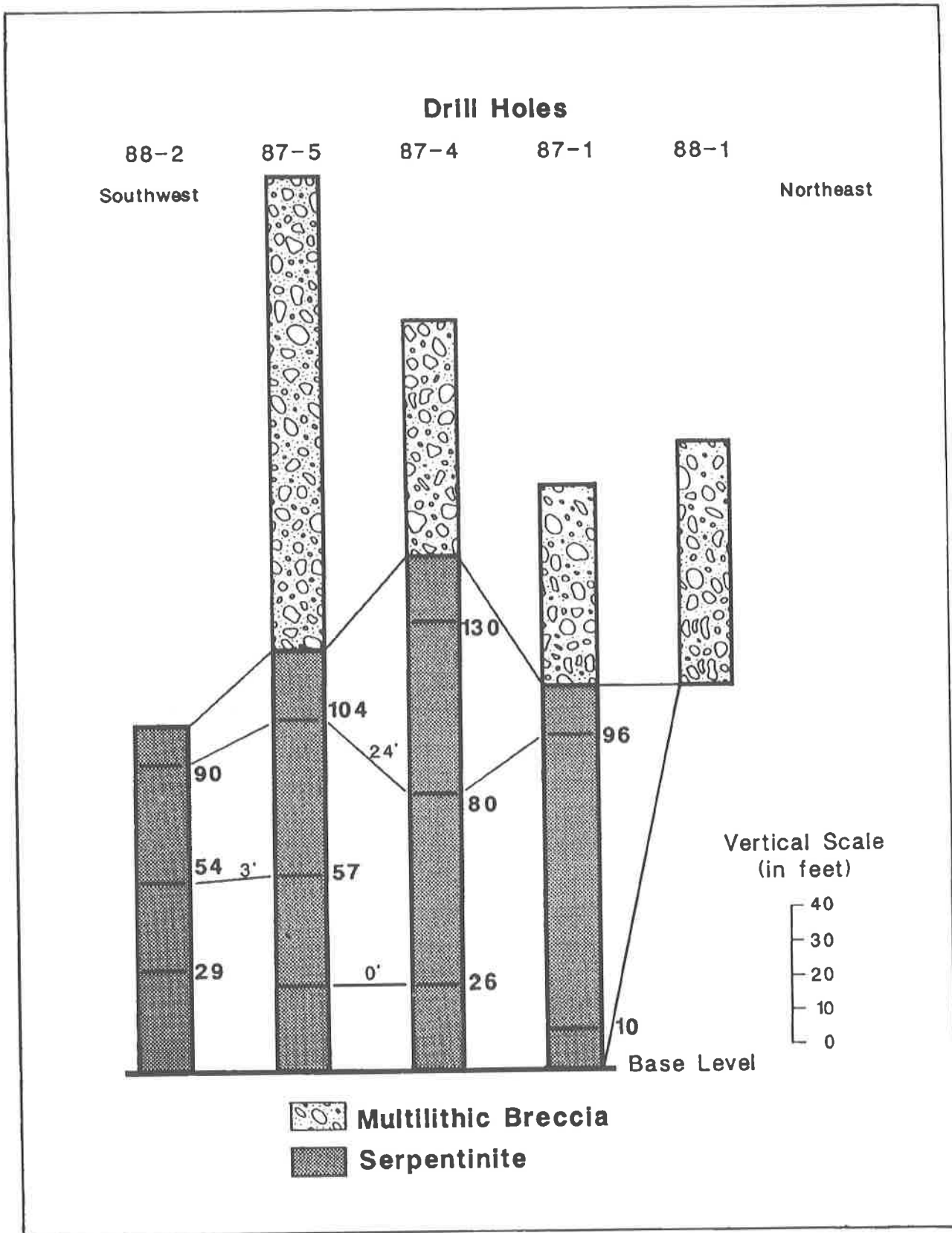
Figure 15. Position of analyses relative to normalized base of serpentinite. The positions of analyses are indicated by the larger, bolder numbers (feet above base). The relative differences in height between analyses with nearly similar norms are shown by the smaller, lighter numbers (0', 3', 24').
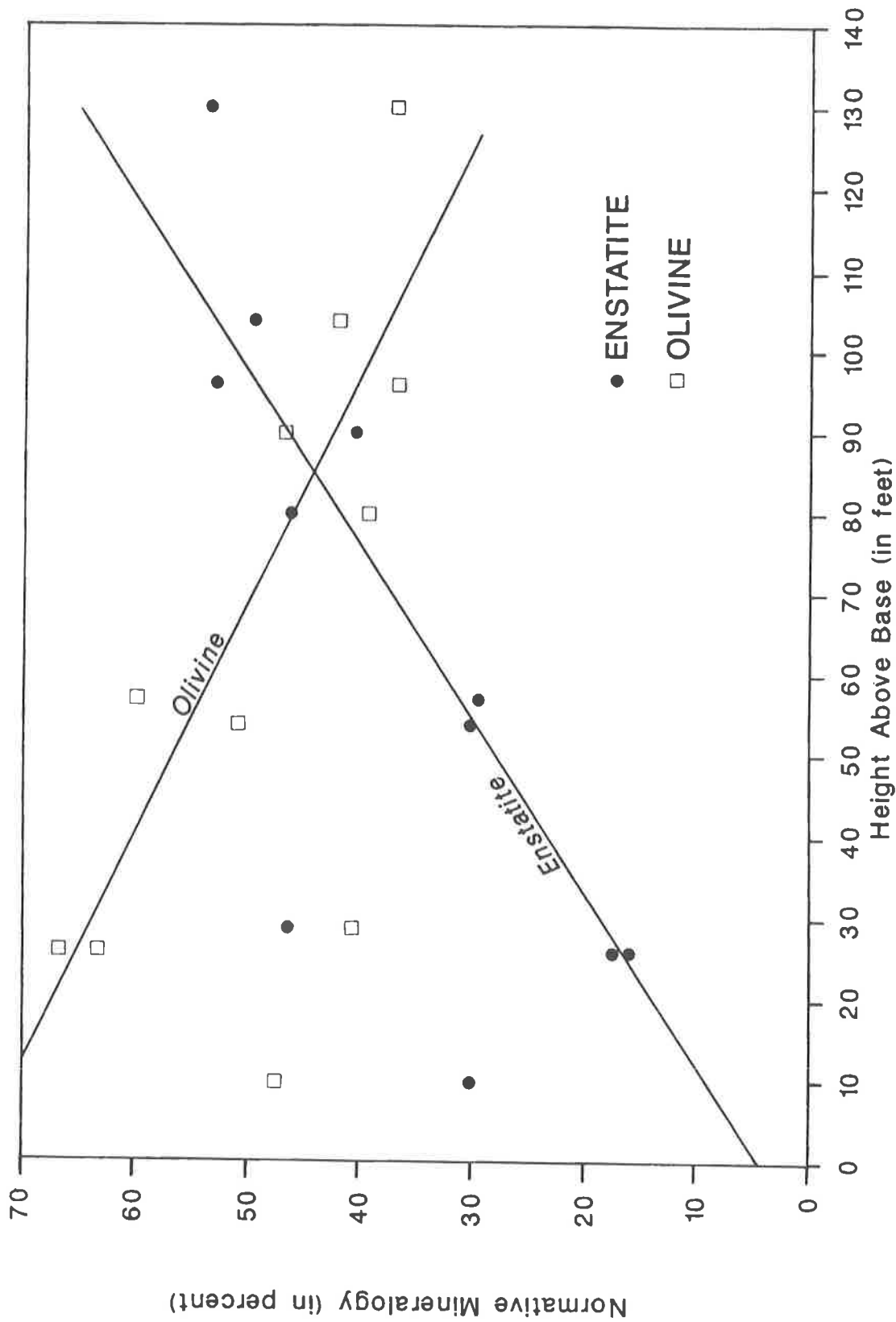
Figure 16. Normative olivine and enstatite versus height above base of the serpentinite. Trend lines suggest a continual change in composition from the base towards the top of the serpentinite and are inferred to represent igneous differentiation. Samples are from DDH's 87-1, 87-4, 87-5 and 88-2. Closely spaced pairs are from different drill holes and reinforce the concept of changing composition at similar horizons during cooling of the magma. The samples at 10 and 26 feet lie off from the main trends. These may contain some talc which has a higher SiO_2 content than the serpentinite. With a higher SiO_2 content, normative enstatite would appear more abundant and normative olivine less abundant than what they really were prior to the addition of SiO_2.
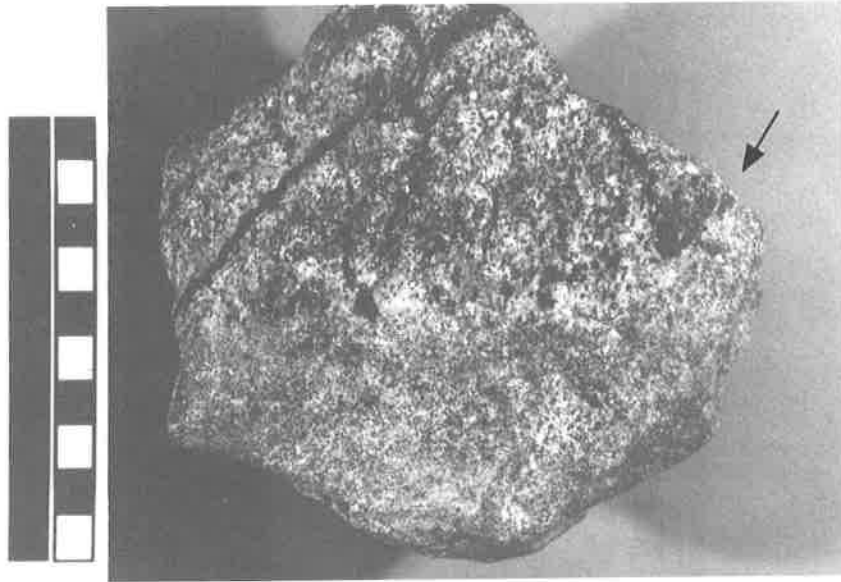
Figure 17. Ti-magnetite and ilmenohematite concentrations. Note curvature of contact (shown by arrow) between Fe-Ti oxide rich layer and lower layer. Veinlets of Fe-Ti oxides (black) do not penetrate lower layer. Sample B-850 from western end of Burks Mountain. Scale on left is in centimeters.
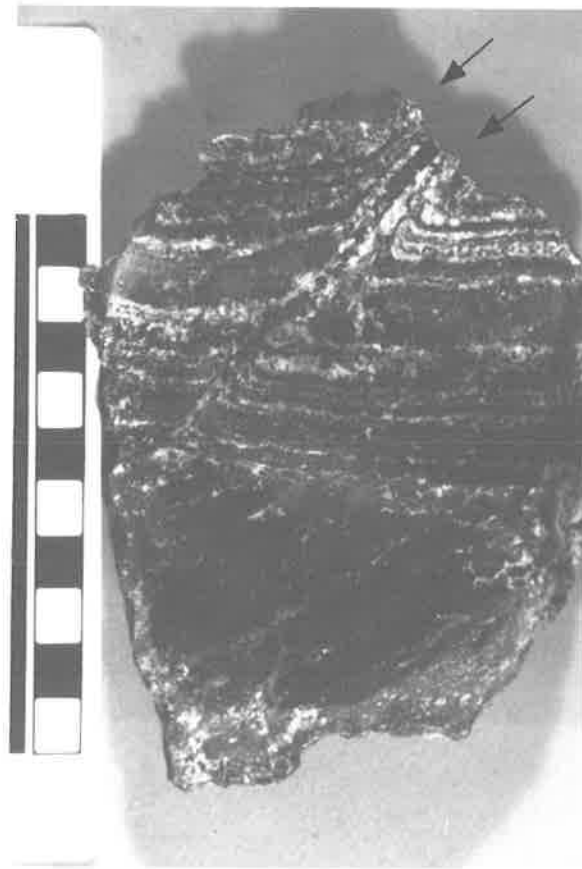
Figure 18. Millimeter-scale layering in contact with massive serpentinite. Layering is composed of olivine plus enstatite and enstatite. The enstatite is altered to talc (light layers), and the olivine is altered to quartz (dark layers). Upward curving of layering (shown by arrows) on both sides of the dark planar feature and the fact that these features do not extend into the underlying massive serpentinite indicate that this is not a fault. This lanar feature may represent a minor amount of late-stage magma injected upward into the layered part of the sample. This sample (B-825) is from the western end of Burks Mountain. Scale on left is in centimeters.
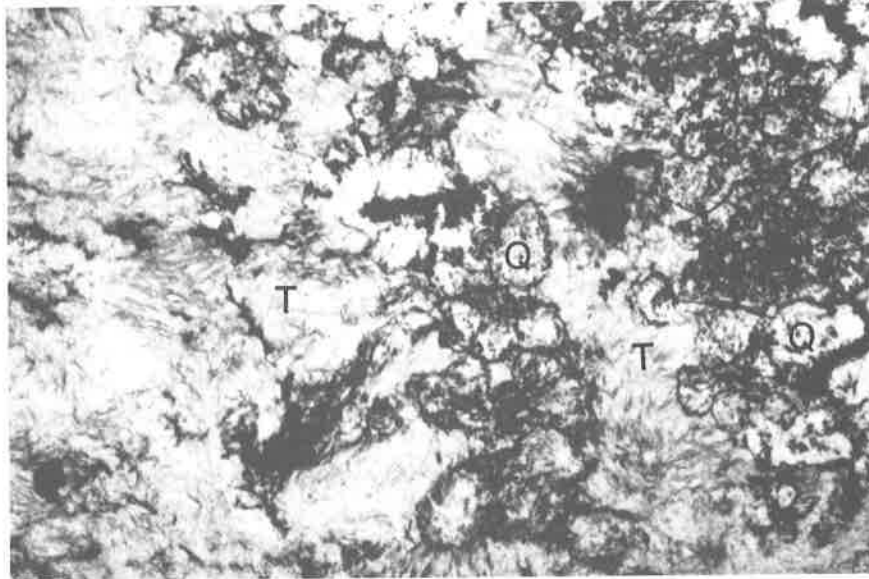
Figure 19. Photomicrograph of millimeter-scale layering. Layering is composed of olivine plus enstatite and enstatite. The enstatite is altered to talc (T), and the olivine is altered to quartz (Q). Outlines of the former olivine and enstatite grains enhanced by magnetite (black). Sample B-825 from western end of Burks Mountain. Width of field of view is 2.65 mm.

Alteration of the serpentinite produced talc, chlorite, carbonate, and quartz. Small (0.05-2 cm) patches of talc, chlorite and carbonate (not necessarily together) are disseminated throughout the serpentinite. Coarse, platy talc forming a cross-fiber texture with an average width of 1 cm, occurs along fractures and edges of ultramafic clasts in the multilithic breccia. This talc may be a pseudomorph after chrysotile or amphibole, but no trace of a previous mineral was found by XRD or petrographic analyses. Massive talc extends from the fibrous talc or from fractures or clast rims into the serpentinite. Coarse-grained chlorite (derived from the alteration of talc and/or crushed serpentinite?) occurs in fractures, as the matrix in a multilithic breccia, and along the country rock-serpentinite contact.

The northern serpentinite is pervasively silicified and cut by stockwork and multistage quartz veining in many parts of the Burks Mountain complex. Petrographic examination of silicified serpentinites indicates that lizardite mesh-texture is preserved but silicification completely replaced all lizardite leaving only the igneous/metamorphic and secondary magnetite. Fibrous foliated talc is overprinted and replaced by silicification. In outcrop, the silicified mafic rocks have a distinct, fine-grained, flinty appearance due to the fine grain size (0.25 to 0.5 mm) of the secondary quartz.

Multilithic breccia

Multilithic breccia is a mappable lithology (mbx in Fig. 3) which overlies the southern serpentinite (Figs. 20 and 21). This breccia is exposed in a roadcut (location shown in Fig. 3) beside the Old Petersburg Road (Fig. 22, 23, 24, 25 and 26) and is penetrated in at least four of the drill holes. In DDH's PC 87-5, -4, and -1, the multilithic breccia overlies the main serpentinite body. In DDH PC 88-1, the breccia directly overlies gneiss, and the main serpentinite mass is missing. Traces of talc and chlorite in DDH PC 87-2, poor recovery in the upper part of DDH's PC 87-3 and 87-2, plus talc boulders on the surface suggest the breccia is present in the drilled section but was not recovered. Additional occurrences of multilithic breccia represented by rounded talc boulders occur to the north at various points around the base of Burks Mountain and to the west overlying a suspected serpentinite mass approximately 0.8 km south of Phinizy on Georgia State Highway 47. The multilithic breccia principally consists of small (<0.5 m), subrounded to rounded, ultramafic clasts with minor (<20 percent) Kiokee gneiss and kaolinized granite clasts enclosed in and supported by a matrix of coarsely crystalline chlorite (Fig. 23, 24, 25 and 26). Ultramafic clasts are rimmed by foliated talc. Complete replacement of the smaller serpentinite clasts by talc is common (Fig. 26), although serpentinite-cored clasts are also present (Fig. 24 and 25).

The breccia matrix, composed of coarse-grained (0.5-1 cm) chlorite, is friable and poorly consolidated (Fig. 24, 25 and 26). During core drilling, the drilling fluids generally wash out and remove the friable chlorite leaving a chaotic mixture of lithologies. Surface weathering removes the chlorite and decomposes gneiss and granite clasts and serpentine leaving the inert talc clasts as a surface residuum of subrounded to rounded pebbles, cobbles and boulders (Fig. 27). Much of the area covered by the talc boulder fields is probably underlain by multilithic breccia.

Drill intercepts of the multilithic breccia indicate a maximum thickness of 137 feet (42 m) in DDH PC 87-5 and a minimum thickness of 85 feet (26 m) in DDH PC 88-1 (Fig. 20 and 21). Potentially thinner breccia intercepts of 20-30 feet (6-9 m) are suggested in DDH PC 87-2 and DDH PC 87-3 because of suspect lithologies and poor recovery. Average thickness in the confirmed intercepts is 76 feet (23 m). The breccia thickens to the west but disappears between DDH PC 87-5 and DDH PC 88-2. Talc boulders several hundred feet west of DDH PC 87-5 indicate the breccia probably extends under that area. The down-dip extent of the breccia was not tested. A three-point solution on the basal contact of the breccia with the serpentinite defines a plane with a strike of N39°W dipping 10°SW.

The breccia provides important evidence concerning the timing of serpentinite brecciation, alteration to talc and formation of chlorite. The presence of Kiokee gneiss and kaolinized granite as clasts (Fig. 23 and 24) within the breccia conclusively indicates that the high grade regional metamorphism and felsic igneous activity that produced the Kiokee gneiss and granite, respectively, occurred prior to brittle deformation and brecciation of the serpentinite. Low temperature and pressure retrograde metamorphism resulting in the formation of the serpentinite also occurred prior to brecciation. Alteration of the serpentinite to talc, carbonate and chlorite along fractures and in breccia clasts occurred subsequent to brecciation and hence after regional high-grade and retrograde metamorphism.

Weathering of serpentinite and talc

Weathering affected the northern and southern serpentinites in distinctly different manners. The northern mass is less affected by weathering principally because of its silicification. Weathering of partially silicified serpentinite produced a type of pseudogossan boxwork consisting of resistant quartz veins, silicified

24
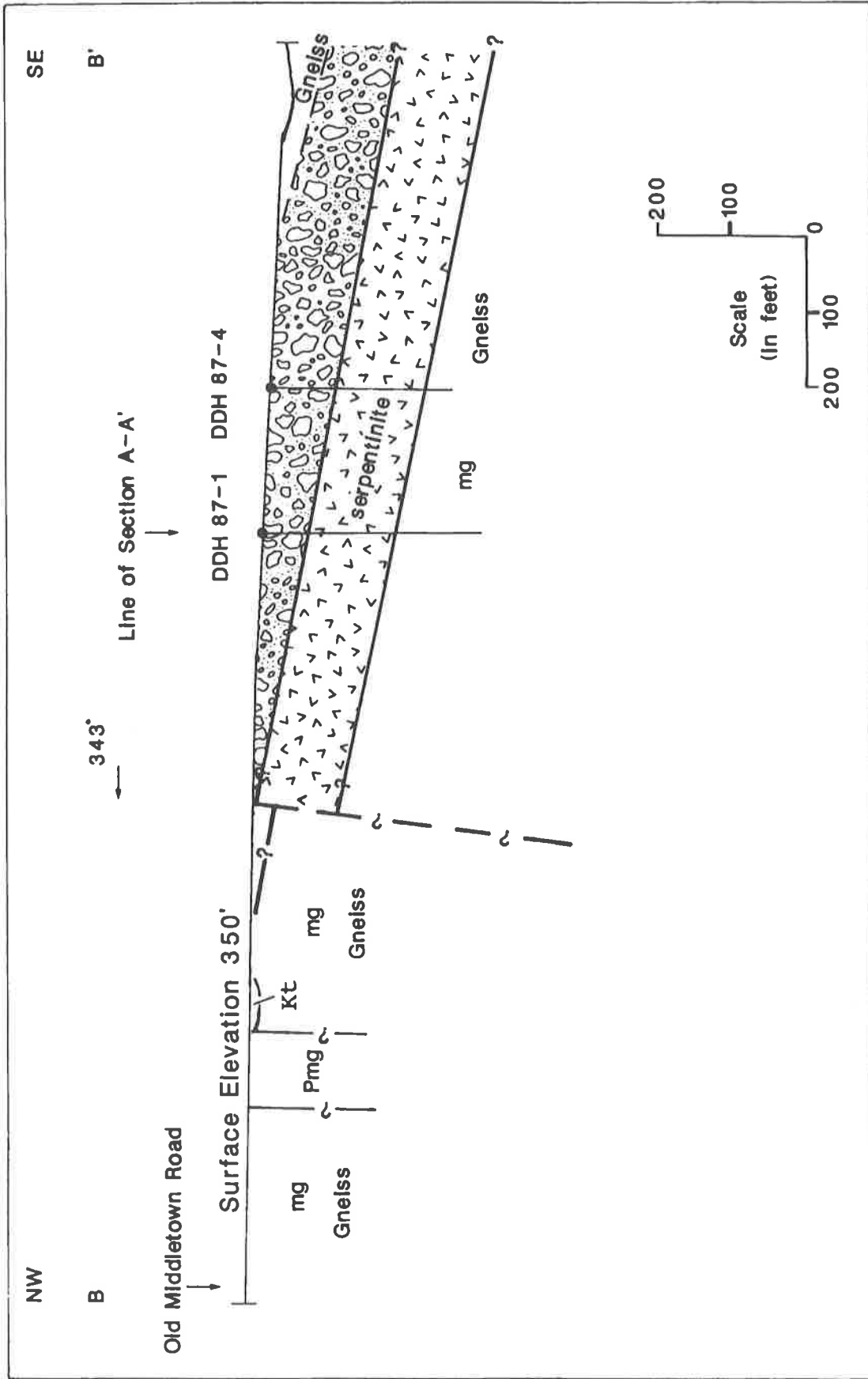
Figure 20. Cross section B-B'. This section was constructed from the surface geology and the geology projected from DDH's 87-1 and 87-4 into the section. This section is oriented at 90° to the long section A-A'. The existence of the fault on the north side of the serpentinite is inferred from the ground magnetic sections (Cocker, unpublished data).
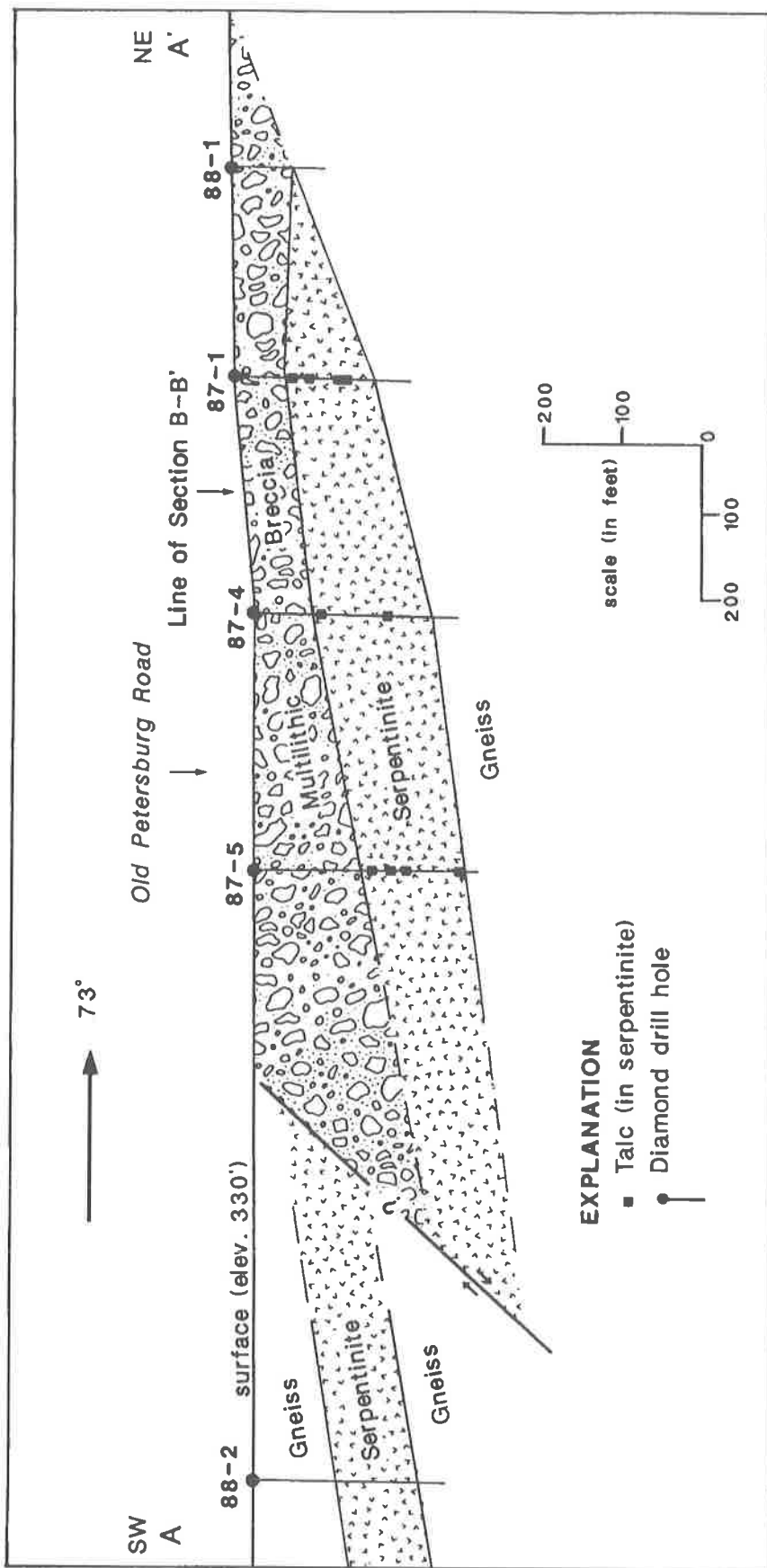
Figure 21. Long section A-A′. This section shows the distribution of the multilithic breccia relative to the underlying southern serpentinite as determined from drill hole data. DDH's 87-4, 87-5, and 88-2 are projected into the section. The existence and attitude of the fault between DDH's 87-5 and 88-2 is inferred from the ground magnetics and the apparent displacement of the serpentinite in this section.
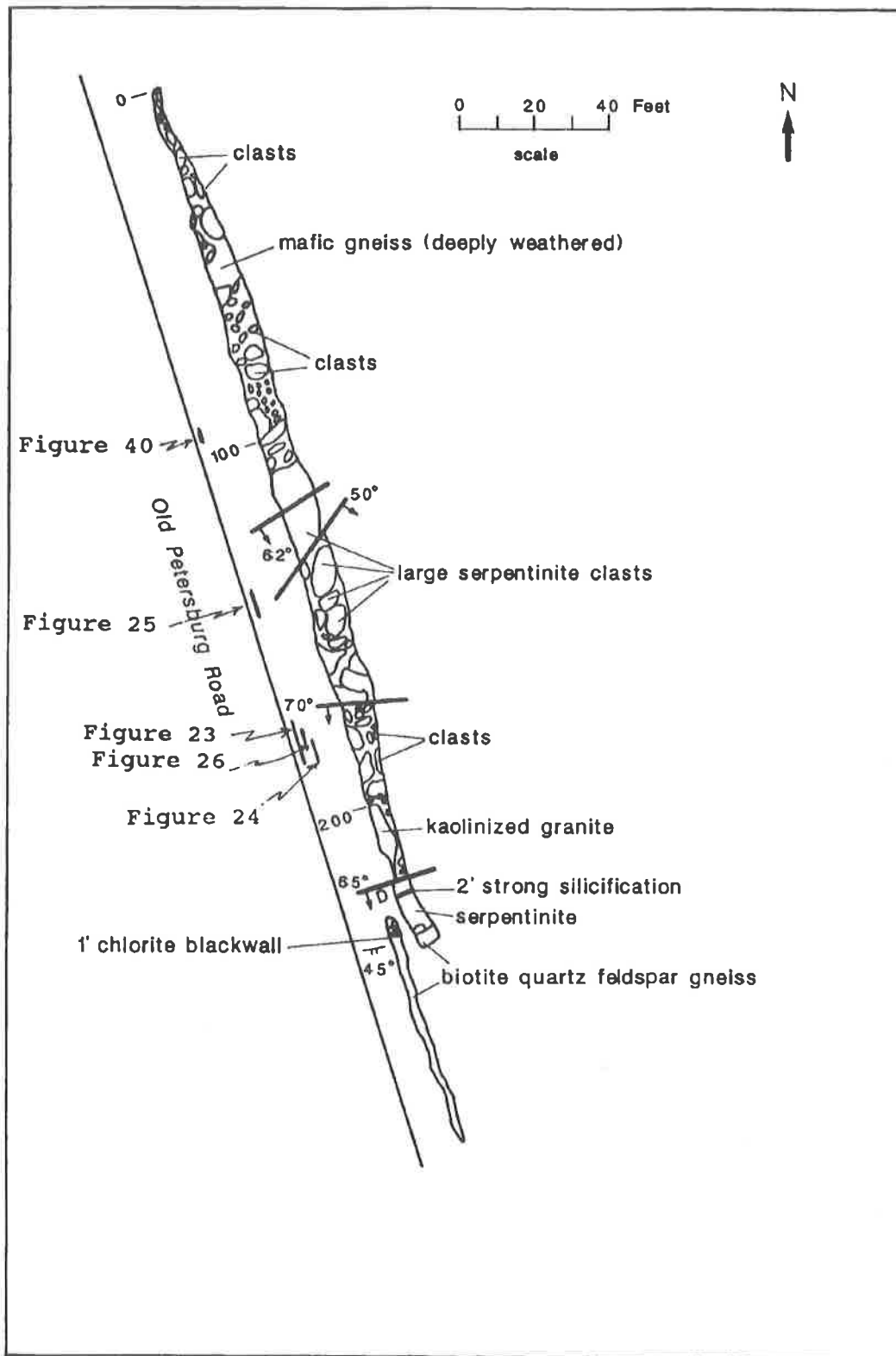
Figure 22. Detailed geology of Old Petersburg Road outcrop. Outcrop map shows the distribution and relative size of clasts in the multilithic breccia (mbx in Fig. 3). Clasts are principally serpentinite although no attempt is made to distinguish the serpentinite clasts from clasts of Kiokee rocks except for those clasts which are of mappable size. Contact with the overlying Kiokee gneiss is at approximately 220 feet. Small faults are indicated by heavy black lines. The numbers along the west side of the outcrop indicate the distance in feet from the northern end of the outcrop. Approximate positions of photographs in the text are shown as small bars alongside of the road. Location of this roadcut is shown in Fig. 3.
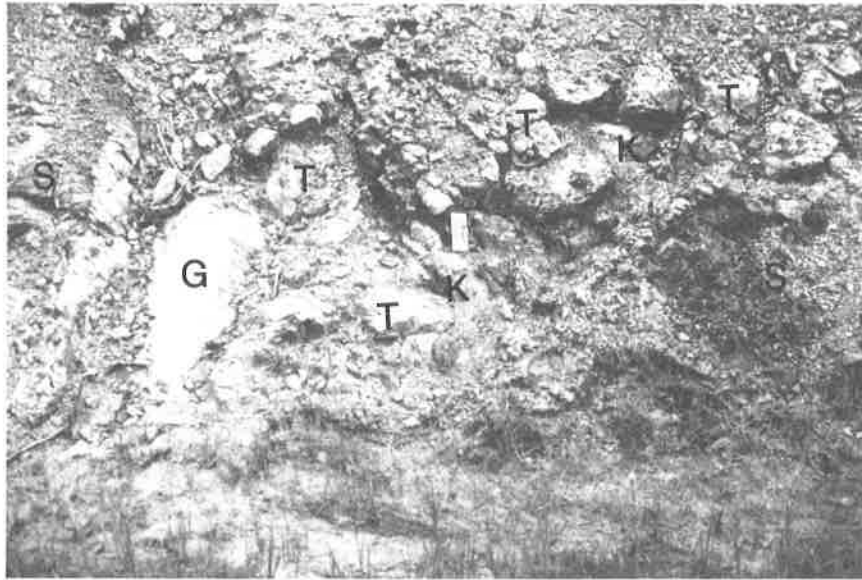
Figure 23. Multilithic breccia. View is of the multilithic breccia with formation of coarse-grained chlorite and talc. Clasts include: kaolinized granite (G), Kiokee gneiss and amphibolite (K), serpentinite with talc rims (S), and talc (T). View is along Old Petersburg Road from 170 to 182 feet south of north end of roadcut (Fig. 22). Scale, located in center of photograph, is 10 cm (4 inches). Figure 24 is a closeup of the area to the upper right of the scale.
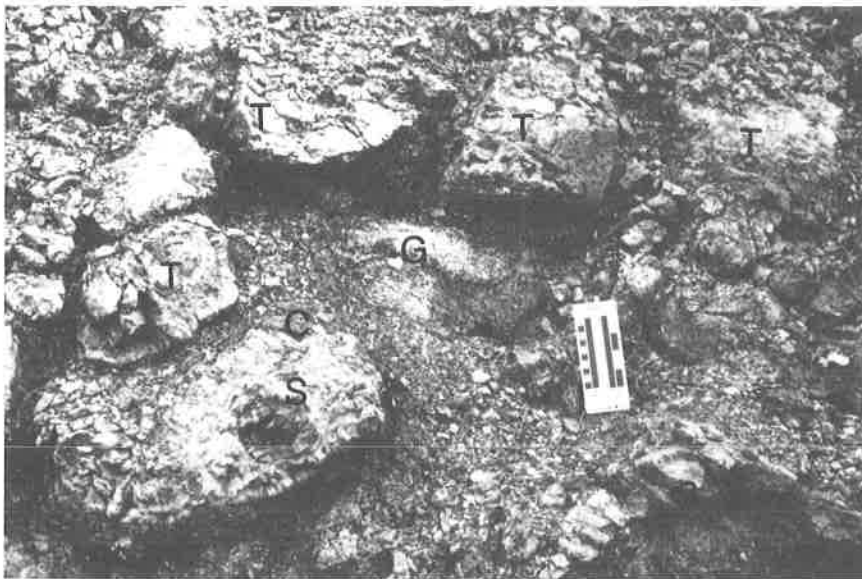
Figure 24. Closeup view of multilithic breccia. Clasts include: Kiokee gneiss (G), serpentinite with talc rims (S), and talc (T). Matrix is coarse-grained chlorite (C). Clast in left center is pictured in Figure 48. Scale is 10 cm (4 inches). View is along Old Petersburg Road at about 177 feet south of north end of roadcut (Fig. 22).
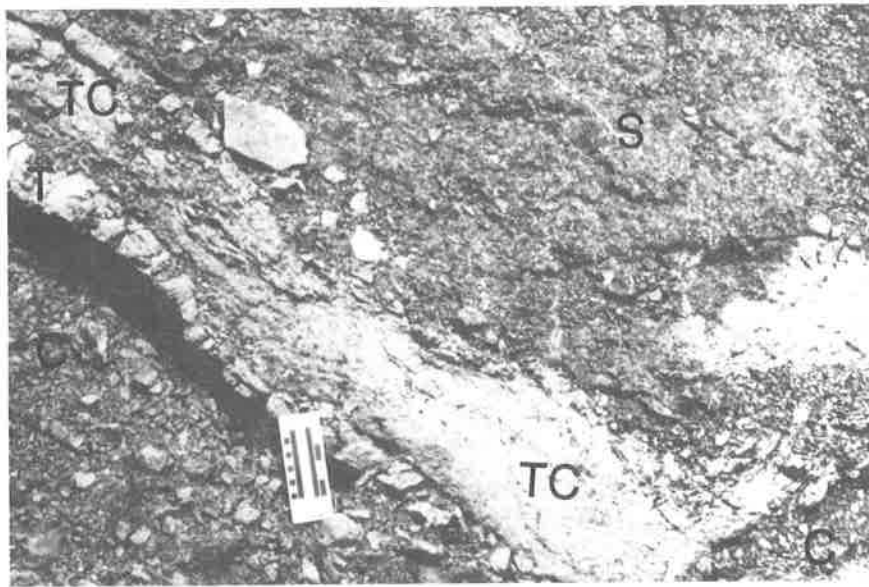
Figure 25. Chlorite, foliated talc and massive talc alteration envelope around serpentinite clast in multilithic breccia. Closeup view of alteration adjacent to edge of serpentinite clast in multilithic breccia, Old Petersburg Road, with coarse-grained chlorite (C); foliated talc rim (T); massive talc + carbonate (TC); and serpentinite with patchy talc (S). Scale is 10 cm (4 inches). View is along the Old Petersburg Road at about 140 feet south of the north end of the roadcut (Fig. 22).
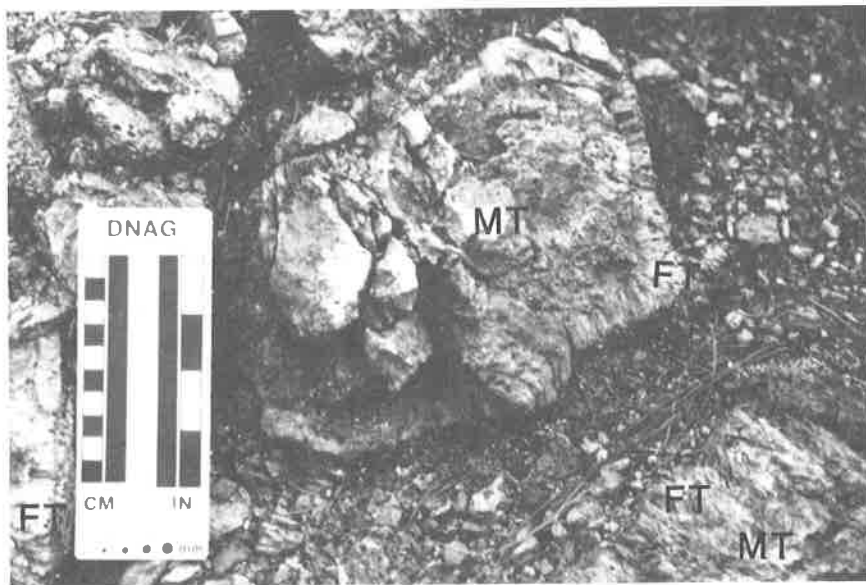
Figure 26. Massive talc clast with foliated talc rim in coarse-chlorite from multilithic breccia. Massive talc (MT) in core of clast with a foliated talc (FT) rim. Other clasts to the left, upper left and lower right also have similar foliated talc (FT) rims. Matrix is coarse-grained chlorite (C). View is along Old Petersburg Road at about 177 feet south of north end of roadcut (Fig. 22). Scale is 10 cm (4 inches).

layers, and oxidized, pitted serpentinite. The lack of significant weathering of a silicified rock produces an organically poor, thin soil which does not retain as much moisture as a thicker, organic rich soil. As a ridge former, there is no drainage onto or over the silicified serpentinite. Weathering is inhibited by the physical nature of the bedrock. Fracturing of the relatively brittle, silicified rock produced numerous open fractures and cavities and greatly enhances subsurface drainage off the ridge. The loss of circulation in numerous cavities and fractured rock during attempts to drill on the western and eastern ends of Burks Mountain by the Georgia Geologic Survey and the J.M. Huber Corporation respectively, is a direct effect of the fractured bedrock.

Clasts derived from the southern serpentinite are exposed in the multilithic breccia in the Old Petersburg Road roadcut (Fig. 23 and 25). This outcrop illustrates the strong degree of weathering typical of a serpentinite in the Georgia Piedmont. Weathering is facilitated by the physical character of the bedrock. The multilithic breccia contains numerous passages, as evidenced by coarse chlorite which surrounds clasts and the numerous through- going fractures, for groundwater movement and retention.

Although serpentinite is strongly affected by weathering, talc appears to be stable under the same conditions. Talc appears fresh in outcrop and forms a surficial residual deposit in certain parts of the project area. The surficial deposit consists of subangular to rounded pebbles, cobbles and boulders commonly so abundant as to form a pavement (Fig. 27). Although the density of surficial talc suggests a similar concentration might occur in the subsurface, drilling indicates considerably less talc. Drilling within the area of surficial talc provided the following results: 1) poor recovery, 2) recovery of a mixture of talc and gneiss clasts, and 3) occasional recovery of coarse-grained chlorite in addition to the talc and gneiss clasts. These results suggest that multilithic breccia similar to that exposed on the surface underlies the surficial talc deposits.

The concentration of talc boulders at the surface depended on development of the multilithic breccia. Brecciation of the serpentinite produced numerous clasts which were subjected to replacement by talc and the development of a chlorite-rich matrix. Rapid decomposition and removal of this breccia matrix and non-talc clasts freed and concentrated the resistant talc clasts.

Talc which formed during metamorphism appears to be stable under intense tropical weathering conditions in Nigeria (Akpanika and others, 1987) and under subtropical conditions in Winterboro, Alabama

(Blount and Vassiliou, 1980). Deep weathering of a dolomite-hosted talc deposit at Winterboro produced yellow, red and brown clays from the illite plus quartz-bearing dolomite and left the talc essentially untouched except for a possible reduction in grain size. Evans and Guggenheim (1988) suggest that deep saprolitic weathering of serpentinites may produce nickel- and ferric iron-rich talc and the Ni-analog of talc, willemsite; these were not recognized in this study, but they may be present.

Coastal Plain sedimentary rocks

Numerous outcrops of arkosic sandstones and conglomeratic sandstones occur unconformably overlying gneisses, schists and granites over much of the mapped area (Kt in Fig. 3). Most outcrops occur along creeks and gullies, but outcrops are also present in shallow roadcuts and drainage ditches (Fig. 28). Gravel-rich layers dip at a shallow angle to the south. The maximum observed thickness in outcrop is about 8 feet (2.5 m). The sandstones are typically massive, light-gray, yellow and pinkish-white, micaceous arkosic and kaolinitic sands with locally crossbedded sands. The gravel consists mainly of subrounded to subangular quartz pebbles with a small percentage of weathered gneiss and granite pebbles.

These clastic rocks are similar to those described by Eargle (1955), LeGrand and Furcron (1956), and O'Connor and Prowell (1976) as belonging to the Cretaceous-age Tuscaloosa Formation. O'Connor and Prowell (1986) question the age and correlation of "Tuscaloosa" sedimentary rocks in eastern Georgia because of palynological studies by Tschudy and Patterson (1975) which suggest some clays may be as young as middle Eocene. Frazier and Schwimmer (1987) indicate that the Tuscaloosa is present in western Georgia but is overstepped in central Georgia by Cenozoic strata. Huddleston (personal communication, 1991) suggests that, in light of recent field work in the Coastal Plain rocks, the sedimentary rocks exposed within the present study area may be part of the Upper Cretaceous Gaillard Formation.

The nearest, previously identified occurrences of the "Tuscaloosa Formation" in Columbia Co. are about 8 miles (12.8 km) down dip to the south near the border with Richmond Co. (LeGrand and Furcron, 1956). In neighboring McDuffie Co., the "Tuscaloosa Formation" extends up to the western end of Greenbriar Creek, about three miles (5 km) south of the project area but approximately along strike. Undifferentiated Cretaceous and Tertiary sands in South Carolina extend to an area approximately 18 miles (30 km) northeast of the Savannah River along strike with the Pol-
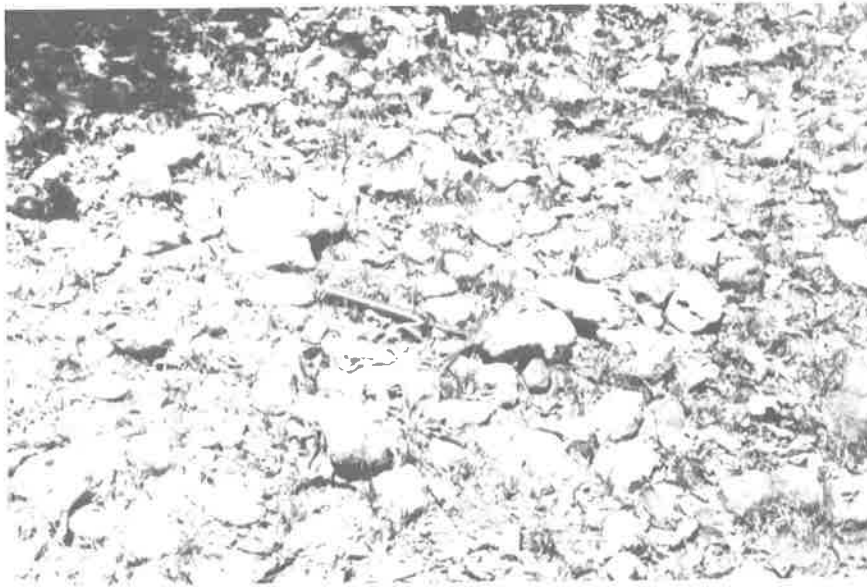
Figure 27. Talc boulder field. Talc boulders are rounded clasts weathered out of the underlying multilithic breccia. Location is approximately 600 feet east of the multilithic breccia roadcut on the Old Petersburg Road (Fig. 22). Approximate location is shown in Fig. 3. Hammer in center of picture is about 1 foot long.

Figure 28. Outcrop of Coastal Plain sandstones. Note white clasts are kaolinite. Outcrop is along drainage ditch on east side of Old Petersburg Road 200 feet south of the intersection with Old Middleton Road (Fig. 3). Scale is 10 cm (4 inches).

lards Corner study area (Secor and others, 1986a).

Thickness of the "Tuscaloosa Formation" (Gaillard Formation ?) ranges from 20 feet (6 m) near Thomson to 190 to 220 feet (58 to 67 m) near the southern edge of McDuffie and Columbia Counties. Average dip of the basal contact is approximately 45 feet per mile (8.6 m per km) (LeGrand and Furcron, 1956). In the study area, maximum elevation of the basal contact with the underlying crystalline rocks, as observed in outcrop, is 320 feet (98 m) above sea level. The highest exposure of the "Tuscaloosa" (Gaillard Formation ?) in the study area is at 350 feet (107 m) suggesting a maximum thickness of 30 feet (9 m) for this unit. Clastic-appearing material recovered from 0 to 100 feet (30 m) in DDH PC87-6 suggests local thicknesses up to 100 feet (30 m). The sharp increase in thickness may be due to late-stage (Cenozoic?) faulting. The elevation of the basal contact at 320 feet (98 m) is similar to that of the Tuscaloosa Formation near Columbus, Georgia at 310 feet (94 m), but considerably lower than the 502 feet (153 m) in Talbott Co., the 545 feet (166 m) in Crawford Co. and the 550 feet (168 m) in McDuffie Co. (Eargle, 1955).

STRUCTURAL GEOLOGY

Structural data were obtained from geologic mapping, core logging, geophysical data, and topographic map lineament analysis. Lineations were compiled for the area from portions of four U.S.G.S. 7.5 minute quadrangle maps: the Appling, Evans, Clarks Hill and Leah quadrangles.

Ductile deformation

The project area is located on the gently dipping southeast limb of the Kiokee antiform. The axis of the Kiokee antiform is located approximately 2 miles (3 km) north of the study area trending in a N60-67°E direction (Fig. 2). Measurements of 62 foliation/banding dips in nine core holes and 32 dips from outcrops within the project area indicate that 55 percent of the foliations dip 10-30°SE with 22 percent dipping 30-55°SE (Fig. 29). Dips measured in outcrops along the Old Petersburg Road tend to steepen adjacent to late, high angle faults. Foliations in surface outcrops generally (50 percent) strike N60-75°E (Fig. 30) which is approximately parallel to the axial strike of the Kiokee antiform. Most structural features originating prior to or associated with this Alleghanian deformation (foliations, stratigraphic contacts, igneous layering in the ultramafic bodies, and strike of gneissic granite) are parallel to this northeast trend (Fig. 30).

Mineral banding is best developed in amphibolites, gneisses and schists and is discernible in older granites (granitic gneisses). The banding is defined by alternating layers of quartz + feldspar and biotite +/- hornblende. Microscopic textures indicate that microscale folding in the gneisses is pre-biotite. Intermediate, outcrop-scale folding was not observed in the project area.

Mylonitization of Kiokee felsic gneisses observed in this study area is manifested as elongated, stressed and broken quartz. Large quartz grains are elongate parallel to the biotite foliation and are extensively strained; abundant fine-grained quartz occurs adjacent to the larger quartz grains (Fig. 4). These features contrast with the relatively non-deformed Kiokee belt rocks to the south of the Burks Mountain area and immediately north of the Augusta fault (Maher, 1987).

In contrast with the felsic and mafic rocks, nearly all of the ultramafic rocks examined during this study and by Vincent and others (1990) show no megascopic or microscopic mineral alignment. Sacks and others (1989) interpret thin, discontinuous layers of chromite grains as a foliation parallel with the regional foliation and suggest that these rocks were penetratively deformed and foliated prior to serpentinization. The present study found magnetite rather than chromite to be the predominant spinel; in addition, this magnetite occurs as disseminated, intricately embayed grains and as primary, layered, magmatic segregations. Elongated blebs of metamorphic magnetite and serpentine in one serpentinite sample collected by Vincent and others (1990) are probably due to localized ductile deformation. An absence of penetrative deformation is indicated also in the preservation of numerous pre-serpentinization textures. Such textures include millimeter-scale primary layering, delicate sprays of acicular tremolite and anthophyllite, intricately embayed primary/ metamorphic magnetite, and pseudomorphs of lizardite after olivine and enstatite.

Brittle deformation

In this part of the Kiokee belt, brittle deformation is complex and multi-stage. Brittle deformation occurs as faults, multilithic breccias, and open-space quartz veining. Some older, brittle structures are preserved by younger granite and pegmatite dikes.

The paucity of outcrops inhibits observations of brittle structures, particularly those structures larger than outcrop scale. Recognition and measurement of the orientation of topographic lineaments (elongate stream segments and ridge crests) may suggest geologic control (brittle structures, resistant and nonresistant rock units, etc.) of these lineaments.
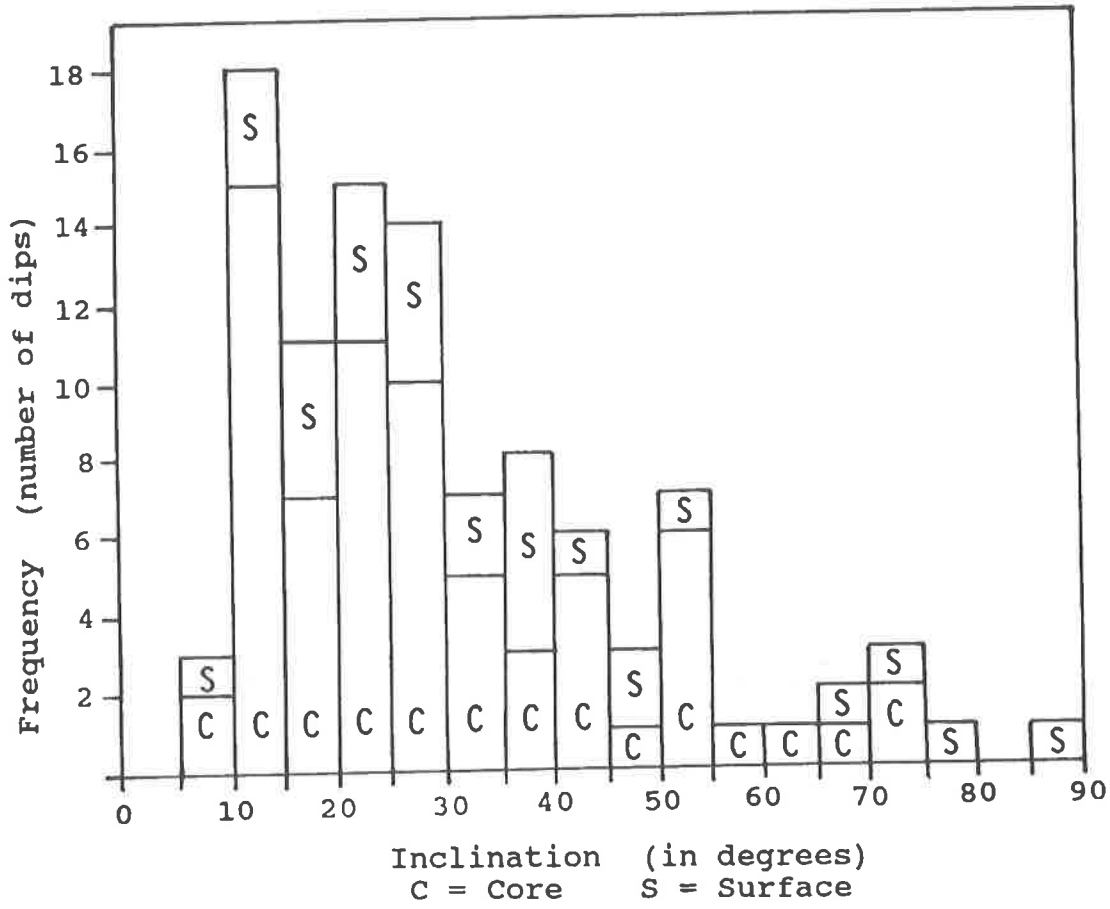
Figure 29. Histogram of foliation dips (core and surface). Angles of veins measured relative to core axis were recalculated to dips from horizontal. Note the concentration of dips from 10-30°. Total number of strikes measured is 101.
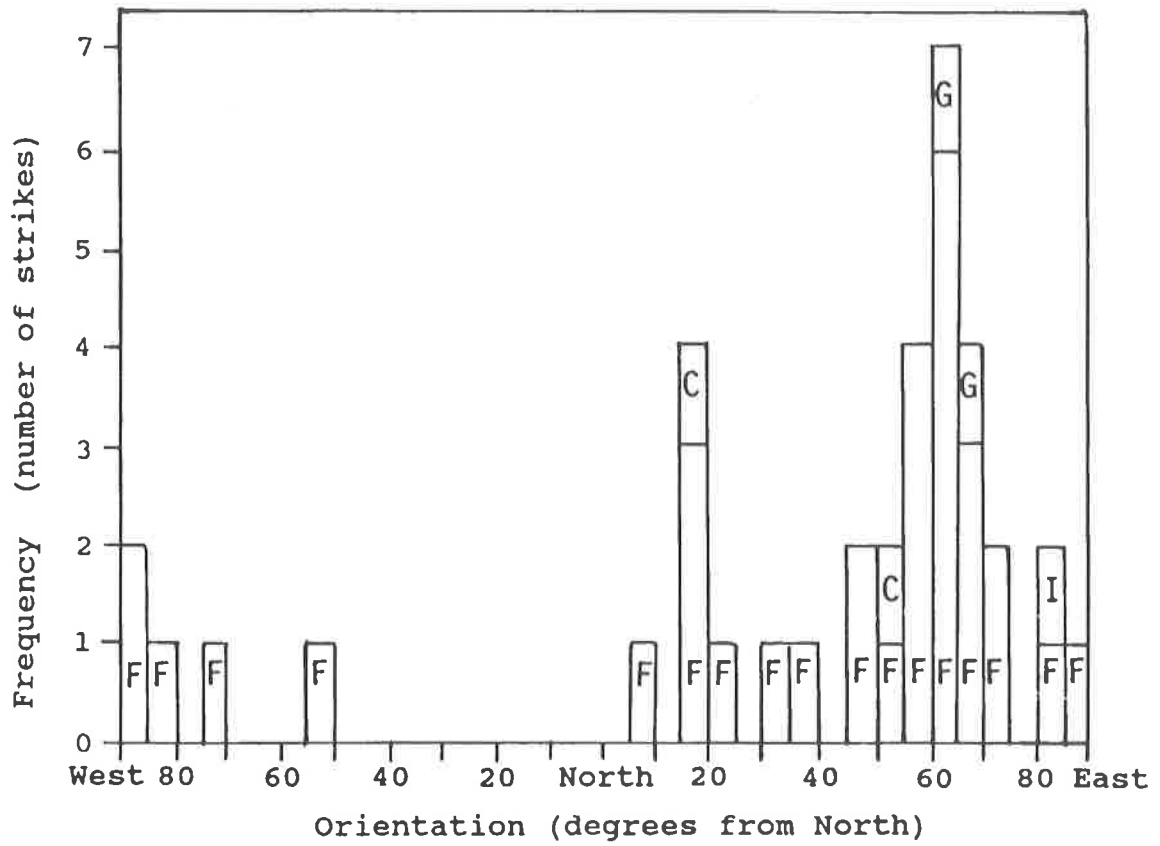
Figure 30. Histogram of strikes of surface foliation, igneous layering, metamorphic contacts, and granite (intrusive) contacts. Note the concentration of strikes from N55-75°E. Total number of strikes is 37.

Talc veins and chlorite fractures

Talc "veins", developed as alteration envelopes adjacent to microscopic fractures, are common in outcrop and in drill core. The talc alteration products include carbonate, principally dolomite and magnesite. These veins are moderately to steeply dipping with 90 percent of the 41 veins in drill core dipping 30-85° (Fig. 31). (Dip azimuths in drill core are unmeasurable without oriented core). One group of veins, dipping 60-65°, contains 22 percent of the veins; this group may represent a major fracture set. Dips of fractures containing coarse-grained chlorite are concentrated (49 percent of the 37 fractures) in the range 40-60° (Fig. 31).

Carbonate veins

White to cream colored carbonate veins in serpentinite are locally abundant in drill core but are virtually absent in surface exposures. Petrographic and geochemical studies indicate that carbonates are completely absent in surface samples probably due to weathering. Carbonate veins appear to show a preferred orientation with 55 percent of the 33 measured veins dipping from 50-65° (Fig. 31). XRD analyses indicate that dolomite is generally more abundant than magnesite and calcite. At least three different stages of carbonate veining and associated alteration observed in thin sections may reflect a temporal change in carbonate mineralogy. Cross-cutting relations indicate that some carbonate veins are younger than the talc and quartz veins.

Quartz veins

Quartz veining is common in the northern serpentinite, but it is uncommon to rare in the southern serpentinite. Dips of 26 quartz veins in six drill holes do not show any preferred orientation. Dips of 5 quartz veins in the northern serpentinite range from 60 to 90°, but this represents too small a sample size to characterize the population. The quartz veins range from small, simple veins, 1-3 mm wide, to large, composite veins, up to 15 cm wide. Cross-cutting relationships, grain size variations, degree of crystallinity, and alteration envelopes suggest a complex period of fracturing and veining; at least 10 distinct episodes of vein filling have been observed.

Multilithic breccia

The multilithic breccia strikes N39°W (based on a 3-point solution on the base of the multilithic breccia in drill holes) and this is essentially parallel to a major group of stream lineaments that strike N30-45°W and to a fracture system that strikes N40°W (Howell and Pirkle, 1976).

The occurrence of the breccia principally along the upper edge of the serpentinite and the mixture of lithologies within the breccia suggests a tectonic origin. The breccia may mark a thrust contact between the serpentinite and the overlying Kiokee metamorphic rocks. The lack of breccia or fracturing in DDH 88-2 suggests that the thrust may extend to greater depths than those drilled.

The presence of multilithic breccia around the base of the serpentinite at Burks Mountain suggests that the northern serpentinite may be underlain by multilithic breccia. The sharp boundaries of the ground magnetic anomaly of that serpentinite (Fig. 10) indicates that the northern serpentinite does not dip beneath the surface between Burks Mountain and the southern serpentinite. These observations suggest that the multilithic breccia may represent a low-angle, brittle deformation zone which broke up a once continuous serpentinite mass into two units moving the upper serpentinite to the north relative to the lower serpentinite.

The absence of this multilithic breccia along the basal contact of the southern serpentinite suggests that the multilithic breccia is not related to emplacement of the Burks Mountain serpentinites. The multilithic breccia was apparently formed after emplacement and appears to represent a low-angle, brittle deformation event which resulted in a relatively minor displacement of approximately several hundred meters.

"Dry" brittle fracturing

Brecciated drill core not accompanied by alteration or mineralization is referred here as brittle fracturing. It is commonly observed in and adjacent to the southern serpentinite and in the northern serpentinite. Measurable fracture surfaces are rare to absent. This fracturing must be younger than all the other brittle deformation, because there is no associated alteration or mineralization and it affects all other brittle features. Long intervals of fractured core suggest that this fracturing is more extensive than surface geologic mapping indicates. Topographic expression of this fracturing may occur as lineament trends as discussed below.

Faults depicted on the geologic map (Fig. 3) and in sections A-A' (Fig. 21) and B-B' (Fig. 20) are interpreted principally from ground magnetic anomalies (Fig. 10) and from abrupt truncation of mapped geologic units. The dry brittle fracturing may be related to development of these inferred faults.

C = Carbonate   Ch = Chlorite   Q = Quartz   T = Talc
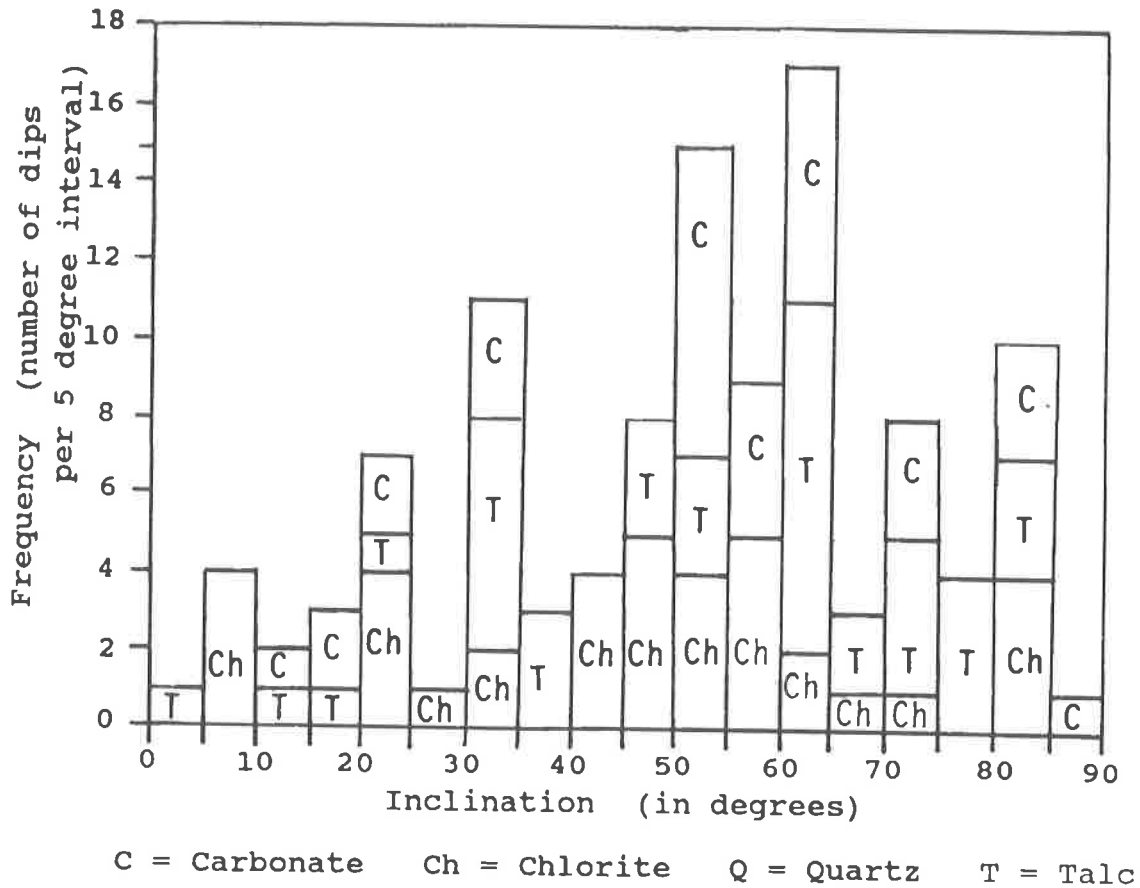
Figure 31. Histogram of dips of talc, carbonate, and chlorite veins and fracture fillings (core). Angles of veins measured relative to core axis were recalculated to dips from horizontal. The strongest concentrations of dips of talc veins is from 60-65°. Chlorite fractures tend to dip from 40-60°. The strongest concentration of carbonate veins dip from 50-65°. The number of each type is 41 talc, 34 carbonate, and 37 chlorite structures. The strongest overall concentration is from 50-65°.

Summary of fracture and vein distribution

The composite distribution of dips measured from 137 veins of carbonate, chlorite, and talc shows a crude bell-shaped distribution with 35 percent of the veins forming an apex in the 50 to 65° range (Fig. 31). The composite distribution of orientations of brittle structures (dikes, faults, veins and abrupt breaks in magnetic anomalies) show concentrations between N25-70°W, N25-40°E and N60-75°E (Fig. 32).

Development of fractures, veins and breccias in the serpentinite with various vein, fracture and breccia fillings and alteration envelopes indicates a prolonged period or several periods of brittle fracturing. Brittle fracturing occurred after serpentinization was completed. This fracturing was accompanied by an influx of "metamorphic/hydrothermal" solutions which altered serpentinite adjacent to the fractures and deposited various minerals in the fractures. Lizardite formation is a volume-for-volume replacement and does not involve expansion of the ultramafite. Also, if the fractures were present at the time of formation of the lizardite, chrysotile would have formed in those fractures. Because no chrysotile is developed, fracturing had to occur after serpentinization.

Geologic relations indicate the following sequence of brittle deformation:

1) mylonitization during the waning stages of the Alleghanian orogen;

2) brittle fracturing and brecciation of the serpentinite with development of talc and carbonate along fractures and rimming breccia clasts; talc occurs with chlorite within the fractures;

3) multistage fracturing occurring with introduction of silica- probably at a lower temperature;

4) multistage fracturing accompanied by carbonate veining;

5) faulting and fracturing with little or no associated veining or alteration.

Topographic lineaments

In northern Columbia County, structural control of topography is not pronounced due a low to moderate topographic relief and deep weathering of the bedrock. No significant ridges are present except for Burks Mountain.

Because streams commonly are controlled by geology, their orientations were measured and plotted to determine whether patterns of structural controls are evident. A total of 370 streams and creeks, in addition to the Savannah River, provide a large database for topographic lineament analysis. Stream orientations were measured in a 30,000 foot x 60,000 foot area centered on the project area. This area is elongate east-west subparallel to regional strike. The size of the area was constrained to the north by the presence of Clark Hill Lake and to the east and west by large granitic intrusions. In an area of such low relief, the orientations of some of the streams may be controlled by bedrock factors such as lithology or fractures.

A visual inspection of stream orientation distributions (Fig. 33) suggests that 30 percent of the population is background (2 to 8 streams per 5° interval). An additional 30 percent appear to be erratically distributed and could be regarded as statistically random clusters. A major cluster, containing 30 percent of the streams, strikes from N25-55°W with the greatest concentration, up to 22 streams per 5° interval, between N35-50°W. The major populations of brittle structures (Fig. 32) and stream lineations (Fig. 33) are roughly coincident suggesting a possible influence of these structures on stream lineations. Small vertical faults, striking at about N40°W and N20°E, are common and cross-cut the cataclastic textures of the Modoc fault zone approximately parallel to the Belair fault (Howell and Pirkle, 1976). It suggests the N40°W faults are controlling stream orientations in this portion of the Kiokee belt. There is no clustering of stream orientations in the N20°E direction. Isolated and unexplained orientations of stream segments are seen at N0-5°W, N40-45°E, and N80-85°E (Fig. 33).

METAMORPHISM AND ALTERATION

FELSIC AND MAFIC ROCKS OF THE KIOKEE BELT

The Kiokee belt consists of metamorphosed igneous and sedimentary rocks with a minor component of syn- or post-metamorphic felsic intrusions. Alleghanian-age, upper amphibolite facies regional metamorphism is predominantly prograde with a minor retrograde overprint. Metamorphic assemblages observed in the present study developed mainly subsequent to penetrative, ductile deformation and prior to development of cataclastic textures.

In the immediate vicinity of the Burks Mountain complex, metamorphic assemblages include:

1) quartz-microcline-plagioclase (oligoclase-andesine)-biotite-muscovite-(epidote) (McLemore, 1965)

2) hornblende-plagioclase(andesine)-almandine-epidote-(quartz-biotite) (McLemore, 1965)
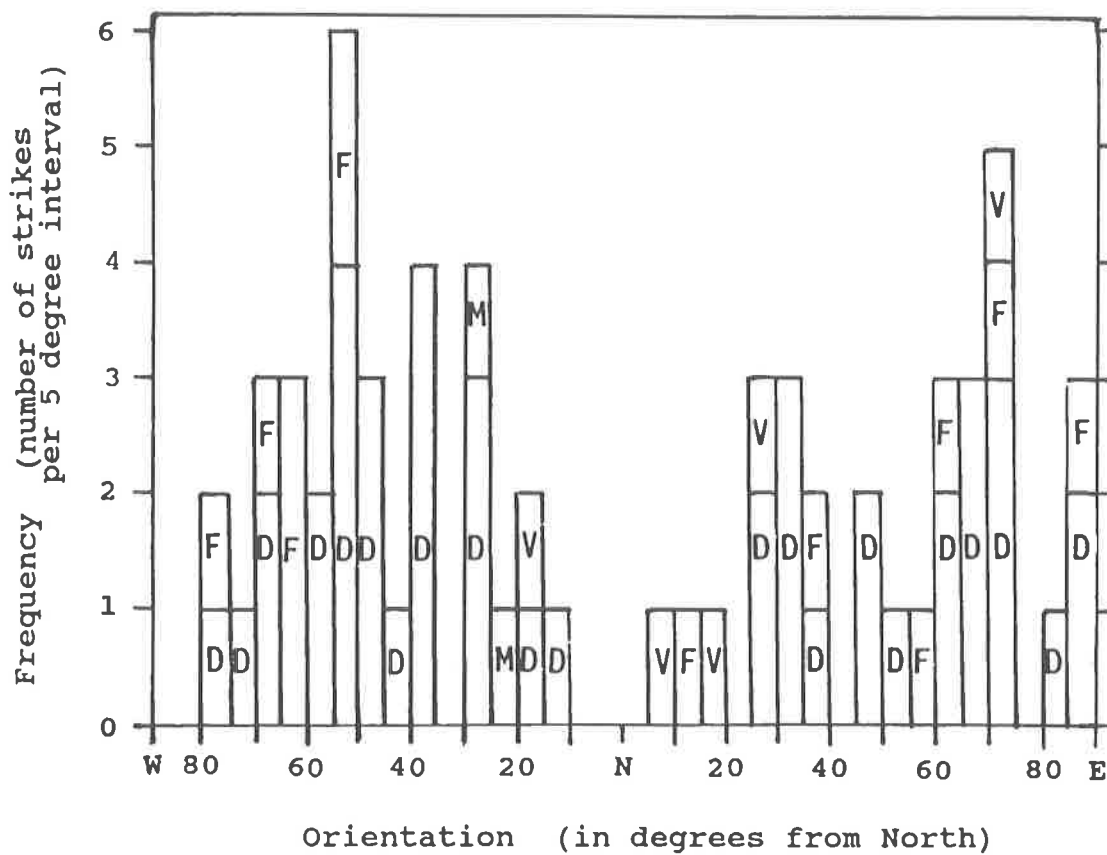
D = Dikes   F = Faults   V = Veins   M = Magnetic data

Figure 32. Histogram of surface brittle structure orientations. Structures are concentrated from N25-70°W, N25-40°E and N60-75°E. The northwest trend overlaps the stream orientation trend in Fig. 33. Orientations are from unpublished field data (Cocker, 1989a) and abrupt breaks in magnetic anomalies from the ground magnetic survey (Fig 10). Total number of orientations is 63.
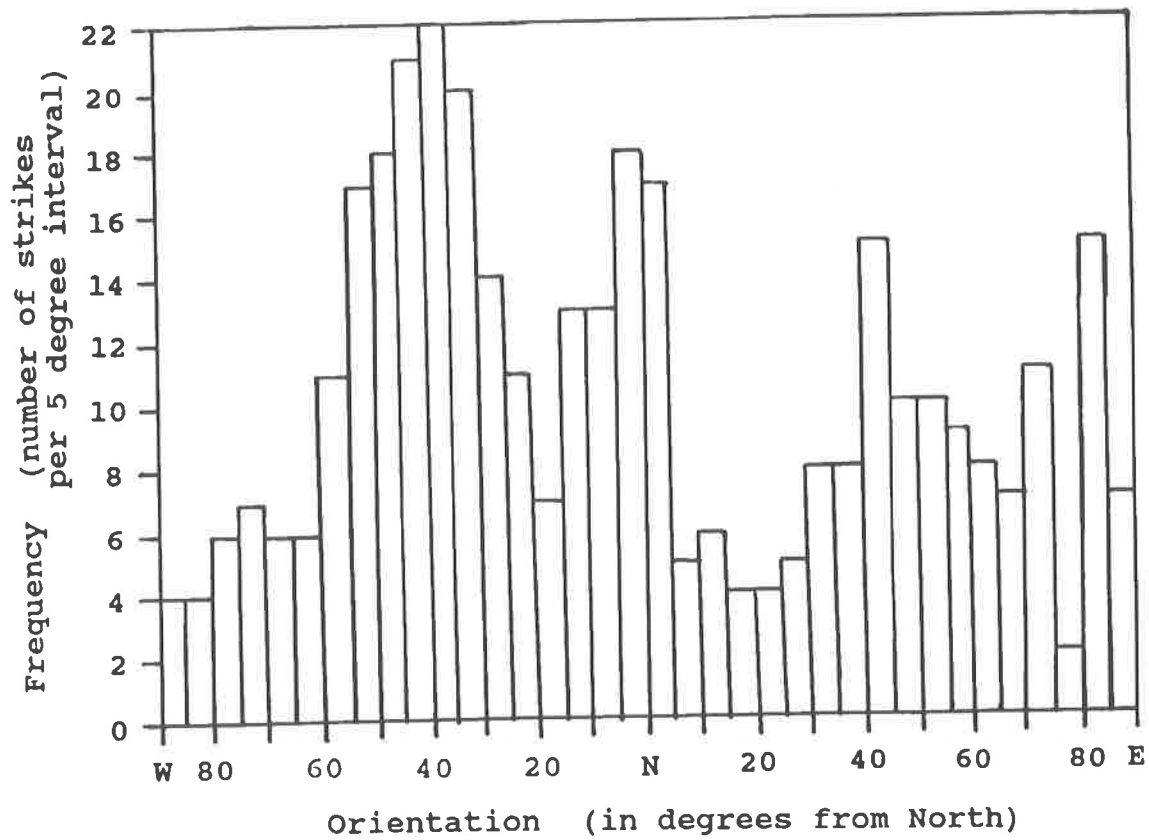
Figure 33. Histogram of stream orientations. Orientations were compiled from all stream segments (total = 371) at least 1000 feet long within an area 30,000 feet east to west and 10,000 feet north to south centered on the project area (Cocker, 1991b). The concentration of orientations from N25°W to N55°W may be influenced by N25°W to N40°W brittle fractures.

3) hornblende-plagioclase (oligoclase)-epidote-(quartz-biotite) (McLemore, 1965)
4) biotite-almandine-hornblende-plagioclase (Howell and Pirkle, 1976).
5) hornblende-plagioclase (oligoclase-andesine)-biotite-ilmenite-titanite (this study)
6) hornblende-plagioclase (oligoclase-andesine)-epidote-magnetite-olivine (this study)
7) biotite-quartz-plagioclase (oligoclase)-ortho-clase-titanite (this study)
8) biotite-quartz-plagioclase (oligoclase)-micro-cline-hornblende-titanite-muscovite (minor) (this study)

The high-grade metamorphism is recorded as muscovite + sillimanite-bearing schists and gneisses and migmatitic gneisses (Maher, 1978, 1987; Secor and others, 1986a, Dallmeyer and others, 1986, Secor and others, 1986b, Secor, 1987; Sacks and others, 1989). The presence of sillimanite schist and gneiss adjacent to some felsic intrusions (McLemore, 1965; Hurst and others, 1966) suggest local heating above the kyanite-staurolite subfacies of the amphibolite facies (McLemore, 1965, and Howell and Pirkle, 1976). More detailed studies are required to determine the overall metamorphic grade and the potential for metamorphic zonation developed during Alleghanian (or older) metamorphism in the Kiokee belt rocks.

The presence of blue-green hornblende, Na-rich plagioclase (An_{14-24}) and epidote in Kiokee belt rocks (this study and Sacks and others, 1989) indicate at least locally developed retrograde metamorphism to the epidote-amphibolite facies (McLemore, 1965). Retrograde metamorphism could result from release of fluids during thrusting of the Kiokee belt rocks onto the North American craton as discussed earlier. A younger, lower-grade metamorphism is suggested by the presence of zeolites in fractures (McLemore, 1965).

ULTRAMAFIC ROCKS

Prograde Metamorphism

Most of the ultramafites belonging to the Burks Mountain complex in Georgia are serpentinized or are altered from a serpentinite. The serpentinization generally conceals the original character of the ultramafic protolith and older metamorphic assemblages. Relicts of prograde metamorphic assemblages in the form of textures and mineral phases provide a picture of events preceding serpentinization. Serpentinization occurred after peak Alleghanian metamorphism. Textural and mineralogical criteria favor retrograde serpentinization in a static environment. Several episodes of serpentinite alteration and fracturing added further complexities to the metamorphic development (Cocker, 1989a).

Evidence of a prograde metamorphic assemblage earlier than the serpentinite is preserved in the form of: 1) earlier metamorphic minerals, 2) pseudomorphs of these minerals, and 3) reactant phases. Sprays of acicular tremolite (Fig. 34) and anthophyllite (up to 5 mm in length) are cut and partially pseudomorphed by lizardite indicating that these amphiboles were formed prior to serpentinization. Elongate, prismatic talc pseudomorphs cross cut and are superimposed on the primary igneous layering (Fig. 35); they are interpreted to be retrograde replacements of porphyroblastic enstatite. Pitted, embayed and corroded, coarse-grained magnetite enclosed in chlorite (Fig. 12 and 13) is interpreted to be the product of a prograde reaction between magmatic chromite/spinel and adjacent serpentine or olivine. Patchy, disseminated talc (Fig. 36) in serpentine is distinct from fracture-related talc (Fig. 24, 25 and 26) and may be a prograde (or retrograde) metamorphic remnant; textural relations with lizardite are inconclusive regarding this relationship.

Lizardite pseudomorphs after primary (?) olivine and pyroxene (Sacks and others, 1989; this study) indicate that olivine and pyroxene were stable phases prior to serpentinization (Fig. 14). The formation of enstatite porphyroblasts (noted above) that cross cut the primary igneous layering and mineralogy indicates that temperature and pressure conditions were sufficiently favorable for local recrystallization of enstatite. This evidence suggests that olivine and enstatite were stable up to and including conditions favorable for the partial recrystallization of enstatite. An assemblage containing olivine - enstatite - tremolite - chlorite - magnetite (spinel group) is approximately equivalent to the sillimanite-muscovite facies (upper amphibolite facies in Table 1). Anthophyllite, a Ca-poor amphibole, is present (this study) in samples from the eastern end of the Burks Mountain complex near the Savannah River.

Kyanite to sillimanite facies prograde metamorphism should have caused the re-equilibration of the ultramafic assemblage existing prior to this metamorphism and formed a high-grade assemblage that would have included olivine + tremolite, +/- talc, +/- enstatite, +/- Ca-poor amphibole, +/- spinel. Olivine, pyroxene, tremolite and anthophyllite are preserved as pseudomorphs and unaltered porphyroblasts (Fig. 14, 19, 34 and 35). Lack of preserved antigorite or chrysotile textures in the serpentinites suggests that these minerals did not develop, or that they reacted completely at a higher grade during progressive metamorphism to form olivine + tremolite + additional phases. Because antigorite is non-pseudomorphic, its development would have obliterated igneous textures. The preser-
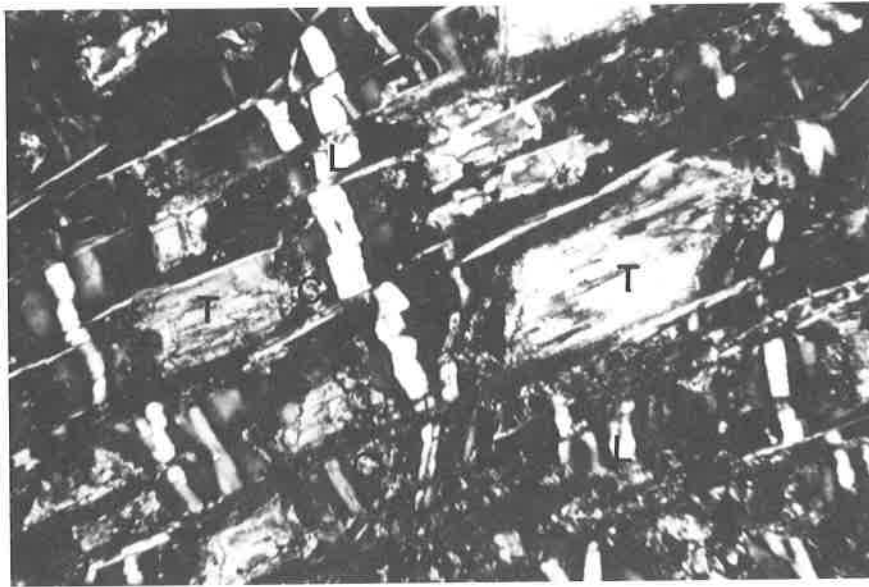
Figure 34. Photomicrograph of acicular tremolite partially replaced by lizardite and calcite. Minerals are tremolite (T), lizardite (L), and calcite (C). Sample is from DDH 87-1, 78 feet. Width of field of view is 1.13 mm.

Figure 35. Talc pseudomorphs after enstatite porphyroblasts. Note porphyroblasts crosscut millimeter scale layering. Sample is from west end of Burks Mountain. Scale is 10 cm.
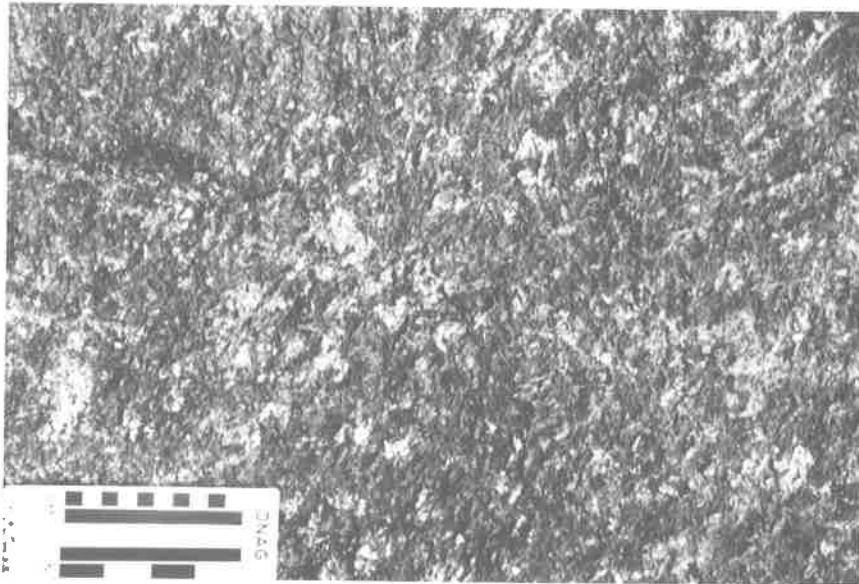
Figure 36. Disseminated patchy talc in serpentinite. Lighter areas are talc. Remainder of rock is weathered serpentinite. View is along Old Petersburg Road at 95 feet south of north end of roadcut (Fig. 22). Scale is 10 cm (4 inches).

vation of these textures indicates that antigorite did not develop. The lack of antigorite suggests that water, which is necessary to form serpentine from an anhydrous phase such as olivine, was not available to the metaharzburgites during prograde metamorphism.

Metamorphism of primary spinel/chromite in alpine-type serpentinites commonly results in the formation of chlorite + ferritchromite +/- Cr-magnetite +/-magnetite (Golding and Bayliss, 1968; Onyeagocha, 1974; Springer, 1974; Bliss and MacLean, 1975; Frost, 1975; Evans and Frost, 1975; Pinsent and Hirst, 1977; Lipin, 1984). The corroded disseminated magnetite in the Burks Mountain serpentinite is remarkably similar to metamorphic chromite in dunites in the Blue Ridge of North Carolina (Lipin, 1984). The reaction to form magnetite in the Burks Mountain serpentinite is probably similar to the following:

chromite + olivine$_1$ + fluid = ferritchromite + olivine$_2$ + chlorite.   During prograde metamorphism, primary spinel is progressively oxidized from the rim to the core to form ferritchromite and magnetite through the substitution of Fe^{+3} for Al, and Fe^{+2} for Mg. Increasing metamorphic grade causes further oxidation with additional replacement of Cr by Fe^{+3} pushing the spinel composition towards that of magnetite (Bliss and McLean, 1975; Pinsent and Hirst, 1977; Lipin, 1984). Primary spinels with a high Al content have a lower stability than high Cr-spinels and are oxidized at lower metamorphic grades than Cr-rich spinels (Pinsent and Hirst, 1977).

The average composition of the Burks Mountain spinels are estimated from whole-rock analyses by assuming the following: 1) spinel is the only phase in this ultramafic rock accommodating appreciable amounts of Cr and Fe^{+3}; 2) the Cr/Fe^{+3} ratio is controlled primarily by the content of Cr and Fe^{+3} (and hence the fugacity of O_2) in the rock; 3) a secondary control is exerted by the modal amounts of serpentine minerals and chlorite which can accommodate modest amounts of Cr and small amounts of Fe^{+3} and by the modal amounts of talc which is virtually free of these elements. Increase in the Cr/Fe^{+3} ratio with increasing grade is interpreted as due to an increase in modal amounts of phases that cannot accommodate Cr. The Al_2O_3 content of spinel is controlled by the coexistence of chlorite, spinel and two magnesium silicates at given P, T and H_2O fugacity. In the Burks Mountain serpentinites, only one magnesium silicate, lizardite, can accommodate appreciable amounts of Al.

Lacking direct analyses of the phases involved, an admittedly indirect and somewhat tenuous path may be used to arrive at an estimate of the original spinel compositions. If one assumes that all the Cr, Al and Fe^{+3} in the ultramafic rock occurs in spinels plus chlorite altering from the spinels and that no Cr, Al and Fe^{+3} has been added to or removed from the rock during metamorphism, the original composition of the spinel can be estimated on a Cr-Al-Fe^{+3} triangular diagram (Fig. 37). Most samples of "fresh" and silicified serpentinite plot in a small area above 86 percent Fe^{+3}, below 6 percent Al and 9 percent Cr. Serpentinite altered to talc contains more Al (approximately 8 percent). The Fe^{+3}:Cr:Al ratios of serpentinite include Fe^{+3} in secondary magnetite as a product of serpentinization. If these ratios are compared with those in talc where the secondary magnetite is absent, there is only a difference of approximately 5 percent less Fe^{+3}.

Evans and Frost (1975) suggest that spinel compositions in metamorphosed ultramafic rocks show a progressive change with increasing progressive metamorphic grade from Fe^{+3}-rich to more Cr-rich with a sharp increase in Al content in upper amphibolite facies rocks. Their study focusses on the non-reacting or more stable spinels instead of the reactant spinels (zoned spinels). The shift in composition reflects only the compositions of the progressively more stable spinels noted in other metamorphosed serpentinites (Bliss and McLean, 1975; Pinsent and Hirst, 1977; Lipin, 1984). The sharp increase in Al-content of spinels during upper amphibolite metamorphism is due to the formation of metamorphic spinels (Frost, 1975).

Chlorite is an ubiquitous phase adjacent to the corroded magnetite except where the chlorite is replaced by younger alteration phases (carbonate and talc). The anomalous birefringence of this chlorite is zoned from brown to medium blue distal to the magnetite. The ratio $(Fe^{total}+Mn+Cr)/(Fe^{total}+Mn+Cr+Mg)$ estimated from the birefringence (Laird, 1988) indicates the chlorite is zoned from Mg-poor to Mg-rich with increasing distance from the magnetite. The chlorite is a reaction product reflecting an Fe and Al contribution from the spinel, and a Mg and SiO_2 contribution from olivine/serpentine. Chlorite adjacent to magnetites in the Burks Mountain serpentinites suggests that the original spinels were Al-rich. Studies by Golding and Bayliss (1968) note that chlorite developed only where the affected chromite is Al-rich, and chlorite is absent where the chromite is Cr-rich. Also, with increasing grade of metamorphism, the Al-content of chlorites increases as a result of the increasing oxidation of spinel and release of Al to form the chlorite (Frost, 1975; Pinsent and Hirst, 1977).

Serpentinization

Based on preserved textures and geochemistry,
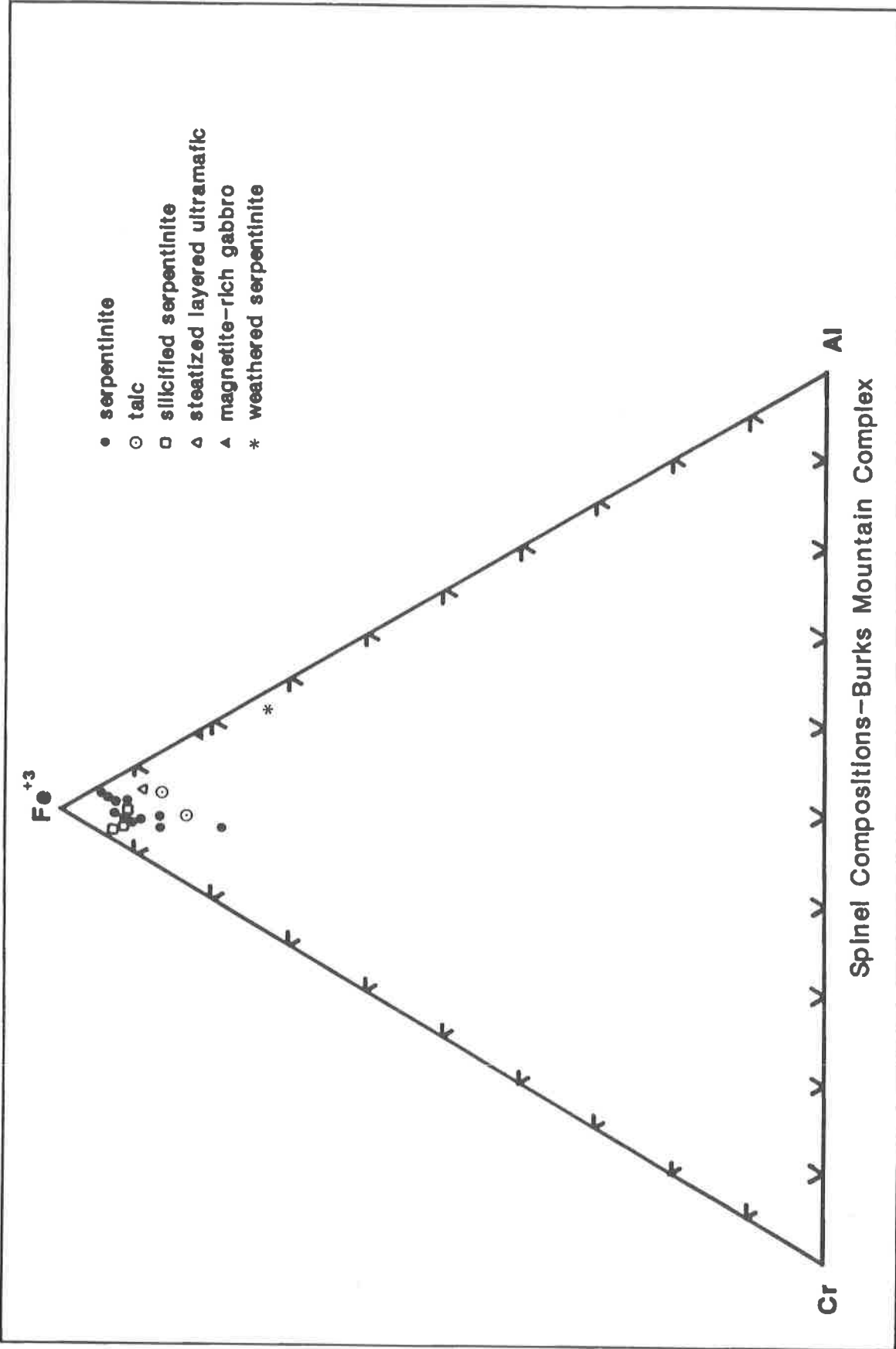
Figure 37. Cr-Al-Fe^{+3} Diagram. Analyses cluster near the high Fe^{+3} corner.

Al

Fe^{+3}

Cr

Spinel Compositions–Burks Mountain Complex

- serpentinite
- talc
- silicified serpentinite
- steatized layered ultramafic
- magnetite–rich gabbro
- weathered serpentinite

44

Table 1.

Typical prograde metamorphic assemblages of serpentinites (modified from Evans and Frost, 1975).

Metamorphic Assemblages	Metamorphic Facies	
chrysotile/lizardite + brucite + diopside	Prehnite-pumpellyite	
antigorite + brucite + diopside	Greenschist	(lower)
antigorite + olivine + diopside		(upper)
antigorite + olivine + tremolite	Amphibolite	(lower)
talc + olivine + tremolite		
Ca-poor amphibole + olivine + tremolite		(to)
enstatite + olivine + tremolite		
enstatite + olivine + tremolite + spinel	Amphibolite	(upper)
enstatite + olivine + diopside + spinel	Granulite	

the typical Burks Mountain complex serpentinite is inferred to have formed from a harzburgite (Cocker, 1989a and 1989b). Mesh-textured lizardite is pseudomorphic after olivine, orthopyroxene (bastite) (Sacks and others, 1989; this study), anthophyllite, and tremolite and is the only serpentine mineral identified in thin-sections or in XRD analyses of core samples. In silicified serpentinites, quartz forms mesh-texture pseudomorphs (outlined by secondary magnetite) which are identical to those in unaltered lizardite. Olivine and orthopyroxene pseudomorphs, which are preserved as quartz and talc, may be remnants of primary igneous olivines and pyroxenes or metamorphic recrystallization products of igneous olivines and pyroxenes. The presence of olivine and orthopyroxene pseudomorphs, the whole-rock chemistry, and the differentiation trends exhibited by their normative vertical distribution strongly suggests that olivine and orthopyroxene were the primary constituents of the original rock.

Serpentinization of Fe-bearing olivine or pyroxene releases iron to form magnetite. This fine-grained magnetite is concentrated during development of a mesh-texture pseudomorphic after the original olivine or pyroxene creating an outline of the mesh-texture (Fig. 11 and 14). This magnetite pattern is preserved in silicified serpentinites but is destroyed in steatized serpentinite (Fig. 38). A decrease in modal magnetite with increasing talc (Fig. 39) and the absence of fine-grained magnetite in talc that has replaced lizardite implies dissolution of the fine-grained magnetite during steatization. The larger magnetite (or ferritchromite) masses show no sign of dissolution perhaps due to compositional differences or reaction thermodynamics.

Previous studies described the Burks Mountain serpentinite as consisting of antigorite with thin veinlets of chrysotile (McLemore, 1965). Antigorite generally is formed during prograde metamorphism and reflects the high temperatures attending the upper greenschist to lower amphibolite facies (Evans and Frost, 1975; Wicks and O'Hanley, 1988). Because formation of antigorite is non-pseudomorphic, its development would have destroyed the igneous textures observed in thin sections and hand samples. Lizardite is the only serpentine mineral observed in thin-sections and identified by XRD (Cocker, 1989a; Sacks and others, 1989). Lower temperatures for the formation and preservation of lizardite (Wicks and O'Hanley, 1988), and the absence of antigorite suggest that serpentinization occurred substantially after peak metamorphism. Textural evidence (pseudomorphic mesh-textures) indicates that this occurred in a static environment.

Serpentinization in a static environment differs significantly from that in a dynamic environment. A static environment is characterized by the lack of a penetrative fabric in the hand sample or thin-section, and is inferred for the isotropic, grid-like framework of fractures that surround olivine and pyroxene fragments in partially serpentinized ultramafic rocks (Wicks and O'Hanley, 1988). These fractures establish sites for the initial lizardite alteration that eventually forms pseudomorphic textures. The pseudomorphic process preserves the outlines of the original grains, textures, fracture patterns and cleavages of the parent minerals. This geometry is compatible with a water-diffusion controlled process (MacDonald, 1984). A dynamic environment is characterized by a penetrative fabric (Wicks and O'Hanley, 1988).

Although Sacks and others (1989) describe apparently foliated chromite from the Burks Mountain complex, this investigation did not find any indication of a penetrative fabric in outcrop, drill core, or thin-section. One sample collected by Vincent and others (1990) is penetratively deformed but this is probably localized. A penetrative fabric (Sacks and others, 1989) should have destroyed the lizardite mesh-texture. Also, the high-grade, progressive metamorphism accompanying the deformation should have recrystallized the lizardite into antigorite. The lack of a penetrative fabric, the presence of lizardite instead of antigorite, the preservation of lizardite mesh-texture, the preservation of acicular amphiboles (tremolite and anthophyllite), and the preservation of mineralogical layering, strongly indicate no widespread penetrative deformation. Penetrative deformation may have occurred locally during a post-serpentinization adjustment event.

ALTERATION OF SERPENTINITE

Movement of fluids and elements between the country rock, generally gneisses and amphibolites, and the serpentinite caused the development of extensive alteration of the serpentinite and subtle alteration of the country rock. Locally, the serpentinites are pervasively altered to talc, chlorite, carbonate, and quartz. Silicification preserved the lizardite mesh-texture, whereas the talc, chlorite and carbonate generally form non-pseudomorphic aggregates. Alteration of the country rocks involved chloritization, biotitization and perhaps albitization; TiO_2 appears to be remobilized to form titanite +/- ilmenite.

Although spatial and temporal overlap of alteration phases has obscured some textural and mineralogical relations, alteration zoning is present. The alteration zoning from unaltered serpentinite to unaltered
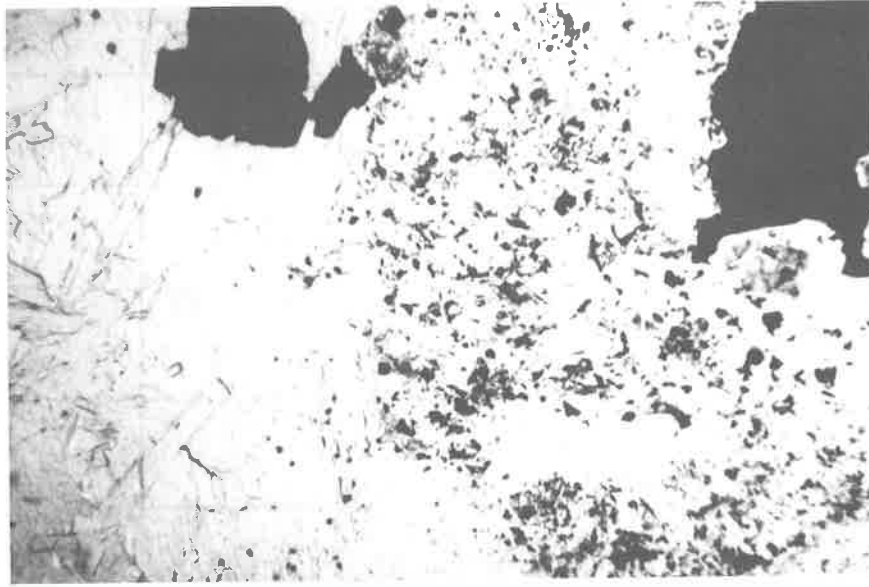
Figure 38. Photomicrograph of magnetite destruction in talc. Right half of picture is lizardite serpentinite plus fine-grained (black specs) magnetite derived from olivine and enstatite during serpentinization. Left half contains coarse-bladed talc that has replaced the lizardite and most of the secondary magnetite. Large black grains in upper center and upper right are magmatic spinels altered to Cr-magnetites during prograde metamorphism. The Cr-magnetite in the talc is not visibly affected by steatization. Sample is PC87-4-67. Width of field of view is 2.65 mm.
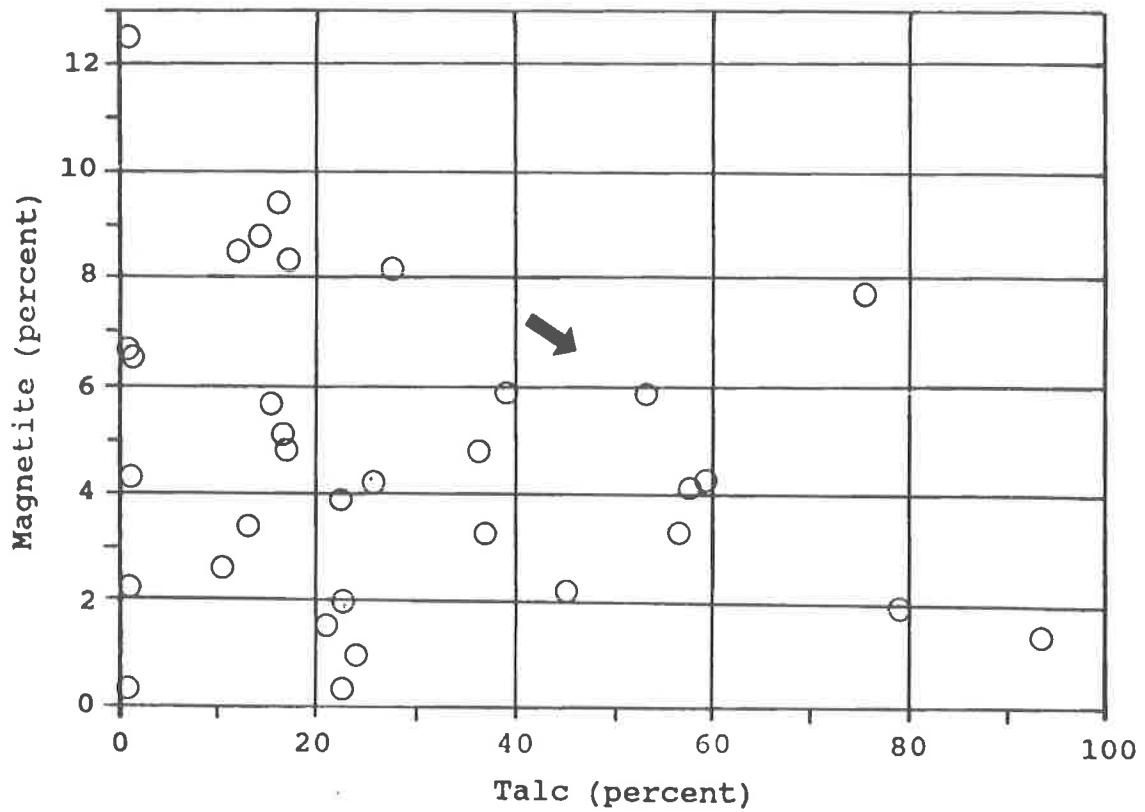
Figure 39. Modal magnetite - talc diagram. Diagram illustrates an overall decrease in total modal magnetite with increasing modal talc in serpentinite. The few percent magnetite in +60% talc is Cr-magnetite. The scatter in the abundance of magnetite may be attributed to the distribution of primary, magmatic Cr-magnetite.

country rock is: 1) "fresh" serpentinite containing disseminated patches of talc, carbonate and Type II chlorite (types of chlorite are discussed below); 2) thin zone of Type II chlorite; 3) talc + carbonate; 4) massive talc; 5) foliated talc; 6) Type III chlorite; 7) altered country rock; to 8) country rock. This zonation is similar to metasomatic alteration sequences commonly developed at ultramafic-country rock contacts: ultramafic assemblage/ talc + carbonate/ talc/ Ca-amphibole + chlorite/ chlorite/ transitional country rock/ country rock (Sanford, 1982).

Talc

Talc occurs: 1) as coarsely bladed, fibrous-appearing rinds, about 1 cm wide, along the edges of fissures and around the rims of ultramafic clasts in the multilithic breccias (Fig. 23, 24 and 26); 2) as a massive, fine-grained replacement of serpentinite adjacent to fractures in the serpentinite, in breccia zones, and in the margins of the serpentinite; and 3) as small, disseminated aggregates in massive serpentinite (Fig. 36). It generally replaces lizardite, enstatite, tremolite and anthophyllite. Lizardite (Fig. 40), tremolite and anthophyllite decrease with increasing talc content. Steatization also causes dissolution of fine-grained secondary magnetite which outlined the lizardite mesh texture (Fig. 38).

Carbonate

Magnesite, dolomite and calcite are texturally and temporally distinct from each other in the Burks Mountain serpentinites. Cross-cutting veins and replacement textures indicate that the carbonates are younger than lizardite, tremolite, and anthophyllite, but overlap with talc, quartz and chlorite. Carbonates are most abundant in rocks with low talc (<25 modal percent) and with 30-50 modal percent lizardite.

The most abundant carbonate is an early stage magnesite with a very fine- to medium-grained (<.01 - 0.1 mm) sugary texture. Magnesite commonly occurs replacing lizardite in the center of the mesh texture of the lizardite, as a patchy replacement of talc and chlorite, and in veinlets cutting talc and chlorite. Dolomite, the next most abundant carbonate, is coarser grained and occurs as euhedral grains or aggregates also in the center of the mesh texture. Dolomite also appears to replace fine-grained carbonate in veins and in the mesh texture. Calcite, the least abundant carbonate, occurs as clean, generally coarse grains rimming tremolite, replacing the centers of the lizardite mesh texture, and as younger veinlets cutting all other veinlets. The veinlets commonly consists of large elongate grains

with an unidentified opaque mineral locally in the center of the veinlet.

Chlorite

Chlorite developed in the Burks Mountain serpentinites in three distinct modes which are indicative of different paragenesis. These are referred to in this report as types I, II, and III. Type I chlorite, discussed earlier, developed as a reaction rim around spinel (Fig. 12 and 13) during progressive metamorphism. Type II chlorite is concentrated along the talc-serpentine contact and is disseminated in serpentinite and talc. Type III chlorite, which is the most conspicuous and abundant chlorite, occurs as coarse-grained flakes filling fractures and forming the matrix of the multilithic breccia (Fig. 24, 25 and 26). Type III chlorite (Fig. 5 and 9) is also commonly known as chlorite blackwall developed between serpentinite and country rock (Chidester, 1962). Type II and III chlorites are more Mg-rich (based on their birefringence) than the Type I chlorite.

Type II and III chlorite replaces talc and to a lesser extent lizardite, tremolite and anthophyllite. These chlorites generally occur as anomalous medium to dark blue birefringent blades elongate up to 3 mm in length and as radiating sprays localized in massive talc near and adjacent to the talc-lizardite contact. Type II chlorite also forms single, dark blue birefringent crystals disseminated in serpentinite, minor light blue-gray birefringent sprays and rosettes replacing lizardite and medium blue-gray birefringent veinlets cutting and replacing lizardite. Some type III chlorite is a coarse-grained (0.5-2 mm) gray chlorite, and it is replaced by light blue birefringent chlorite and possibly by dark blue to brown birefringent chlorite. Fine-grained, light blue birefringent chlorite occurs along fractures and cleavages in gray birefringent chlorite. In drill core and outcrop type III chlorite forms massive, coarse-grained, non-foliated, platy intergrowths in open structures. Type III chlorite consists of poorly bound coarse flakes which are very susceptible to weathering and washout by drilling fluids.

Silicification

Silicification and quartz veining are widespread in the northern Burks Mountain serpentinite, but are only locally developed in the southern serpentinite. Attempts to drill through the silicified and veined northern serpentinite to examine the distribution of silicification and veining with depth were unsuccessful because of loss of circulation and caving during drilling. The much greater abundance of silica in the
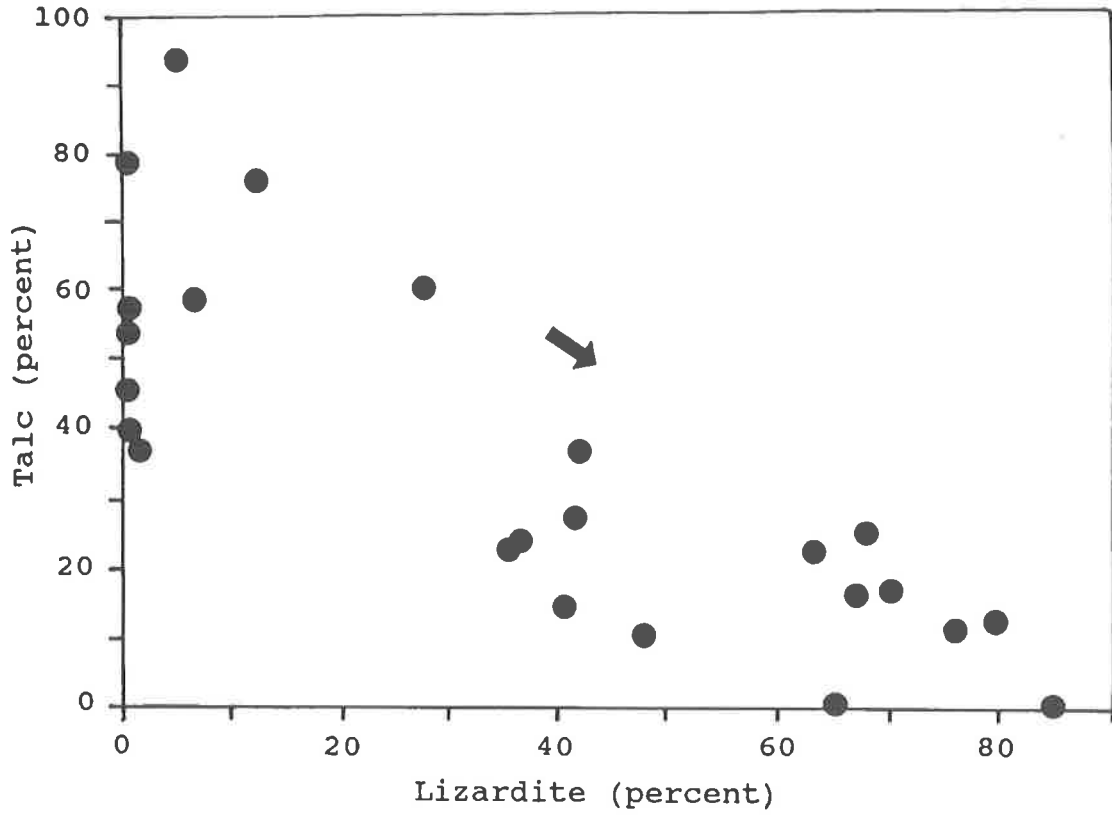
Figure 40. Modal talc-lizardite diagram. Diagram illustrates a strong negative correlation between talc and lizardite reflecting the replacement of lizardite by talc.

northern serpentinite and its virtual absence in the southern serpentinite is unexplained. Silicification was not observed in any country rocks from drill core, outcrop or float. Also, resistant ridges or hills which might indicate silicified country rock are not present.

Quartz veins cut across talc, chlorite, and serpentine, with quartz commonly replacing these minerals. The intensity of silicification is directly related to the density of quartz veining. The above relations suggest silicification and quartz veining are probably simultaneous and directly related. Veining is multistage based on the following observations: 1) quartz-veining consists of banded quartz veins; 2) quartz veins cross-cut other quartz veins; and 3) vein mineralogy changes from quartz to chalcedony to opal? in progressively younger veins. Crustiform vein quartz is common, indicating open-space filling.

The SiO_2 content increases dramatically from an average of about 40 weight percent in normal serpentinite to 80-90 weight percent in silicified serpentinite. No major volume changes are evident, for the modal magnetite and weight percent Fe_2O_3 are essentially the same in unsilicified and silicified rocks.

ALTERATION OF COUNTRY ROCKS

Secondary biotite

Secondary biotite (8 modal percent) occurs as numerous anastomosing veinlets cutting hornblende (Fig. 41), biotite, quartz and plagioclase and as irregular aggregates replacing plagioclase in an amphibolite (Fig. 42) 5 feet (1.5 m) below the lower serpentinite-gneiss contact (PC 1-175). Closer to the serpentinite the veinlets are composed of chlorite instead of biotite. The secondary biotite is similar to the pleochroic, yellowish-brown (resembling rust in thin-section) secondary biotite occurring as irregular branching patterns in country rock schist in many localities in New England (Chidester, 1962; Sanford, 1982) and Virginia (Burfoot, 1930).

The formation of secondary biotite begins with chloritization of biotite in the country rock immediately adjacent to the ultramafic body. Chloritization mobilizes potassium which diffuses further into the country rock. Biotite forms at the expense of calcic amphibole (hornblende (Fig. 41)) or plagioclase (Fig. 42) (Sanford, 1982; Chidester, 1962). At Newfane, Vermont, epidote replaces chlorite which, in turn, replaces biotite. Further out in the country rock, biotite, albite and minor chlorite replace hornblende. This may be the origin of biotite blackwall zones around many ultramafic bodies (Sanford, 1982).

Secondary albite

Extensive albitization of plagioclase occurs along fractures and commonly forms irregular masses to euhedral porphyroblasts within the plagioclase (Fig. 43). Albitization probably was initiated by chloritization of plagioclase. Chloritization mobilized Na_2O further into the country rock immediately adjacent to the chlorite zone. Albitization of plagioclase mobilized CaO, some of which may have formed secondary titanite. Albitization resulting from chloritization of plagioclase is a commonly reported phenomenon developed adjacent to Alpine-type serpentinites in the eastern United States (Chidester, 1962; Jahns, 1967).

Ti- bearing phases

Titanite is an abundant but minor phase occurring as individual grains and as overgrowths on Ti-oxides in gneisses and amphibolites adjacent to the serpentinite. Similar occurrences adjacent to New England ultramafics consist of: 1) ilmenite with overgrowths of leucoxene or of rutile and/or titanite; 2) rutile with overgrowths of titanite; and 3) ilmenite, rutile and titanite with no overgrowths (Chidester, 1962). A pronounced increase in Ti and titanite in the chlorite zone was recognized by Sanford (1982). The chloritization of biotite plus the chloritization and albitization of plagioclase probably mobilized the Ti and Ca necessary to form the secondary Ti-oxides and titanite. Metamorphosed chlorite blackwall at Paddy-Go-Easy Pass, WA contains spinel enclosing rutile suggesting a reaction of chlorite + ilmenite = olivine + spinel + rutile + water (Frost, 1975). Ilmenite replaces amphibole, and titanite rims ilmenite and replaces ilmenite, epidote and amphibole in association with talc deposits in Virginia (Burfoot, 1930). Recrystallized aggregates of anhedral titanite, commonly up to 2 mm in size, occur in hornblende schists and gneisses, amphibolites and hornblende gabbro associated with talc and asbestos deposits in Georgia (Hopkins, 1914).

PETROCHEMISTRY

Petrochemistry can be used to determine: the origin of a rock or a suite of rocks; igneous differentiation trends; the effects of metamorphism; and the effects of alteration. The data discussed in this section are presented in Appendices I-VI. Additionally, some ratios discussed in this section are derived from the data in those appendices.

FELSIC AND MAFIC ROCKS
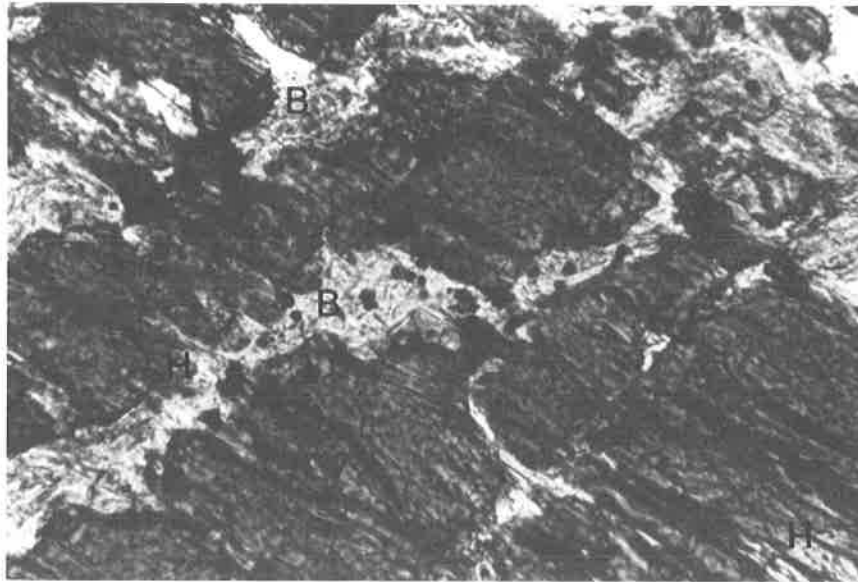
Figure 41. Photomicrograph of secondary biotite cutting and replacing hornblende. Minerals include hornblende (H) and biotite (B). Sample is from DDH 87-1, 175 feet. Width of field of view is 1.13 mm.
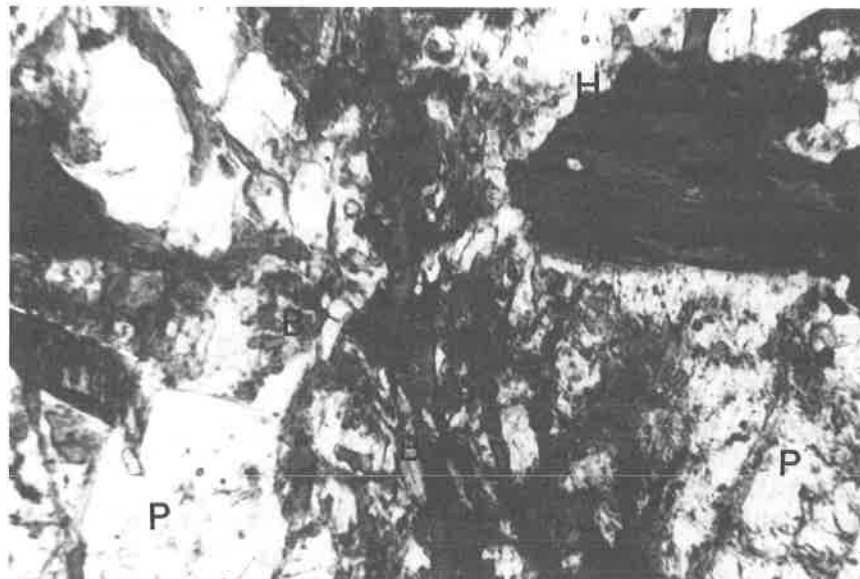
Figure 42. Photomicrograph of secondary biotite cutting and replacing plagioclase. Minerals include biotite (B), plagioclase (P), and hornblende (H). Sample is from DDH 87-1, 175 feet. Width of field of view is 1.13 mm.
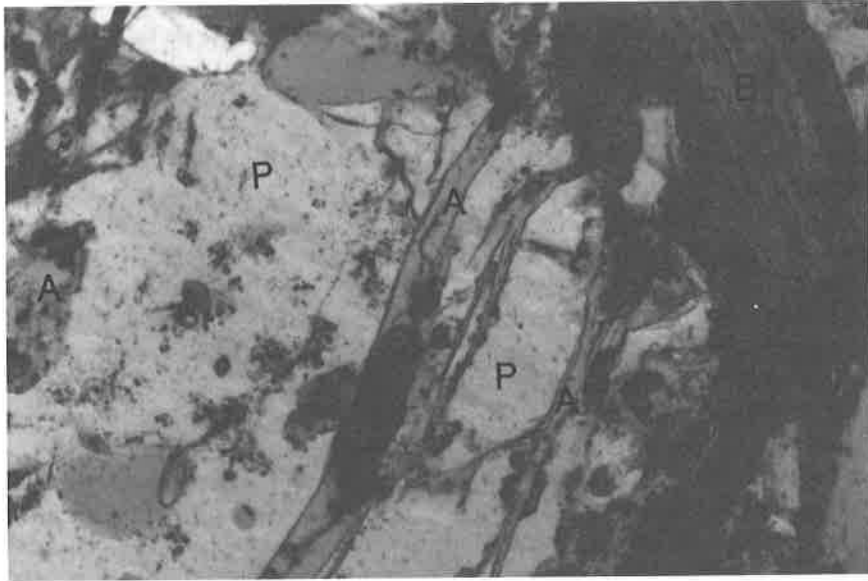
Figure 43. Photomicrograph of secondary albite. Albite (A) veinlet cuts plagioclase (P). Also apparent are patches of secondary albite replacing plagioclase. Other mineral is biotite (B). Sample is from DDH 87-1, 175 feet. Width of field of view is 1.13 mm.

Primary igneous or sedimentary textures are not preserved in the felsic and mafic rocks in the vicinity of the Burks Mountain complex. The nature of these rocks may be suggested by their petrochemistry. Studies of amphibolites indicate that variation trends can be used to distinguish between ortho- and para-amphibolites (Leake, 1964).

Trends in the Niggli values of igneous rocks differ from those trends caused by mixing pelitic and carbonate sedimentary rocks (Leake, 1964). Niggli values are: $mg = (MgO/(FeO + MnO + 2Fe_2O_3 + MgO))$, $c = (CaO)$, and $al\text{-}alk = (Al_2O_3 + Na_2O + K_2O)$ (Leake, 1964). Igneous rocks show a systematic decrease in mg with a subsequent increase in al-alk. On a triangular plot of mg, c and al-alk, the mixing line joining dolomite and typical pelite and semi-pelite is perpendicular to a typical basic igneous series trend. Mixtures of pelite and semi-pelite with limestone should plot in a different part of the diagram and should show a characteristic trend of their own. The mafic gneisses/amphibolites in the Burks Mountain area follow a normal igneous trend (Fig. 44) indicating that they may have igneous (including volcanic) protoliths. The felsic gneisses also plot along this trend suggesting that they may also have igneous (including volcanic) protoliths. The inclusion of several granitic rocks in these trends tends to support, but does not prove an igneous parentage for the felsic gneisses.

A $CaO\text{-}Na_2O\text{-}K_2O$ diagram (Fig. 45) shows several distinct clusters of rock analyses. Field A consists of very high-CaO metagabbros. Field B consists of high-CaO metabasalts. Field C is composed of granites and felsic gneisses with high Na_2O and K_2O.

The CaO and $Na_2O + K_2O$ contents of these rocks are about equal at 58 weight percent SiO_2 suggesting that they may be part of a calc-alkaline rock series (Peacock, 1931). On an AFM diagram (Fig. 46), the felsic gneisses and granites from the Burks Mountain area occur along a calc-alkaline enrichment trend. Mafic gneisses/amphibolites (metabasalts) from the Burks Mountain area lie on a tholeiitic Fe-enrichment trend.

On a normative $SiO_2\text{-}NaAlSi_3O_8\text{-}CaAl_2Si_2O_8$ (quartz-albite-anorthite) diagram the analyses define a trend intersecting at about 750°C (Fig. 47). This defines the minimum melting temperature at 5 kb pressure and is reasonable for generation of partial melting associated with migmatitization. This temperature is similar to the anticipated maximum temperature (700°C) proposed for peak metamorphism in this part of the Kiokee belt (see discussion on conditions of metamorphism).

The TiO_2 contents of the mafic rocks range from 1.1 to 1.3 weight percent, and appear to be greater than those indicative of a subduction-related environment (Feiss, 1982).

Rare earth element (REE) analyses of the amphibolites (Cocker, 1989c) show a slight enrichment in light REE suggesting an island-arc or continental margin origin.

The Kiokee belt rocks analyzed in this study are markedly different from the Little River Series rocks (Carolina Slate belt) analyzed by Whitney and others (1978). The Kiokee belt rocks display a variation in Al_2O_3 from <13 to >17 weight percent in mafic to felsic rocks while the Little River Series rocks show no variation. The Kiokee belt rocks analyzed in this study show a strong enrichment in K_2O; rocks with 70-75 weight percent SiO_2 contain 2.5 to 4.7 weight percent K_2O versus 0.5-1.5 weight percent in Little River Series rocks. Despite the limited number of analyses, a continuous trend in SiO_2 content (unimodal) appears to be present the Kiokee belt rocks.

The spatial association of abundant felsic rocks with the mafic rocks (metabasalts), the light REE enrichment, and the calc-alkaline trend suggest, but do not prove a continental margin environment (+/- a minor island arc component) for the Kiokee belt rocks in this area. Another, alternative explanation for the Kiokee belt rocks is the mixed environment intermediate between continental margins and island arcs (Rogers, 1982). This mixed environment has characteristics of both the continental margin and island arc setting and is believed to have developed over a crust intermediate, both in thickness and in composition, between continental and oceanic crust.

ULTRAMAFIC ROCKS

Magmatic trends

Concentrations of major and trace elements in the Burks Mountain serpentinites are generally related to their stratigraphic height in the serpentinite, which is the elevation above the lower serpentinite-country rock contact. Vertical chemical variation trends within the serpentinite are interpreted as: 1) metasomatic changes towards the edges of the serpentinite, and 2) vertical primary differentiation trends which have persisted despite metamorphism and metasomatism. Where present, pervasive silicification severely changed the whole-rock chemistry of the altered ultramafite on a broader scale apparently unrelated to present contacts.

Variations in the concentrations of SiO_2, MgO, MnO, Fe_2O_3, and CaO probably reflect primary igneous differentiation trends in the ultramafic body from

54
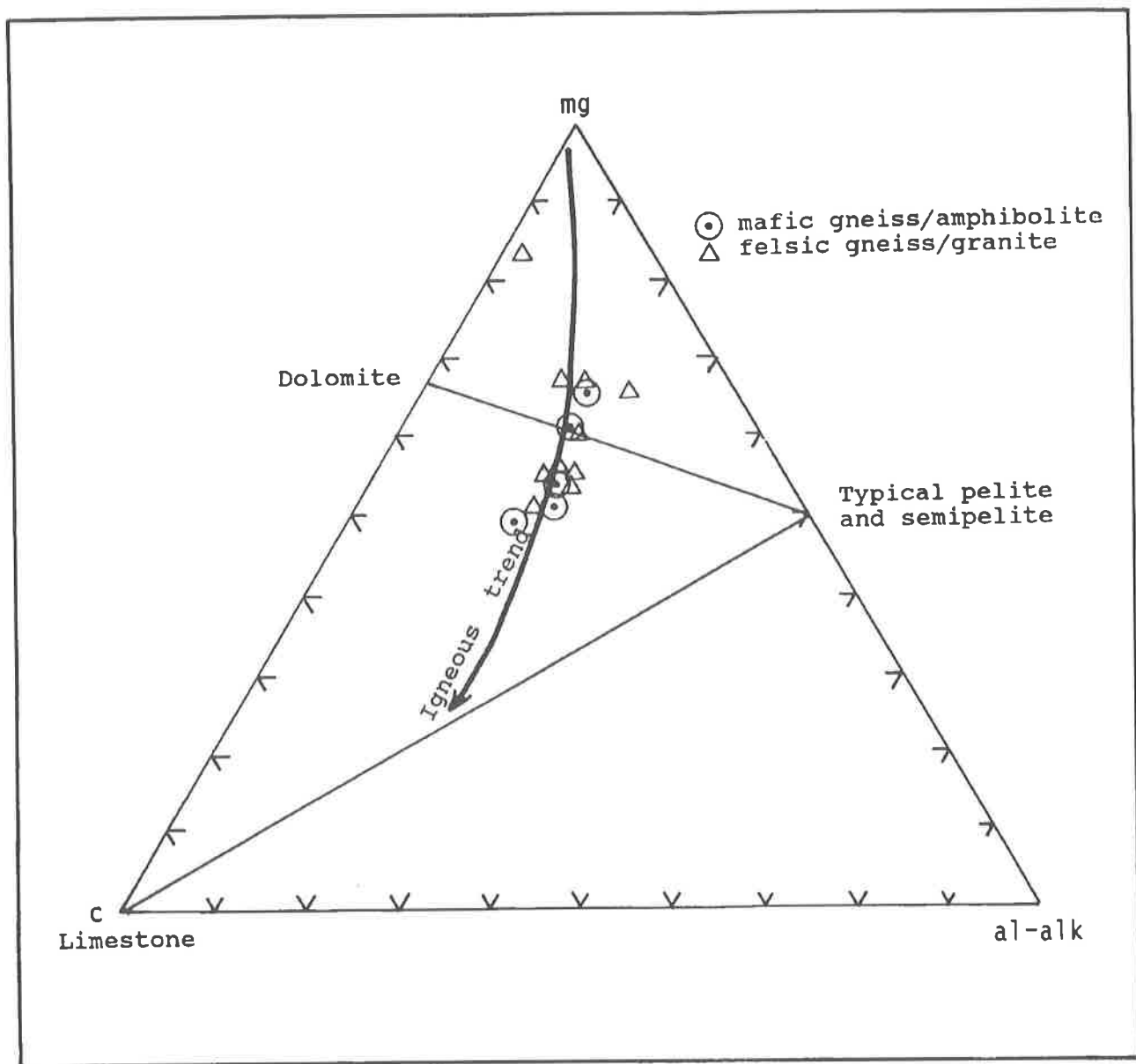
Figure 44. Niggli mg-c-(al-alk) triangular diagram. The mafic gneisses/amphibolites plot along the igneous rock trend and suggest these have igneous protoliths. The felsic gneisses and granites also plot along this trend and may suggest that they also have igneous protoliths. Calculation of c, mg, al-alk are explained in the text. Rock fields and the igneous rock trend are from Leake (1964).
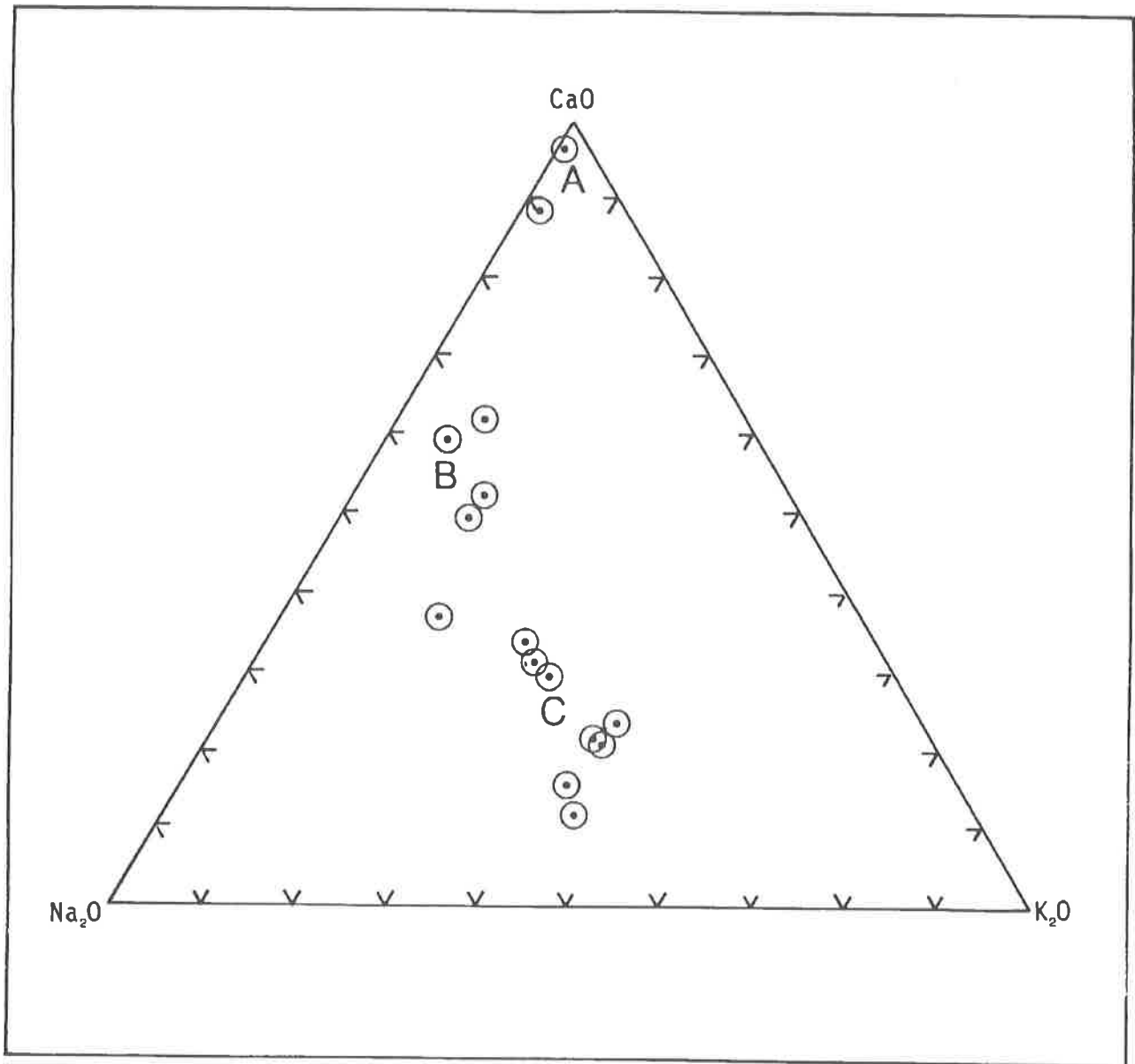
Figure 45. CaO-Na$_2$O-K$_2$O triangular diagram of felsic and mafic gneisses and granites. Analyses of felsic and mafic rocks included in the appendicies are shown as dots. Three fields are evident: A) a high CaO field corresponding to the metagabbros; B) an intermediate field containing mafic gneisses/amphibolites; and C) an Na$_2$O + K$_2$O field containing felsic gneisses and granites.
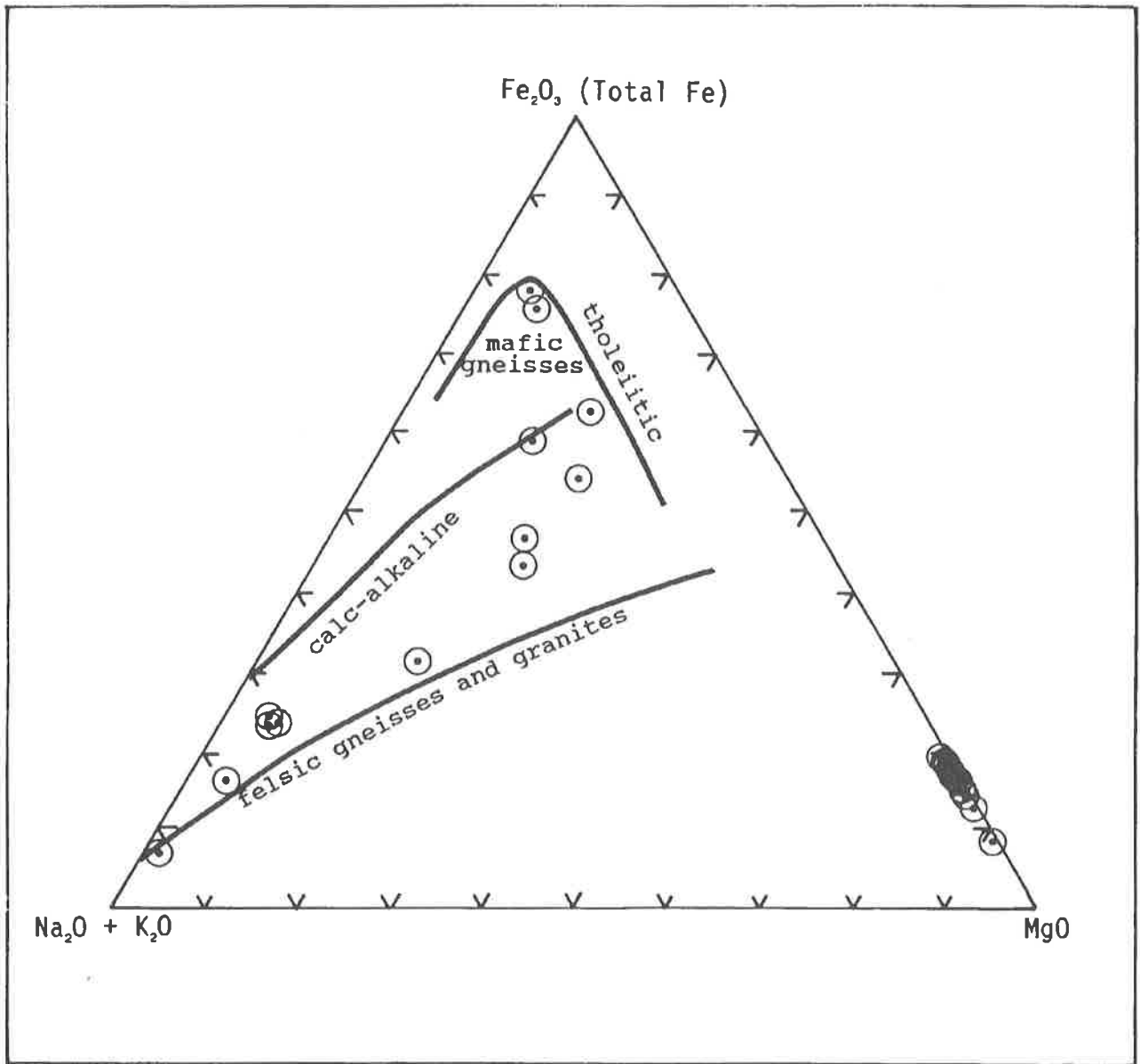
Figure 46. AFM triangular diagram of serpentinites, felsic and mafic gneisses and granites. Analyses of serpentinites, felsic and mafic rocks included in the appendicies are shown as dots. The felsic and mafic rocks follow two well-established trends: the mafic gneisses follow the tholeiitic Fe-enrichment trend; the felsic gneisses and granites follow the calc-alkaline trend. The serpentinites plot in the lower right corner (MgO).
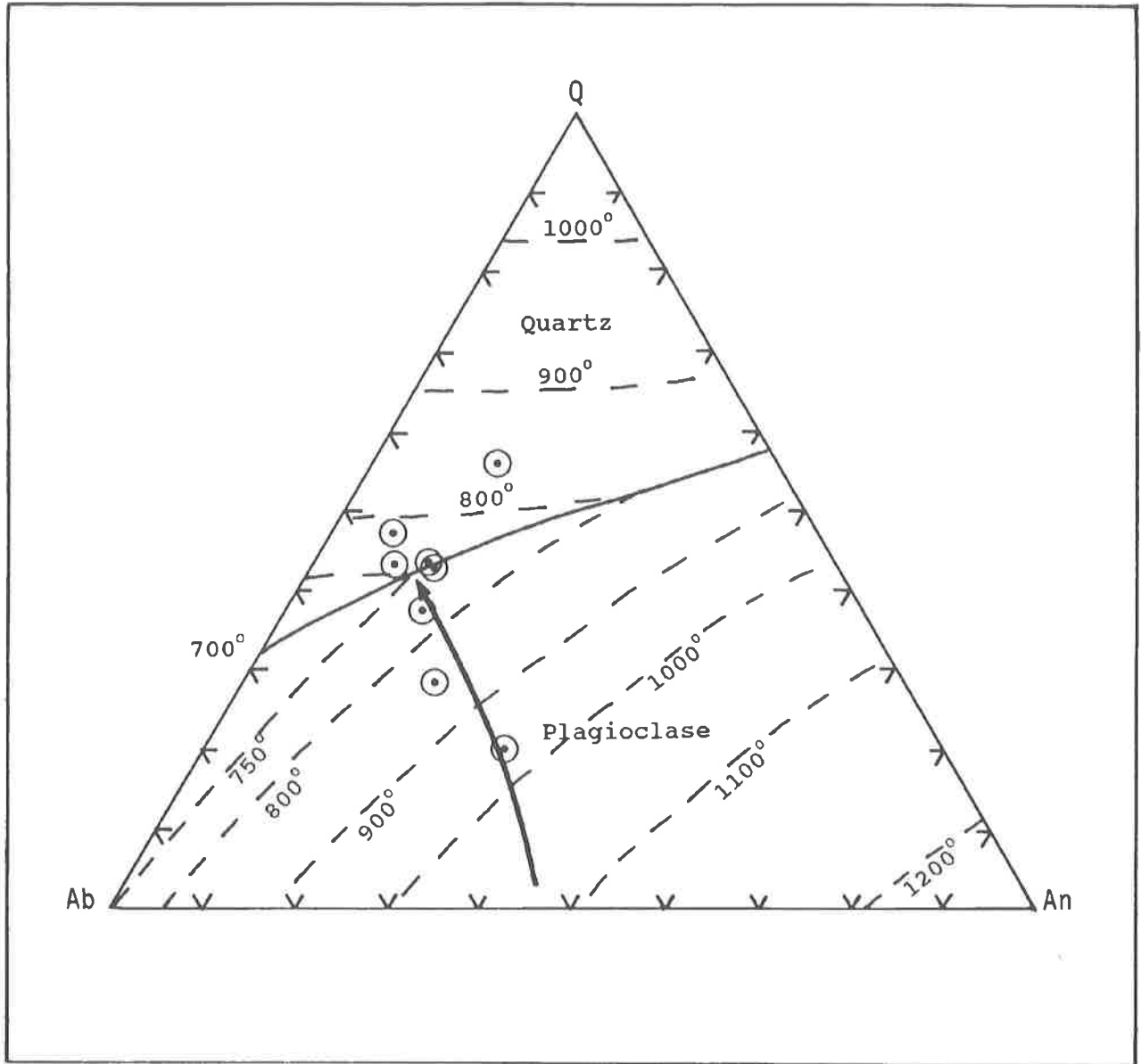
Figure 47. Normative Ab-An-Q diagram for felsic gneisses and granites at $P_{vap.}$=5 kb. An = anorthite, Q = quartz, Ab = albite. The norms of these rocks cluster near the intersection of the two liquidus surfaces and the 750°C isotherm. Several of these norms appear to lie on a path which intersects the boundary curve at this point. Diagram modified from Yoder (1968).

an olivine-rich base to an orthopyroxene-rich top. SiO_2 shows two subparallel enrichment trends (Fig. 48): 1) in the more silica-rich trend, SiO_2 increases from about 38 weight percent near the base to 41-42 weight percent in the upper part of the serpentinite; 2) in the more silica-poor trend, SiO_2 increases from about 33-35 weight percent near the base to about 36-37 weight percent in the upper part of the serpentinite. The increase in SiO_2 content may reflect a change from SiO_2-poor olivine (Mg_2SiO_4) to SiO_2-richer enstatite ($MgSiO_3$). MgO exhibits a gradual increase from about 35 weight percent near the base to about 36.5-37 weight percent near the top of the serpentinite (Fig. 48). Sharp increases between 20-30 feet and about 57 feet may reflect local increases in the magmatic olivine content. FeO also shows a sharp increase between 20-30 feet above the base. Concentrations of MnO generally decrease from about 0.12 weight percent to about 0.055 weight percent toward the upper part of the serpentinite. Fe_2O_3 decreases slightly from about 6-7.5 weight percent to about 5 weight percent possibly reflecting a decrease in the overall magnetite/chromite content of the original igneous body.

A distinct decrease in CaO from 3.5 weight percent to less than 0.1 weight percent with increasing stratigraphic height (Fig. 49) may result from a decrease in primary Ca-pyroxene (represented by a small diopside ($CaMgSi_2O_6$) component). A similar concentration of Ca along the borders of a harzburgite from Burro Mountain, CA is attributed to release of Ca from pyroxenes through progressive serpentinization (Coleman and Keith, 1971). Because Ca is not compatible with the crystal structure of serpentine minerals, it will leave serpentinite to form rodingite or remain to form tremolite or diopside (Wicks and O'Hanley, 1988). In the Burks Mountain serpentinite, influx of carbonate-bearing solutions from the country rock is suggested by the increase in the CO_2 content of the serpentinite towards its base (Fig. 50).

The average TiO_2 content of the Burks Mountain serpentinites and talc is normally 0.01 weight percent. Near the top of Burks Mountain is a layered, magnetite + ilmeno-hematite (38.2 weight percent Fe_2O_3) rock enriched in TiO_2 (9.2 weight percent), V (750 ppm), P_2O_5 (0.34 weight percent) and rare earth elements (REE) (273 ppm La to 1.9 ppm Lu) (Cocker, 1989c). The Cr content of this rock is unusually low (100 ppm) especially when compared to the rest of the serpentinite body (550-4500 ppm). Textural relations and geochemical data suggest separation of an immiscible TiO_2-V-P-REE-Fe-rich melt in the upper part of the ultramafite which subsequently sank to the base of a crystal mush (Fig. 17). Below the crystal mush the remainder of the harzburgite was apparently crystallized and was not penetrated by the sinking of the TiO_2-V-P-REE-Fe-rich melt. The V content of serpentine and talc is normally on the order of 5-15 ppm and 5-20 ppm respectively. Challis (1965) noted that V tends to concentrate in the pyroxenes (90-200 ppm) in New Zealand ultramafic rocks. In disseminated chromite in dunite and harzburgite, V is 180 ppm but is concentrated in massive chromite at 900-1400 ppm (Challis, 1965). Polished sections of this rock indicate a minor amount of strongly resorbed chromite with the remainder being magnetite and ilmeno-hematite. The REE, Ti and V are probably concentrated in these latter minerals.

Vanadium also tends to concentrate along with apatite and REE in the later crystallizing titan-magnetites in the Stillwater (Helz, 1985) and Bushveld layered mafic intrusions (Reynolds, 1985). The similar association of V, Ti, P and REE in iron oxide-rich rocks in the upper levels of the Burks Mountain complex suggests a similar paragenesis to iron oxide-rich rocks in the layered mafic intrusions.

In the Burks Mountain ultramafites, Ni generally ranges from 0.2 to 0.25 weight percent in serpentinite and from 0.12 to 0.19 weight percent in talc, chlorite and silicified serpentinite. If most of the Ni is assumed to be in one phase common to the talc, chlorite and silicified serpentinite, the Ni is probably in Cr-magnetite. The higher Ni content of the serpentinite suggests that Ni may occur in lizardite in addition to the Cr-magnetite.

The behavior of Ni and Co in ultramafic rocks is dependent on olivine. At high temperatures during crystallization from an ultramafic magma, Ni substitutes for Mg in the olivine lattice. During the serpentinization of Ni-bearing olivine, Ni tends to partition into oxides, sulfides or alloys rather than into lizardite. This is attributed to the low water fugacity during serpentinization of olivine (Wicks and O'Hanley, 1988). Co tends to follow Ni in olivine, so their distribution in the serpentinite should reflect that of normative olivine. In Figure 51, Co and Ni show a positive correlation to each other. In the southern Burks Mountain serpentinite, Co, Ni, and Cr tend to increase toward the base of the serpentinite. This is best illustrated by Co (Fig. 52). The serpentinite contains two Cr populations: one greater than Ni (0.255-0.45 weight percent), and the other lower than Ni (0.055-0.2 weight percent). Cr tends to have a greater degree of variability than Co and Ni within the serpentinite.

Effects of serpentinization

The chemical aspects of serpentinization are quantified using a method devised by Shteinberg (1960)
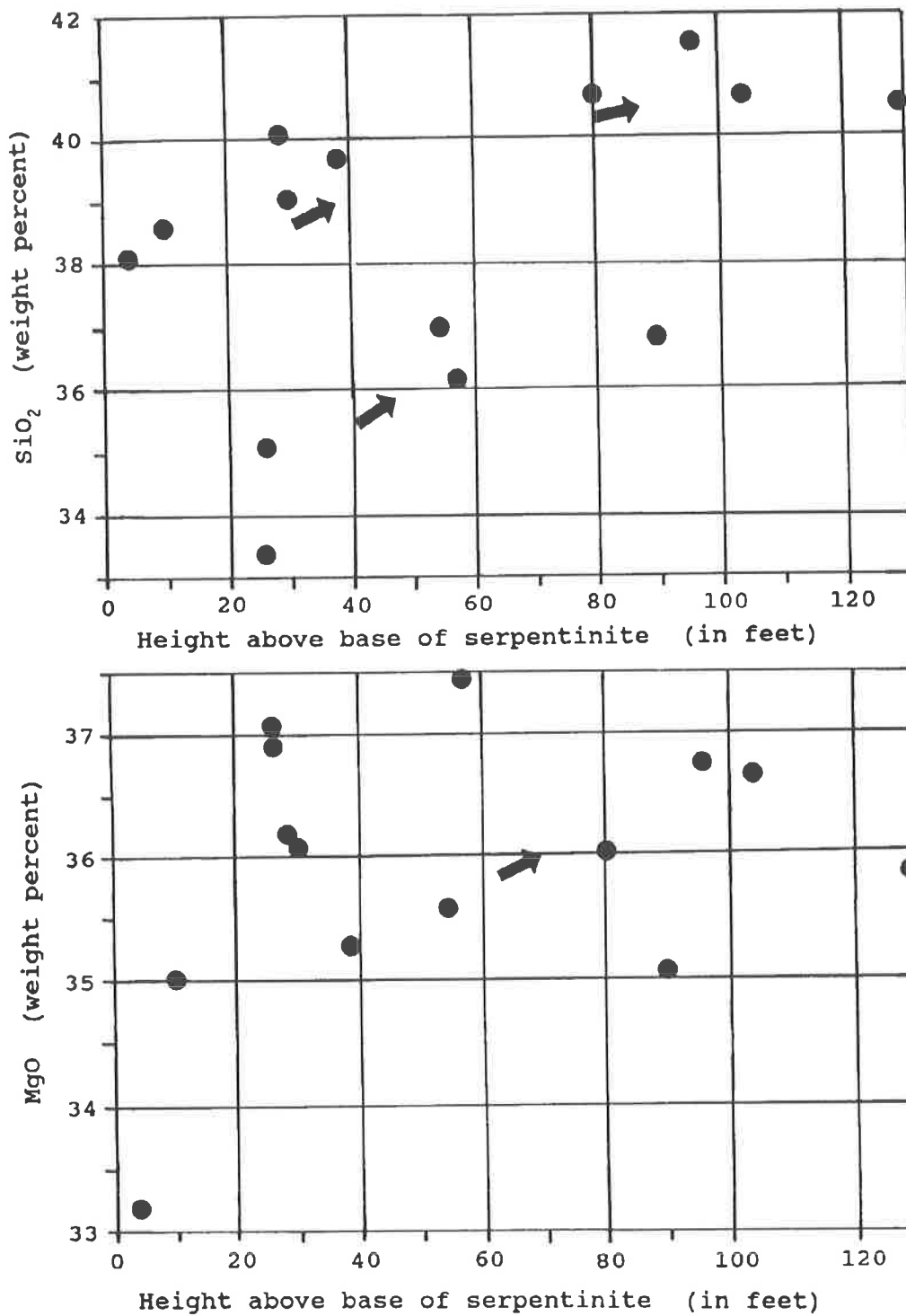
Figure 48. SiO$_2$ and MgO versus height above base in the serpentinite. The main SiO$_2$ trend shows an increase from about 38 weight percent to about 41 weight percent with increasing height. A lower trend is subparallel to the upper trend. The general trend in MgO shows an increase from about 35 weight percent to about 36.5-37 weight percent. Variations above and below these trends may reflect primary, magmatic variations and/or alteration of the serpentinite.
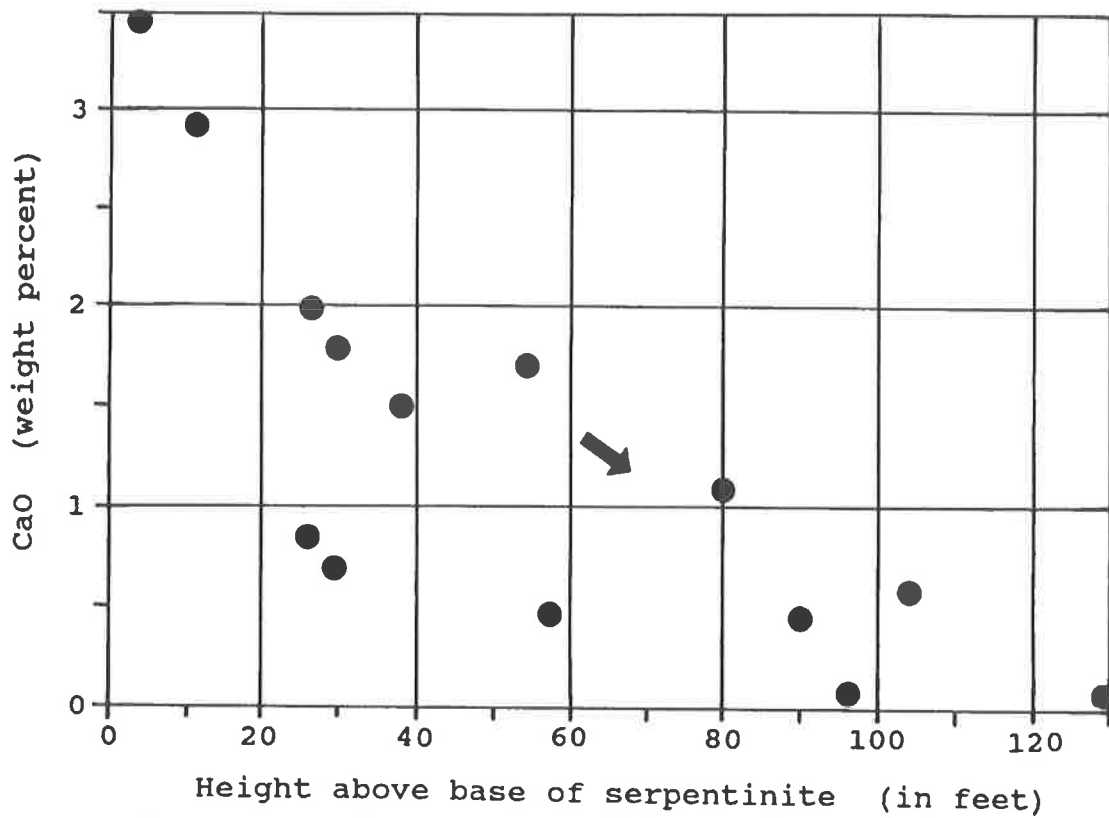
Figure 49. CaO versus height above base in the serpentinite. The CaO shows a definite decrease of 3.5 weight percent to 0.1 weight percent from the base to the top of the serpentinite. This trend may be related to a higher concentration of carbonates toward the base or to a primary, magmatic distribution. The latter may be due to a higher diopside component toward the base of the ultramafite.
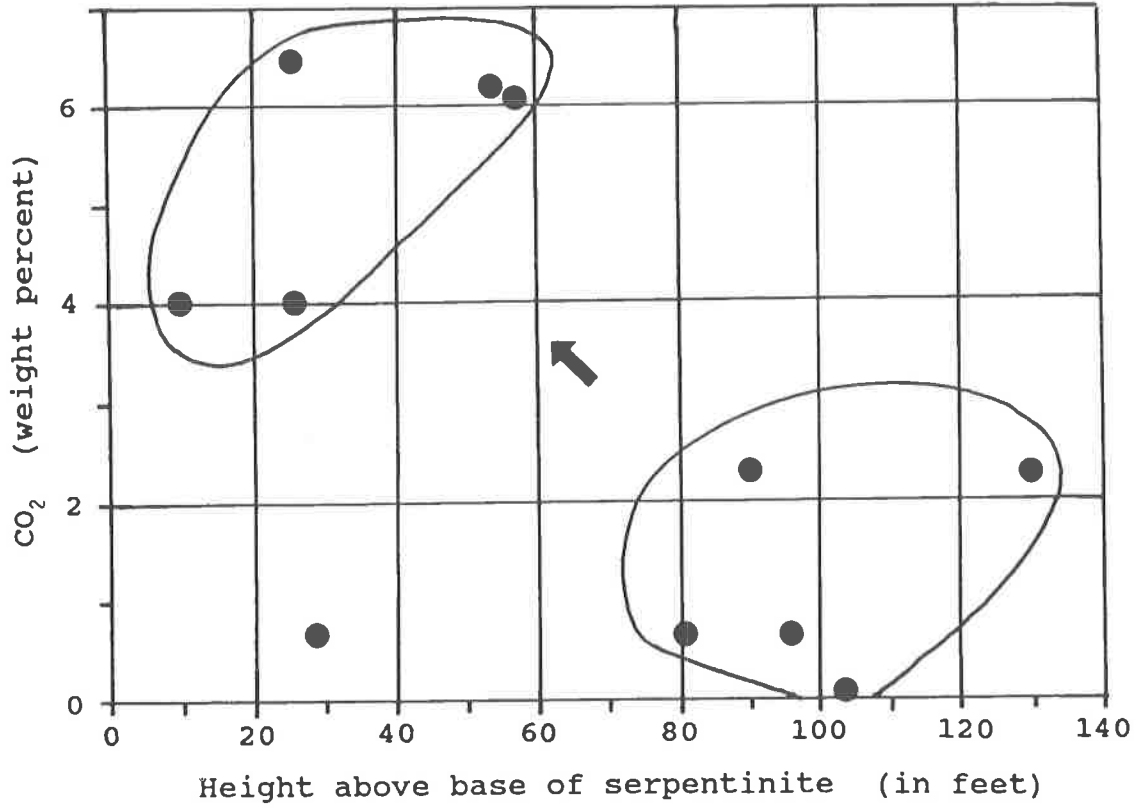
Figure 50. CO_2 versus height above base in the serpentinite. The carbonate content is distinctly higher, 4-6.5 weight percent, near the base of the serpentinite than in the upper part of the serpentinite, 0-2.3 weight percent. This may reflect the influx of CO_2 from the basal country rock-serpentinite contact.
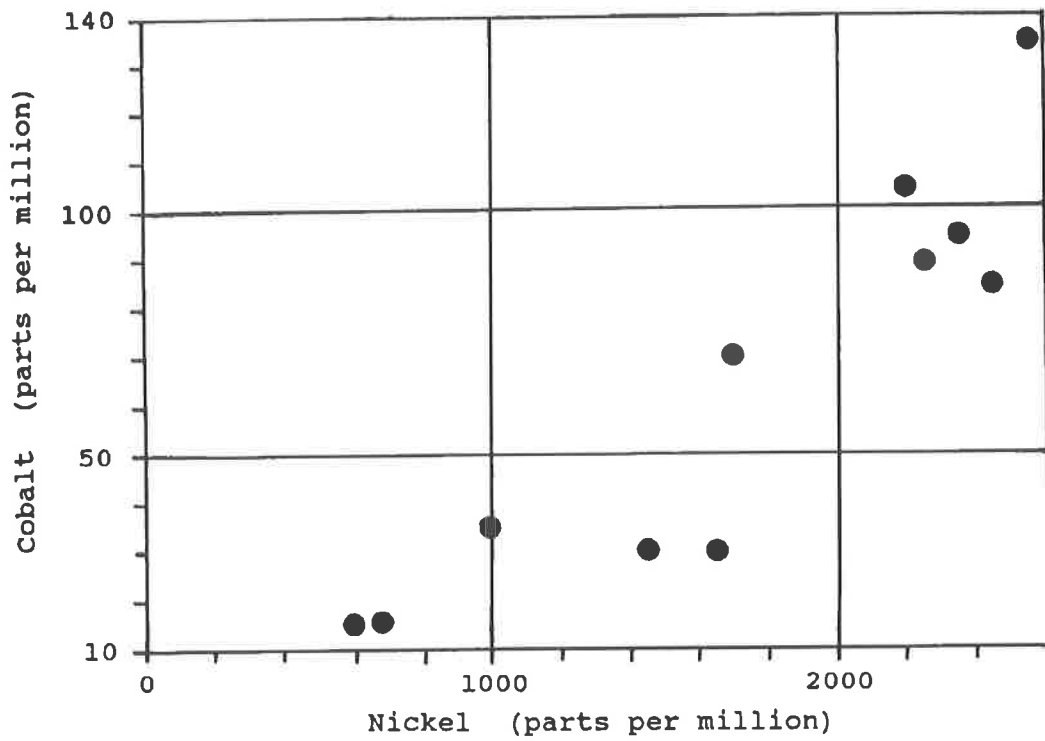
Figure 51. Co versus Ni in serpentinite. Co shows a positive correlation with increasing Ni.
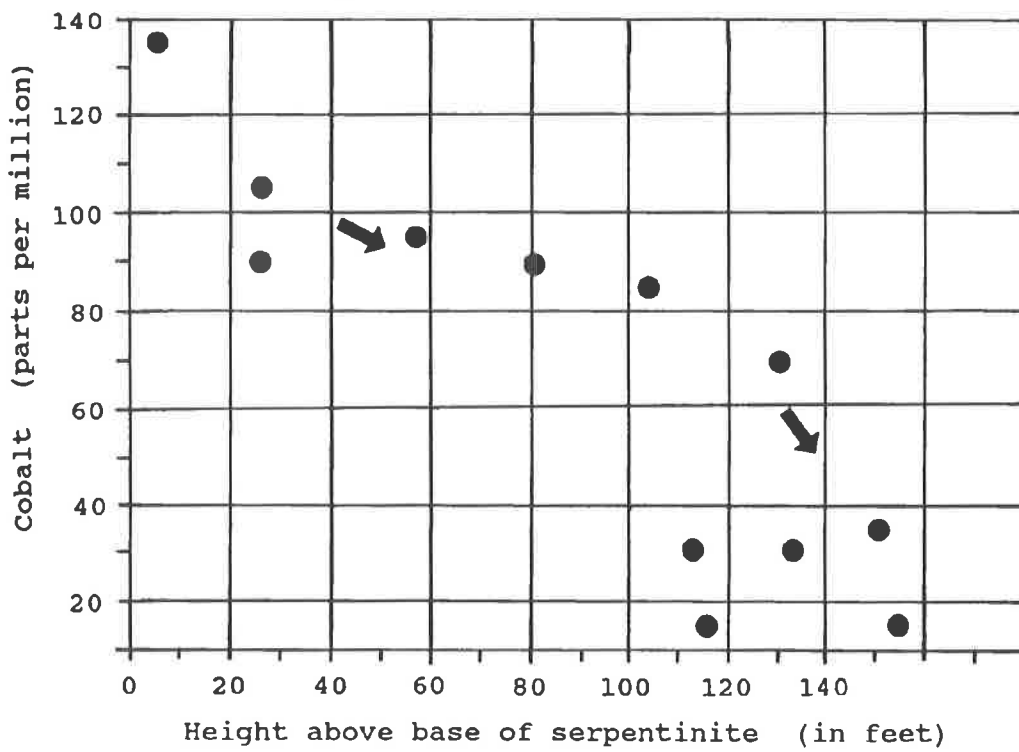
Figure 52. Co versus height above base in serpentinite. Co shows a well defined decrease with increasing height above the base of the serpentinite.

and employed by Coleman and Keith (1971). In Shteinberg's chemographic plot, the ratios RO'/SiO_2 and H_2O/SiO_2 (in molecular amounts) are employed in a triangular diagram (Fig. 53) with apices RO' (representing the molecular sum of the amounts of MgO, total Fe as FeO, CaO, MnO, and NiO reduced by the molecular amounts of Cr_2O_3 and Al_2O_3), SiO_2 and H_2O. If silica, iron or magnesia do not change appreciably during progressive serpentinization of dunites and harzburgites, the RO'/SiO_2 ratio should be relatively constant with only H_2O/SiO_2 increasing toward serpentine which has a H_2O/SiO_2 ratio equal to 1. Variations in the RO'/SiO_2 ratio for harzburgites result from variations in the original orthopyroxene-olivine contents (RO'/SiO_2=2 for olivine, 1.6 for serpentine, and 1.0 for enstatite).

When the Burks Mountain serpentinites are plotted using loss-on-ignition (LOI) for H_2O, they are scattered over a wide range of H_2O/SiO_2 between 1.0 and 1.8. Because other components, principally CO_2, contribute to the LOI component, an adjustment could be made to the LOI if the proportion of CO_2 is estimated. The LOI content for the Burks Mountain serpentinites increases proportionally with increasing carbonate content above 10 weight percent LOI. The 10 weight percent LOI can be attributed mainly to the H_2O content of serpentine. Subtraction of an increasing percentage of CO_2 with increasing LOI provides a closer estimate for H_2O. Most of the data then plots to within +0.1 H_2O/SiO_2 of serpentine (Fig. 53). Additional data scatter may be due to analytical error, contamination by phases other than serpentine, or a correction factor for CO_2 which is slightly too low.

Variation in the RO'/SiO_2 ratio (Fig. 54) may be related to the original orthopyroxene-olivine content. As discussed earlier, the relatively orthopyroxene-rich harzburgite becomes increasingly olivine-rich with increasing depth. The shift in RO'/SiO_2 towards higher metal content with progressive serpentinization might suggest metal enrichment or silica depletion with increasing serpentinization; however, neither is known to occur. The orthopyroxene (enstatite) content of the harzburgite ranges from 20 percent to 62 percent. Serpentinization generally appears to increase with depth. Increasing olivine content, which is usually more susceptible to serpentinization than orthopyroxene (Coleman and Keith, 1971), with depth may account for the increase in serpentinization.

The decrease in H_2O/SiO_2 with increasing stratigraphic height in the serpentinite (Fig. 55) may be related to the increasing SiO_2 content reflecting the change in olivine-enstatite content and to a decrease in H_2O content away from the wallrock-serpentinite contact. A decreasing RO'/SiO_2 ratio with increasing

height suggests that the variation in the primary mineralogy may be the controlling factor.

The oxidation ratio ($100 \times Fe_2O_3/(Fe_2O_3+FeO)$) should increase with increasing degree of serpentinization. The increase in Fe^{+3} is taken up by serpentine and an increase in modal magnetite. Coleman and Keith (1971) suggested the oxidation ratio would not be a good estimate for the degree of serpentinization because of the uncertainty in the oxygen activity and other factors. However, the oxidation ratios of Burks Mountain serpentinites increase as the H_2O/SiO_2 ratio moves toward 1.0 = serpentine (Fig. 56).

Effects of metasomatism

Metasomatic alteration of the serpentinite is suggested by changes in Al_2O_3, Na_2O, K_2O and possibly FeO from the center to the outer edges (top and base) of the serpentinite. Al_2O_3 decreases from about 0.4-0.46 weight percent in the core of the serpentinite to about 0.32-0.37 weight percent near the upper and lower margins of the serpentinite (Fig. 57). Near the present contacts, the Al_2O_3 content increases sharply - up to 0.58 weight percent. From the core to the upper and lower margins of the serpentinite, Na_2O increases from 0.005-0.01 to 0.02-0.04 weight percent (Fig. 58), and K_2O increases from 0.01-0.012 to 0.02-0.03 weight percent (Fig. 58). Circulating fluids may have leached Al_2O_3 from the serpentinite to form chlorite and leached Na_2O and K_2O from the country rocks and transported them into the serpentinite. Because the amount of variation in Al_2O_3, Na_2O, and K_2O is rather minimal (and may be more apparent than real), mineralogic changes are not detectable in modal analyses of these rocks. The Al_2O_3 required to form the abundant chlorite present in the fractures and the monolithic breccia matrix must have come from the country rock, because the normal Al_2O_3 content of the serpentinite is too low.

The FeO content of the serpentinite is generally lower in the core (about 0.4-0.7 weight percent) and increases toward the upper and lower margins (about 0.8-2.3 weight percent). The FeO content decreases near the lower margin of the serpentinite body. As noted earlier, the FeO content may be related to the distribution of magmatic olivine, or the FeO content may be related to the relative abundance of talc and serpentine. As the H_2O/SiO_2 ratio increases above 1.0 (H_2O/SiO_2 is equal to 1.0 for serpentine), the amount of serpentine decreases. In the Burks Mountain serpentinite, the FeO content does increase with an increase in the H_2O/SiO_2 ratio (Fig. 59) and thus is related to a decrease in serpentine. The increase in FeO
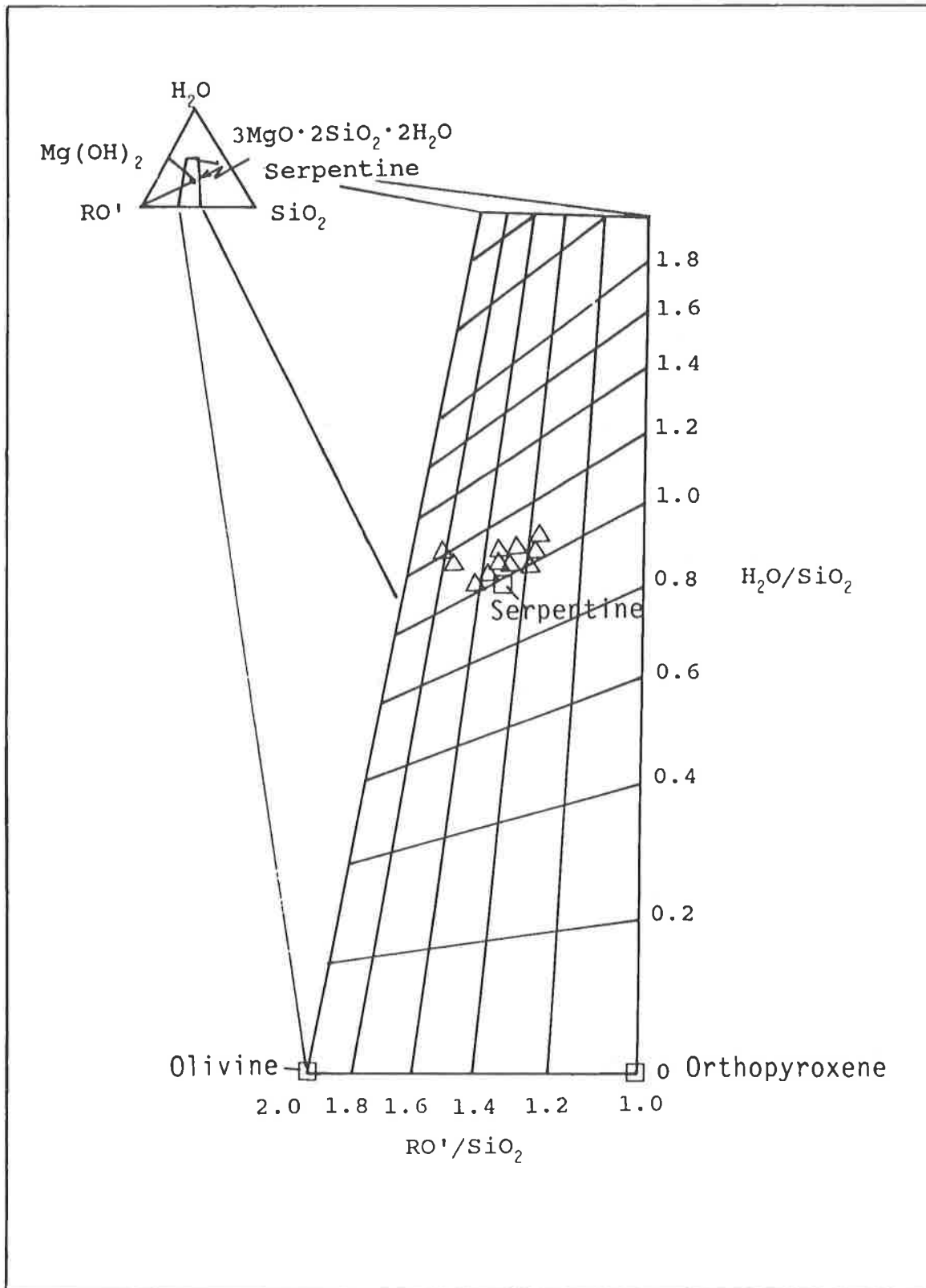
Figure 53. RO' versus SiO₂-H₂O. RO' represents the molecular sum of MgO, total Fe as FeO, CaO, MnO and NiO reduced by the molecular amounts of Cr_2O_3 and Al_2O_3. The Burks Mountain complex serpentinites (represented by dots) all plot near the ideal serpentinite composition (S). Ideal olivine, orthopyroxene and serpentine compositions are denoted by squares. Assuming isochemical serpentinization, except for addition of H_2O, the original rock should range from about 80-30% olivine and 20-70% orthopyroxene (After Shteinberg, 1960).
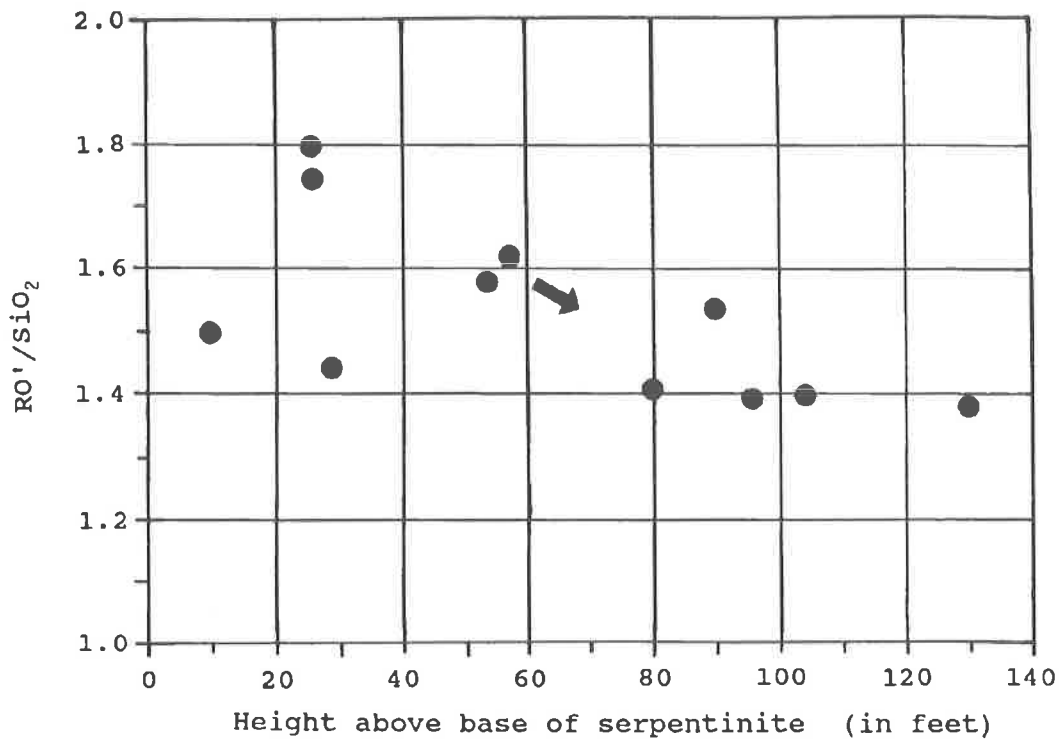
Figure 54. RO'/SiO$_2$ versus height above base in the serpentinite. Decrease in this ratio with increasing height probably reflects an overall change in normative mineralogy with height.
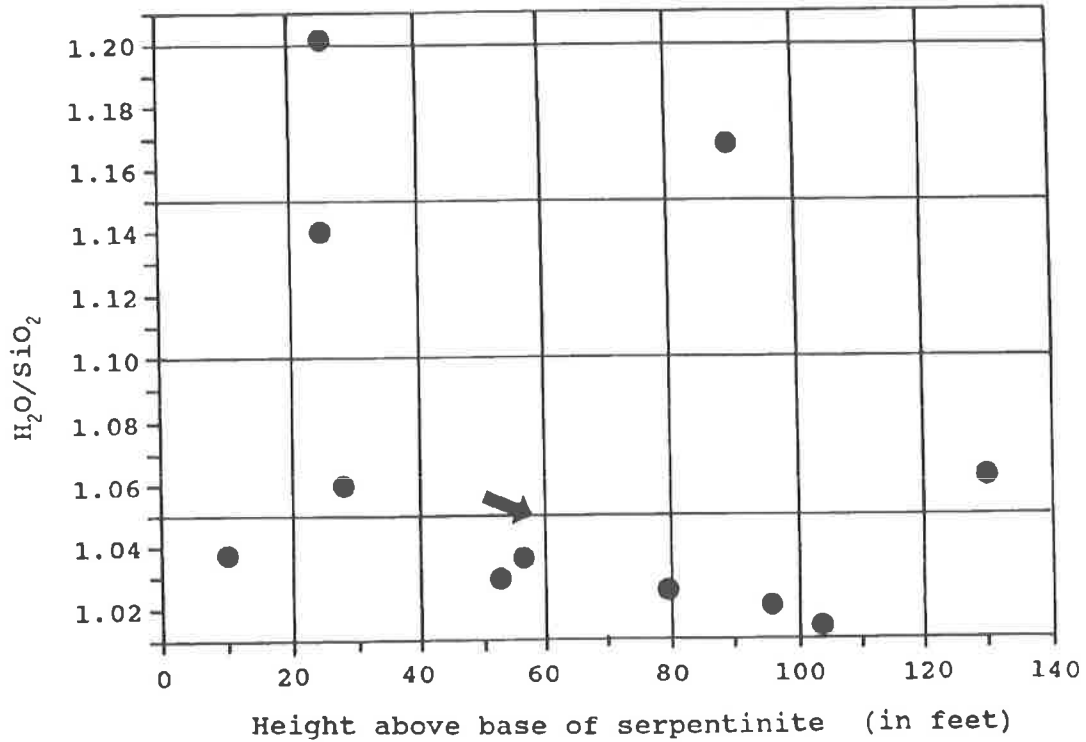
Figure 55. H$_2$O/SiO$_2$ versus height above base in the serpentinite. See text for discussion.

66
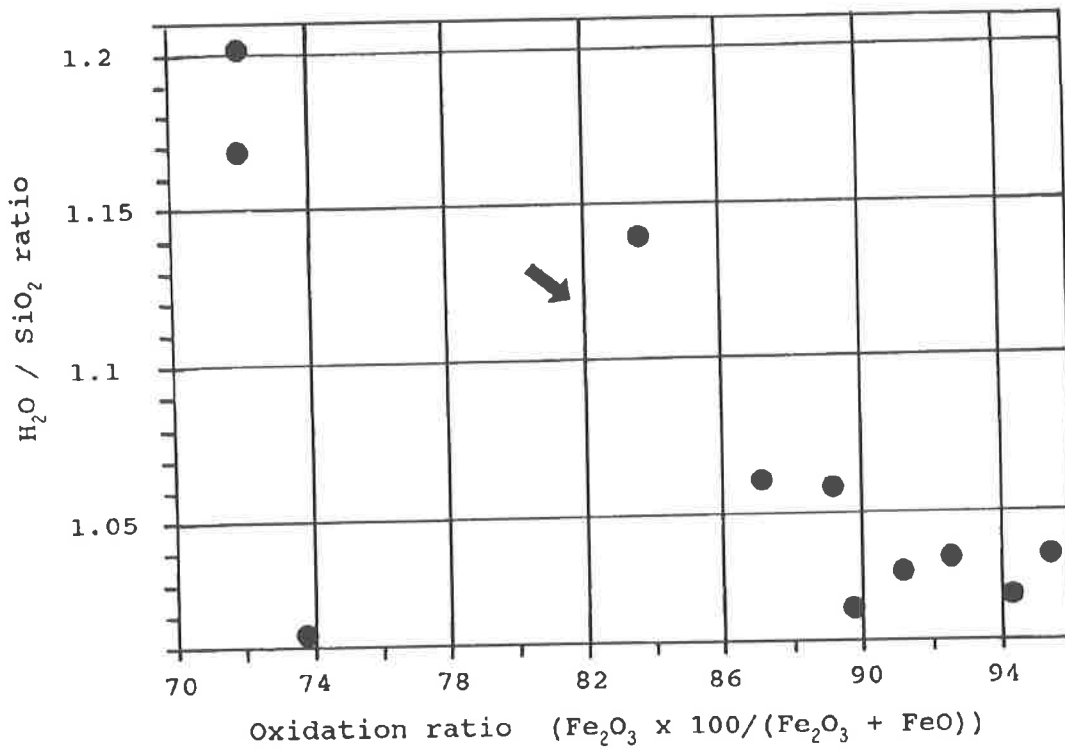
Figure 56. Oxidation ratio versus H_2O/SiO_2. The oxidation ratio increases as the ideal ratio ($H_2O/SiO_2 = 1$) for serpentine is approached.
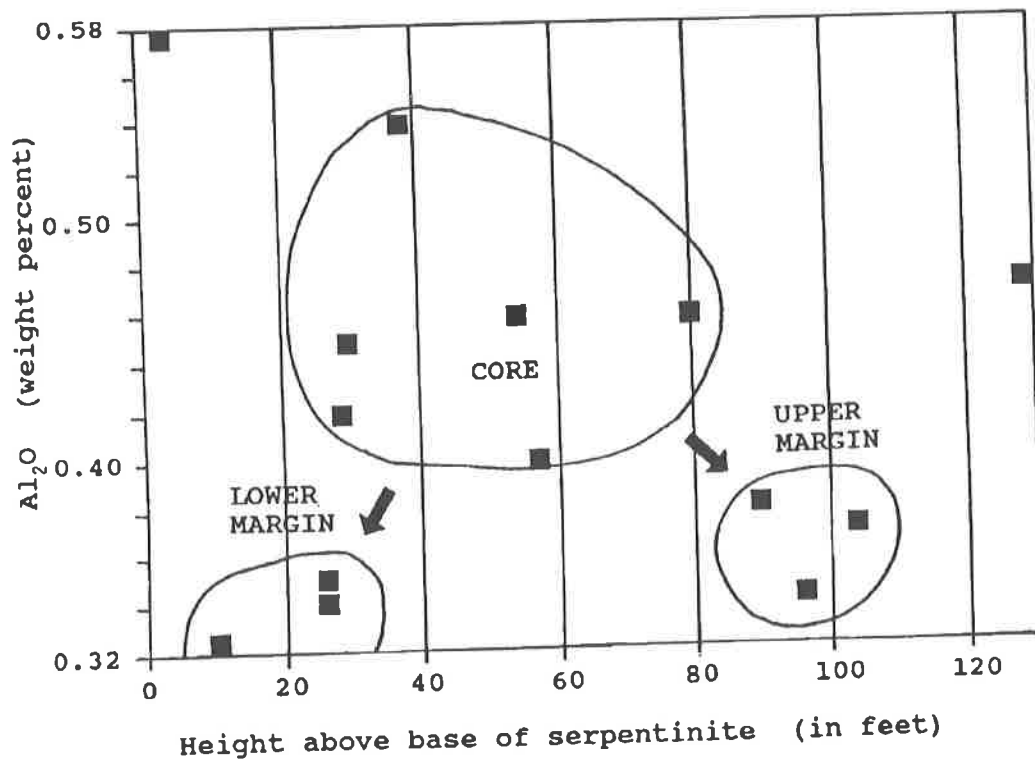
Figure 57. Al_2O_3 versus height above base in the serpentinite. In the core of the serpentinite the Al_2O_3 content varies from about 0.39 to 0.46 weight percent. It decreases to about 0.32 weight percent towards the upper and lower margins, and then it increases to 0.58 weight percent near the lower and upper contacts. The variation near the contacts may reflect migration of Al_2O_3 to form chlorite.

67
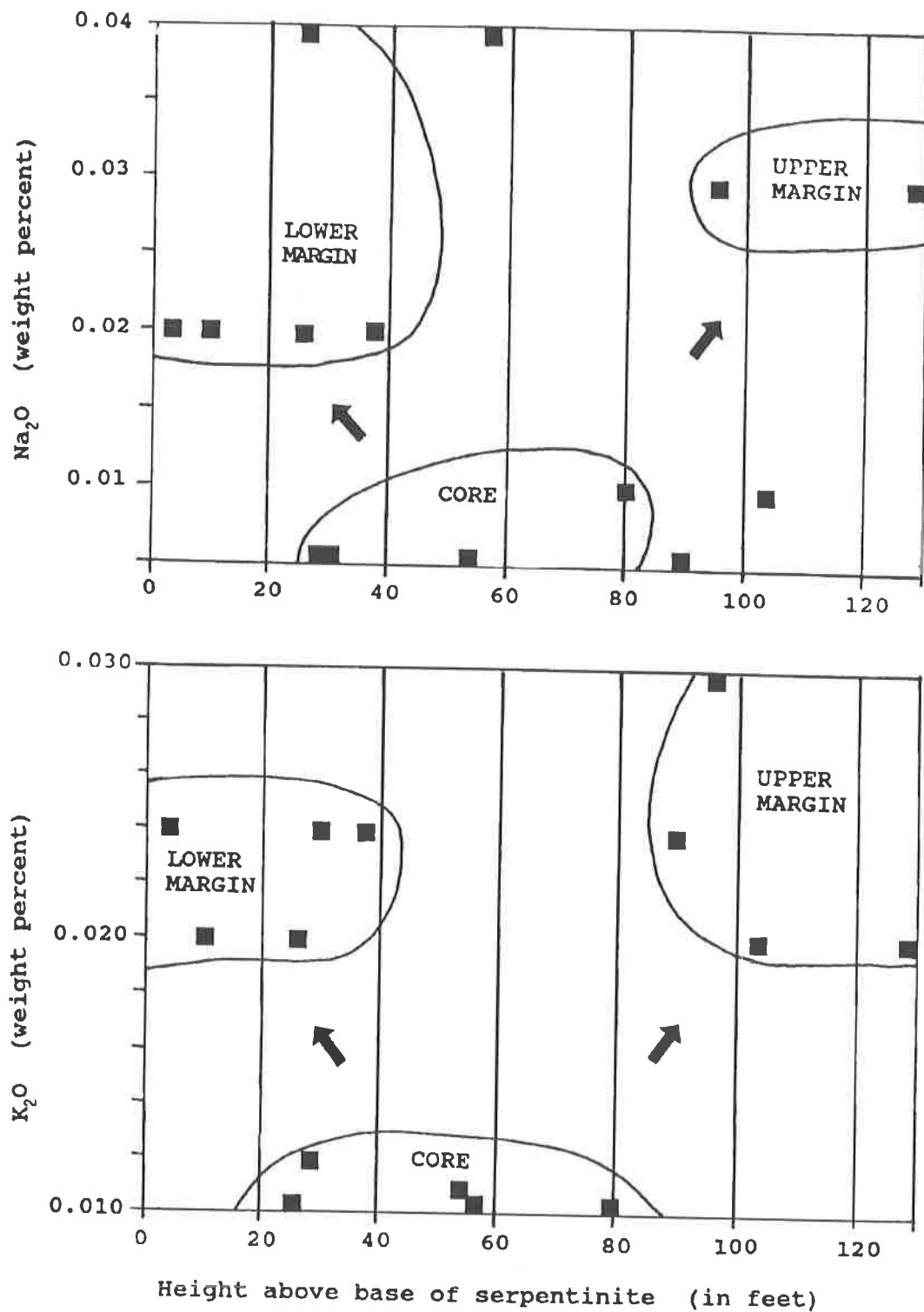
Figure 58. Na_2O and K_2O versus height above base in the serpentinite. In the core of the serpentinite the Na_2O content ranges from 0.05-0.1 weight percent. Towards the upper and lower margins, the Na_2O content increases to 0.02-0.04 weight percent. This slight increase towards the base may reflect influx of Na_2O associated with chloritization of plagioclase in the country rock. In the core of the serpentinite K_2O ranges from 0.01-0.012 weight percent. In the upper and lower margins of the serpentinite, the K_2O content ranges from 0.02-0.03 weight percent. This may reflect an influx of K_2O associated with chloritization of biotite in the adjacent country rock.
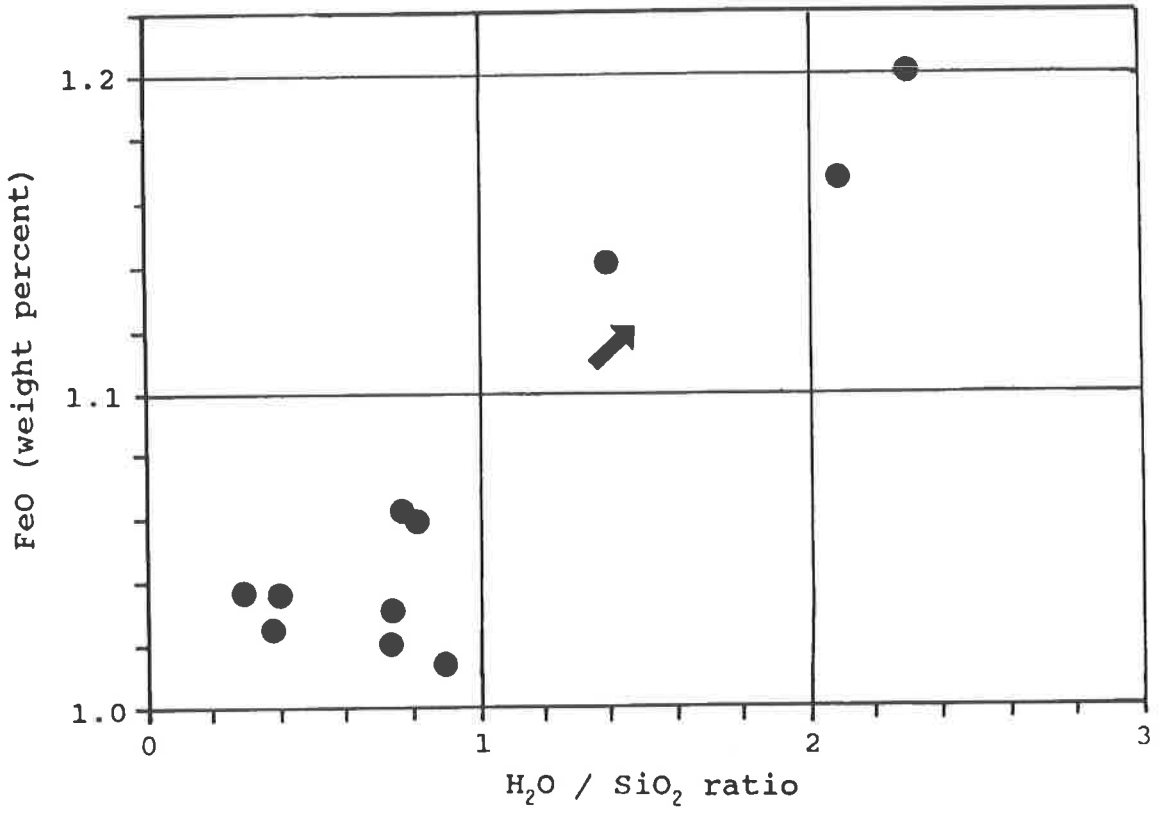
Figure 59. FeO versus H₂O/SiO₂ ratio. Increase in FeO may reflect increasing steatization and subsequent destruction of secondary magnetite.

may be caused by the substitution of Fe^{+2} for Mg^{+2} in talc and/or an increase in the talc content toward the outer edge of the serpentinite. The presence of secondary magnetite in the serpentinite and its absence in talc causes a generally higher oxidation ratio in serpentinite (72-95 percent) than in talc (42-82 percent).

The change in major and trace element chemistry accompanying alteration of serpentinite to talc, chlorite and quartz is illustrated by a series of graphs (Figures 60-62). The oxides SiO_2 and MgO (total 70-90 weight percent), reflect the changes in mineralogy accompanying each type of alteration (Fig. 60). MgO (34-37.5 weight percent) is relatively constant in serpentinite, and SiO_2 varies from 33.4-41.6 weight percent. In talc-rich rock, SiO_2 is significantly enriched (up to 61 weight percent) but is highly variable due to different amounts of carbonate in the analyzed rocks. In chlorite-rich rock, the SiO_2 content is generally similar to that of serpentinite. The decrease of MgO in talc-rock is related to increases in silica or carbonate. In chlorite-rock, the decrease in MgO is caused by an increase in Al_2O_3 (Table 2).

The higher content of CaO and CO_2 near the base of the serpentinite (Figs. 49 and 50) suggests influx of CaO and CO_2-bearing solutions from the country rocks. The CaO content increases from less than 3 weight percent in serpentinite to as much as 8.5 weight percent (average 4.06 weight percent) in talc and to 4.2 weight percent in silicified talc (Fig. 61). The association of talc and carbonate commonly is attributed to addition of CO_2 to serpentine.

The Fe_2O_3 and FeO contents (generally 5-8 weight percent and 0.3-2.3 weight percent respectively) vary considerably in serpentinite (Fig. 60) suggesting a wide range in the amount of magnetite, both metamorphic and secondary (serpentinization-related). The decrease in Fe_2O_3 content from serpentinite (generally 5-8 weight percent) to talc (1-5 weight percent) resulted from dissolution of secondary magnetite during steatization. The decrease in modal magnetite with increasing talc content is shown by Fig. 38 and 39. In chlorite, the Fe_2O_3 content is highly variable (1.8-9.5 weight percent) but on average is equal to that in serpentinite. The small variation of FeO in talc (1.1-1.5 weight percent) may reflect the relatively stable metamorphic magnetite content and lack of secondary magnetite.

Several major element-oxides (Al_2O_3, TiO_2, Na_2O, and K_2O) are significantly enriched in chlorite relative to serpentinite, talc, silicified serpentinite, and silicified talc. Al_2O_3 is enriched from <0.5 weight percent up to 12.3 weight percent (Fig. 61). Because the Al_2O_3 content of the Burks Mountain serpentinites are uniformly very low, it is likely that the Al_2O_3 was introduced by Al-bearing solutions which then reacted with serpentine and talc. The fluids migrated along fractures extending well into the serpentinite and through the relatively porous multilithic breccia. The TiO_2 content increases sharply from 0.01 weight percent in serpentinite and talc to 5.1 weight percent in chlorite (Fig. 62) also suggests mobilization and transport of TiO_2 from the country rock. Normally considered immobile, significant amounts of both Al_2O_3 and TiO_2 have migrated considerable distances along fractures and through the multilithic breccia. Both Na_2O and K_2O (Fig. 62) increase from less than 0.05 weight percent in serpentinite to 0.1 weight percent Na_2O in talc and to 0.28 weight percent Na_2O and 0.75 weight percent K_2O in chlorite. These six- to fifteen-fold enrichments further suggest influx of major oxide-bearing fluids from the enclosing country rocks.

In general, the major chemical changes accompanying metasomatism of serpentinite include enrichment of SiO_2, FeO, and CaO during steatization and enrichment of SiO_2, Al_2O_3, Na_2O, K_2O, and TiO_2 during chloritization relative to average Burks Mountain serpentinite. During steatization, Fe_2O_3, MgO, LOI, Ni and Cr decrease, and during chloritization, CaO, MgO, LOI, Ni and Cr decrease relative to average Burks Mountain serpentinite.

Effects of silicification

In the silicified ultramafites, silicification is nearly complete. The SiO_2 content increases to 85.8-90.4 weight percent (Fig. 60) and most of the other oxides are reduced to minimal levels (Figures 60, 61 and 62). Preservation of metamorphic and secondary magnetite in serpentinite noted in thin sections is further demonstrated by similar concentrations of Fe_2O_3 (5.4-6.7 weight percent) in silicified serpentinite and non-silicified serpentinite (5-8 weight percent).

Chemical Effects of Weathering

The geochemistry of a weathered serpentinite clast (sample D139) from the Old Petersburg Road roadcut shows significant depletion of certain elements and an apparent enrichment in others when compared to fresh serpentinite from the drill core.

The decrease of CaO and in the loss-on-ignition (LOI) component reflect the weathering and removal of carbonate. The absence of carbonates in all thin-sections of exposed serpentinites examined in this study might suggest that carbonate is absent in unweathered serpentinite at depth; however, these chemical analyses confirm that carbonates are removed almost completely by weathering. Deep-weathering
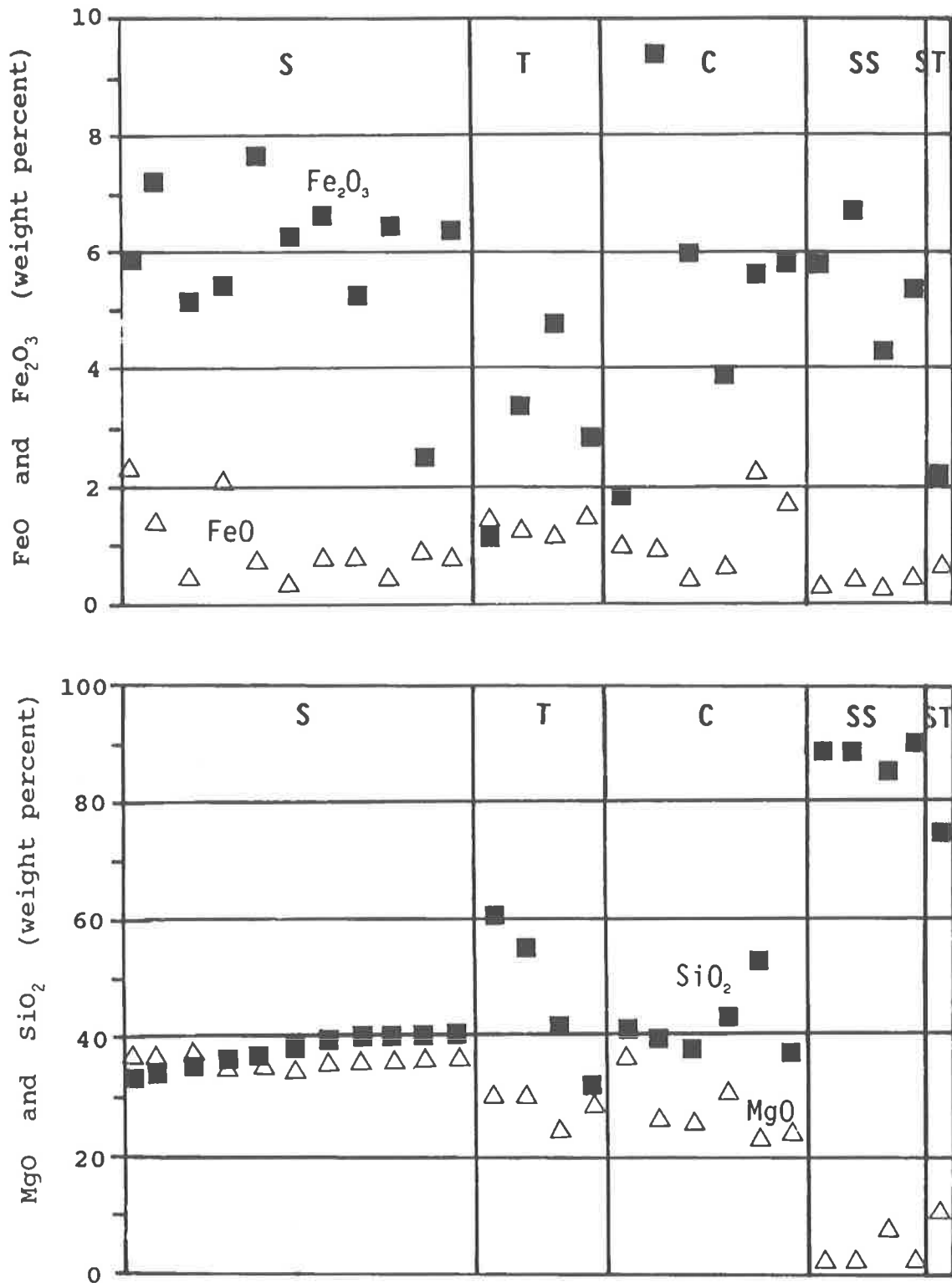
Figure 60. SiO$_2$ and MgO, Fe$_2$O$_3$ and FeO versus serpentinite alteration type. Weight percent of oxide is plotted versus the principal rock type. Each rock type is essentially a monomineralogic alteration "assemblage". Variations in compositions of each rock type are due principally to trace amounts of other minerals such as talc, chlorite and carbonate in serpentinite. S = lizardite serpentinite, T = talc, C = chlorite, SS = silicified serpentinite, ST = silicified talc.

71
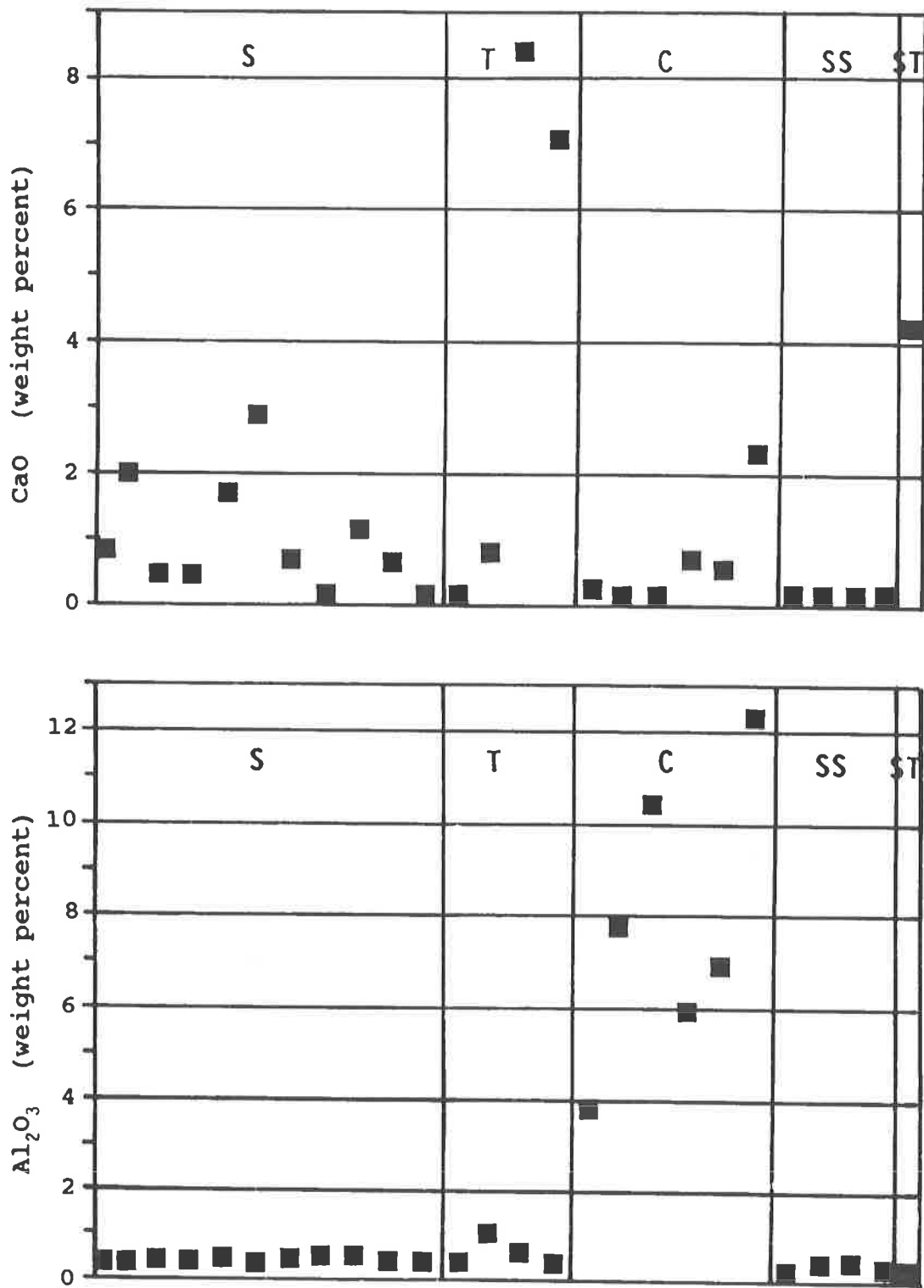
Figure 61. Al_2O_3 and CaO versus serpentinite alteration type. Weight percent of oxide is plotted versus the principal rock type. Each rock type is essentially a monomineralogic alteration "assemblage". Variations in compositions of each rock type are due principally to trace amounts of other minerals such as talc, chlorite and carbonate in serpentinite. S = lizardite serpentinite, T = talc, C = chlorite, SS = silicified serpentinite, ST = silicified talc.
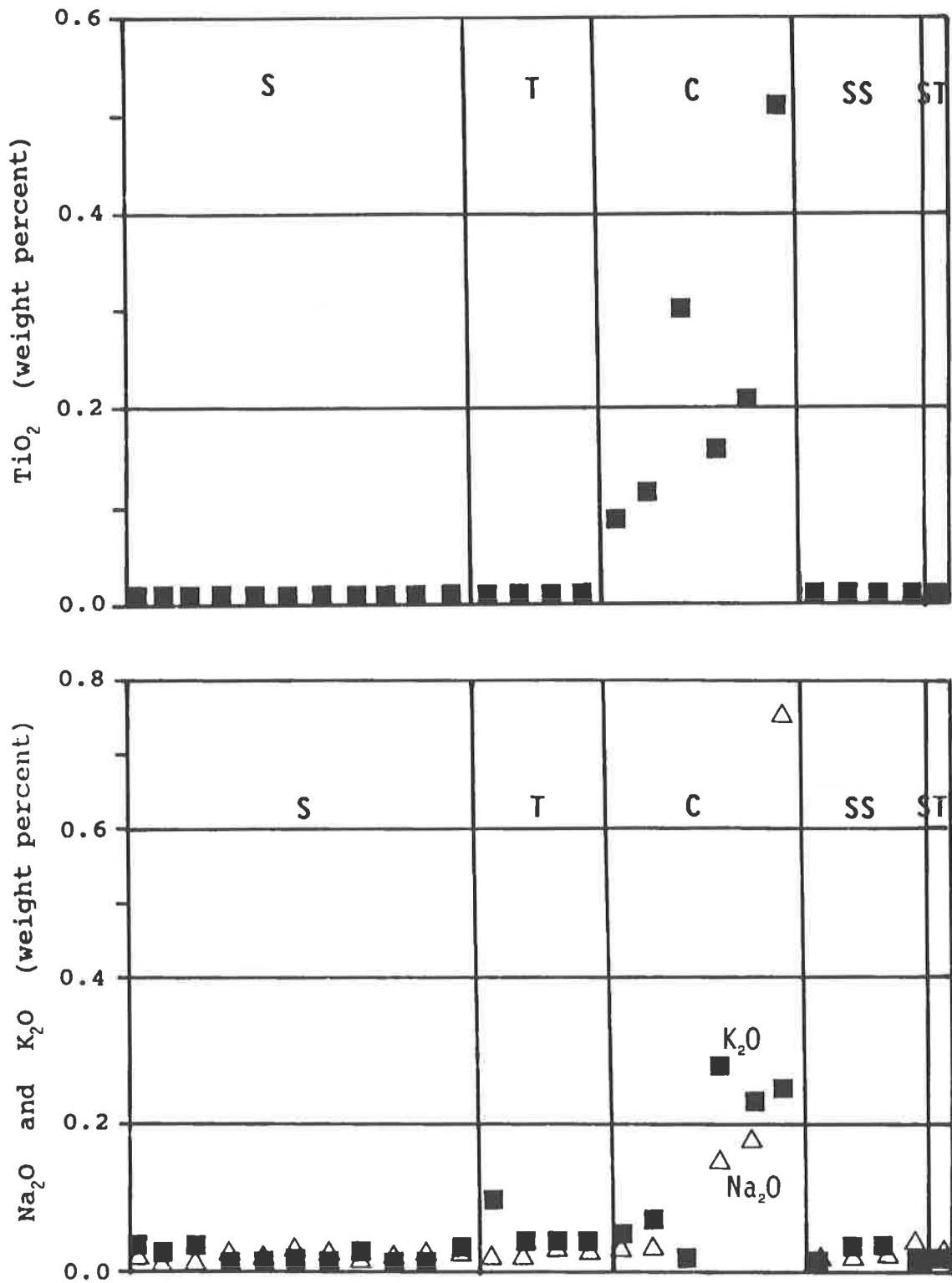
Figure 62. Na₂O and K₂O, and TiO₂ versus serpentinite alteration type. Weight percent of oxide is plotted versus the principal rock type. Each rock type is essentially a monomineralogic alteration "assemblage". Variations in compositions of each rock type are due principally to trace amounts of other minerals such as talc, chlorite and carbonate in serpentinite. S = lizardite serpentinite, T = talc, C = chlorite, SS = silicified serpentinite, ST = silicified talc.

Table 2.

Average Chemical Composition of Ultramafic Rocks Burks Mountain Complex (this study)

	Serpentine			Chlorite			Talc		
	AVG	STD	VAR	AVG	STD	VAR	AVG	STD	VAR
SiO_2	38.28	2.60	6.76	42.17	5.22	27.27	47.52	11.53	132.85
Al_2O_3	0.39	0.05	0.00	7.85	2.81	7.90	0.58	0.26	0.07
Fe_2O_3	5.89	1.31	1.72	5.45	2.28	5.19	3.05	1.32	1.75
FeO	0.99	0.64	0.41	1.13	0.63	0.39	1.35	0.17	0.03
MgO	36.26	0.78	0.60	27.72	4.86	23.60	28.22	2.48	6.13
CaO	0.99	0.83	0.70	0.64	0.78	0.61	4.06	3.68	13.57
Na_2O	0.02	0.01	0.00	0.15	0.11	0.01	0.06	0.02	0.00
K_2O	0.02	0.01	0.00	0.20	0.25	0.06	0.02	0.01	0.00
LOI	15.29	1.92	3.68	13.43	3.10	9.58	12.72	7.68	59.06
TiO_2	0.01	0.00	0.00	0.23	0.14	0.02	0.01	0.00	0.00
P_2O_5	0.01	0.00	0.00	0.08	0.16	0.02	0.01	0.00	0.00
MnO	0.10	0.03	0.00	0.12	0.08	0.01	0.14	0.14	0.02
SrO	0.002	0.00	0.00				0.0005	-	0.00
Rb_2O	0.001	-	-				0.0005	-	0.00
Ni	0.221	0.019	0.00	0.157	0.115	0.013	0.163	0.032	0.00
Cr	0.235	0.108	0.116	0.108	0.045	0.002	0.215	0.005	0.00
TOTAL	98.720			99.426			98.144		

AVG = average
STD = standard deviation
VAR = variance
The original analyses for serpentinite, chlorite and talc are presented in Appendix II.

Table 3.

Chemistry of Fresh and Weathered Serpentinite
(values are in weight percent)

	Average Fresh Serpentinite	Weathered Serpentinite
SiO_2		
MgO	36.26	9.70
Al_2O_3	0.39	11.10
Fe_2O_3	5.89	24.70
FeO	0.99	0.38
Na_2O	0.02	0.04
K_2O	0.04	0.06
CaO	0.99	0.03
LOI	15.29	9.90
Ni	0.22	0.19
Cr	0.24	0.46
TiO_2	0.01	0.26

Average fresh serpentinite is from Table 2.

of serpentinites in many parts of the world produces Ni-rich saprolites which are an important source of that metal. The results of this study do not suggest that weathering enriched Ni in the study area.

The weathering index of a silicate rock provides a chemical index for quantifying the intensity of weathering (Parker, 1970). The weathering index is calculated from the expression:

$100 \times [(Na)a/0.35 + (Mg)a/0.9 + (K)a/0.25 + (Ca)a/0.7]$

(where $(X)a$ is the atomic percentage of element X divided by its atomic weight). The weathering index, normally 96-104 for fresh serpentinites, decreases to 27 for serpentinite in the roadcut.

GEOPHYSICS

Rocks with different physical properties can be distinguished by measuring those properties with geophysical instruments. Serpentinites and other ultramafic and mafic rocks are commonly significantly different from felsic rocks in their physical properties. Generally, they differ most in density and/or magnetic susceptibility. Geophysical methods aided in the subsurface delineation of the Burks Mountain complex serpentinites because of their extremely poor exposures; especially of the southern serpentinite. Initial geophysical work conducted by Long (1987) used gravity methods. A second survey by Cocker (1989a) employed ground magnetic methods.

GRAVITY

Unaltered ultramafic rocks are generally very dense with a specific gravity of 3.3 for dunite and harzburgite. Alteration of ultramafic rocks changes their mineralogy and hence their density.
Specific gravity of serpentine minerals ranges from 2.55 for chrysotile and lizardite to 2.61 for antigorite (Coleman, 1971). The presence of antigorite instead of lizardite, massive talc (specific gravity 2.7-2.8, average 2.71, Telford and others, 1976), as well as other minerals such as magnetite, carbonate, chlorite and actinolite will affect the density of an ultramafite to different degrees. Amphibolites have densities ranging from 2.90 to 3.04 with an average of 2.96 (Telford and others, 1976) and may be misinterpreted as ultramafic rocks.

Long (1987) attributes a subtle gravity anomaly in the Burks Mountain area to talc mineralization but found the anomaly to be indistinguishable from an anomaly over higher density mafic rocks. This lack of a distinctive gravity signature is attributed to similar densities of the talc and mafic rocks. However, the densities of talc and serpentine should be less than the densities of the mafic rocks and, in principle, should be distinguishable from them.

Similarities in the densities of talc and serpentinite to felsic rocks may significantly increase the difficulty in distinguishing the ultramafic from the felsic rocks. Felsic rocks have densities which are normally lower than ultramafic rocks. Granite has a density range of 2.50 to 2.81 with an average of 2.64, and gneiss has a range of 2.59 to 3.0 with an average of 2.80 (Telford and others, 1976). The densities of serpentinite and talc can range from 2.55 to 2.8 overlapping that of granite and gneiss.

MAGNETICS

The abnormally higher concentrations of magnetite in serpentinite compel the choice of magnetics as the most highly suitable geophysical technique to delineate serpentinites associated with ultramafic rocks (Breiner, 1980). Primary magmatic magnetite and/or chromite is commonly significantly more abundant in mafic/ultramafic rocks than in more felsic rocks. Prograde amphibolite facies metamorphism of mafic/ultramafic rocks produces a more magnetite-rich spinel which is more magnetic than the magmatic spinel. Also, serpentinization of Fe-Mg silicates releases additional iron to form finely disseminated magnetite.

The ground magnetic survey consisted of two main parts: an initial orientation survey followed by the main survey. The orientation survey was run alongside of the Old Petersburg Road with stations every 50 feet. The orientation of the line was chosen to cross the previously mapped regional geologic trends (McLemore, 1965). The interval was chosen to determine the minimum spacing required to detect the serpentinite.

The orientation survey identified a very prominent anomaly coincident with the serpentinite (Fig. 63). A grid was constructed to cover the serpentinite and subsequently was expanded to cover additional areas of interest. Numerous N-S and E-W ground magnetics profile lines were constructed and the results are similar to the orientation survey line in defining the serpentinite. A ground magnetic map (Fig. 10) compiled from these data successfully delineated the subsurface extent of the serpentinite. The subsurface presence of serpentinite was confirmed by drill testing. Discontinuities in the magnetic anomalies suggest the presence of faults which break the serpentinite into smaller segments. Smaller anomalies correspond with isolated ultramafite masses identified by surface float. Extension of the survey to a wider line spacing over the western end of Burks Mountain uncovered currently unexplained discontinuities in the magnetic expression of the serpentinite. These discontinuities include
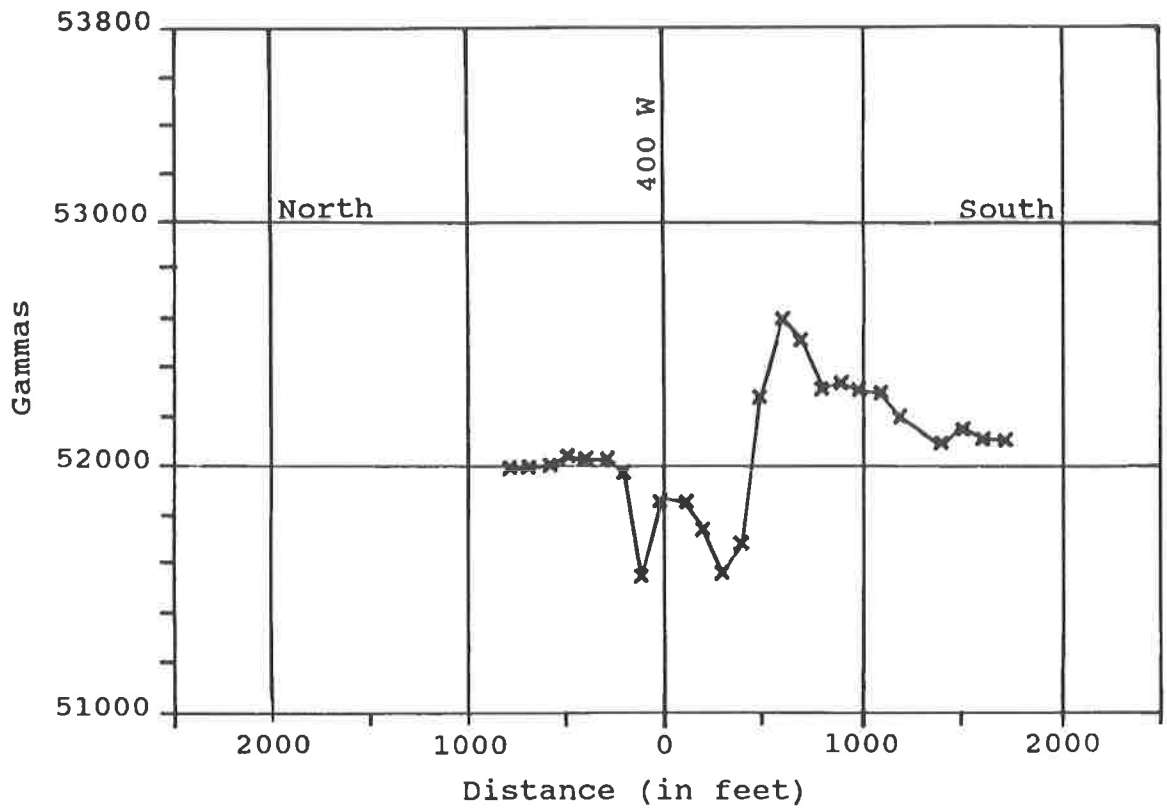
Figure 63. Ground magnetic survey line. This line (400W) is oriented north (left) to south (right) with the view towards the east. Pronounced positive magnetic anomaly (greater than 52,100 gammas) is associated with the underlying serpentinite. Relatively non-magnetic Kiokee gneisses and granites occur north of the serpentinite.

exceptionally high and narrow magnetic anomalies and serpentinite with an abnormally low magnetic response. The scale of the ground magnetic map (Fig. 10) prohibits the inclusion of these narrow anomalies.

The ground magnetic anomaly over the southern serpentinite is roughly coincident with a positive anomaly detected in an airborne survey (Daniels, 1974). These results suggest that the southern serpentinite extends to the southwest at a relatively shallow level for approximately several thousand feet.

DISCUSSION AND CONCLUSIONS

PHYSICAL CONDITIONS DURING PROGRADE METAMORPHISM

Studies in the northeastern portion of the Kiokee belt in the vicinity of Lake Murray, S.C. (Dallmeyer and others, 1986) provide a framework for estimating the physical conditions during the metamorphism in and adjacent to the Burks Mountain complex (Fig. 64). Maximum metamorphic conditions during Alleghanian metamorphism are suggested to be approximately 4.5 kb with a minimum temperature of 530°C (Secor and others, 1986a), although a more recent study (Snoke and Frost, 1988) indicates pressures of up to 7 kb and 575°C were attained in Kiokee belt rocks located in South Carolina. Subsequent rapid cooling from above 500°C to below 300°C is attributed to rapid uplift from mid-crustal depths and erosion in the latest Carboniferous and Early Permian (Dallmeyer and others, 1986). Slower cooling to about 100-125°C occurred over the following 170 million years (Zimmerman, 1979; Naeser and Cebula, 1978; Dallmeyer and others, 1986).

Mineral equilibrium relations suggest peak metamorphic conditions were probably much higher than the minimum 530°C. Dallmeyer and others (1986) show a maximum temperature on their thermal evolution curve of 600°C with an error of +/- 70°C. During amphibolite facies metamorphism, temperatures are between 600 and 700°C (Ehlers and Blatt, 1982). The relict upper amphibolite assemblages identified in the serpentinized metaharzburgite (Cocker, 1989a) are similar to upper amphibolite facies assemblages in other serpentinites (Springer, 1974; Frost, 1975; and Pinsent and Hirst, 1977). Maximum temperatures estimated for these similar assemblages are: 775°C (Springer, 1974); 750°C (Frost, 1975); and 725°C (Pinsent and Hirst, 1977). The presence of anthophyllite places a minimum temperature of formation at 2-4 kb of approximately 600°C (Evans and Guggenheim, 1988).

The clustering of granite and granite gneiss (migmatites) compositions near 750°C at 5 kb pressure (Fig. 47) is in reasonable agreement with the 700°C estimated from the above metamorphic relations. Intrusion of the granites in association with or subsequent to the migmatization during the Lake Murray deformation event (discussed earlier) is thought to have produced the amphibolite facies metamorphism in the Kiokee belt (Secor and others, 1986a and 1986b; Dallmeyer and others, 1986; and Secor, 1987).

PHYSICAL CONDITIONS DURING SERPENTINIZATION

Physical conditions during serpentinization can be determined through the use of phase diagrams, textures, mineralogy and chemical analyses. As discussed in previous sections, the only recognized serpentine mineral is lizardite; the lizardite forms a pseudomorphic mesh texture after olivine and enstatite; and the lizardite is relatively low in Al_2O_3.

Using these parameters, the physical conditions during formation of the Burks Mountain lizardite serpentine can be estimated from P-T phase diagrams. The stability fields of each of the three primary serpentine minerals, lizardite, chrysotile and antigorite, can be shown in P-T space, because each is known to replace or be replaced by the other two serpentine minerals.

Two types of P-T phase diagrams, which are constructed from experimental relations and thermodynamic data, include the MSH (MgO-SiO_2-H_2O) and the MASH (MgO-Al_2O_3-SiO_2-H_2O) diagrams (Wicks and O'Hanley, 1988). The MSH diagram contains six phases: lizardite, antigorite, chrysotile, brucite, forsterite, enstatite, talc and water, and 3 components (MgO-SiO_2-H_2O). The MASH diagram includes a seventh phase, clinochlore, through the addition of a fourth component (Al_2O_3). Reactions involving two serpentine minerals have not been calibrated experimentally, so only the topologic relations can be shown (Fig. 65 and Fig. 66). These phase diagrams are for low-Al (less than 1 weight percent Al_2O_3) lizardite and high-Al (greater than 3.5 weight percent Al_2O_3) lizardite respectively.

Lizardite should be the stable serpentine phase at pressures above 500 bars and at temperatures below 200°C (Wicks and O'Hanley, 1988). The invariant point [LT] in Figures 65 and 66 is at 500 bars and 200°C. The stability of lizardite is dependent on its Al-content as illustrated by the intersection of the following two reactions. The equilibrium lizardite = forsterite + talc + clinochlore + water and antigorite = forsterite + talc + water intersect at 700°C and 35 kb for a(H_2O)=1 with a lizardite containing 9 weight percent Al_2O_3. A decrease in Al-content to 3.5 weight percent moves this
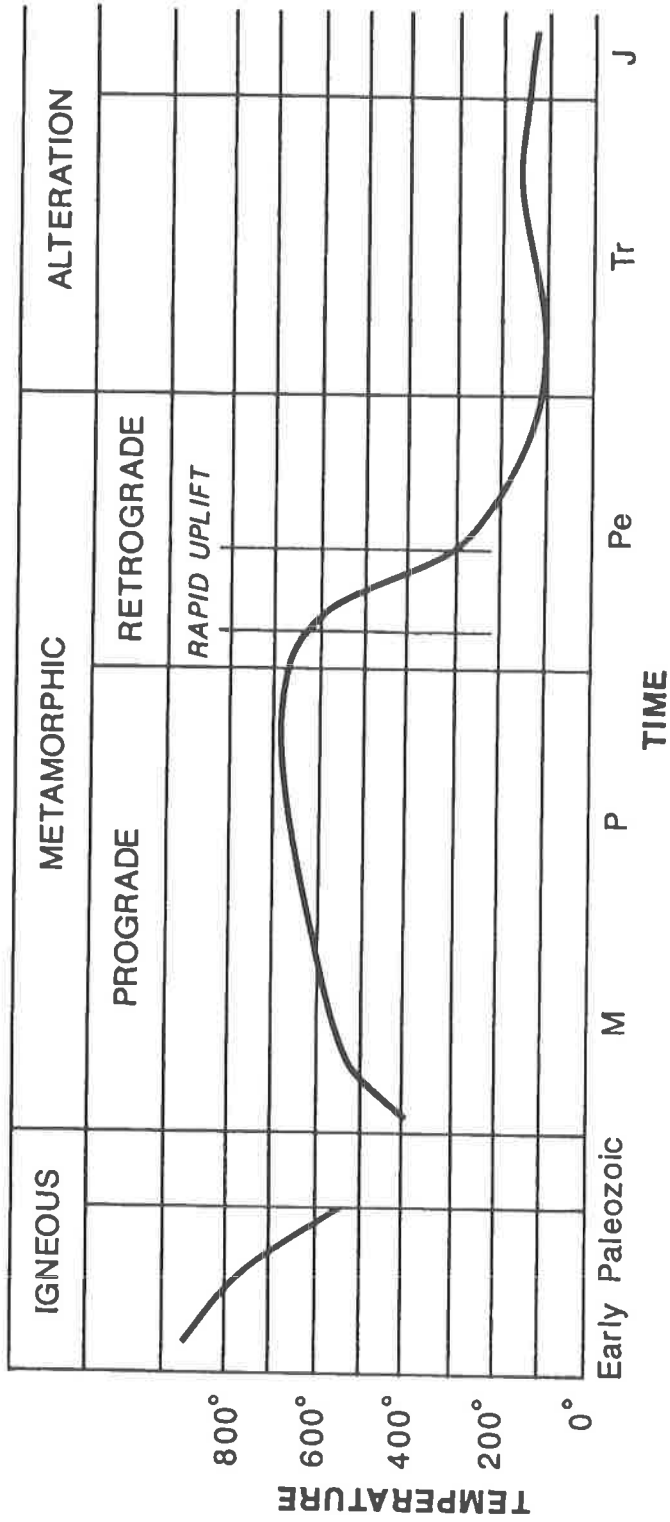
Figure 64. Time-temperature diagram for Alleghanian metamorphism. Graph illustrates relative cooling for the ultramafic complex during the Early Paleozoic. After emplacement into the Kiokee section, the ultramafites were heated and metamorphosed during the Mississippian (M) and Pennsylvanian (P). This was followed by rapid uplift and cooling during the Permian. Serpentinization probably occurred below 250°C during the Late Permian (Pe). Alteration to talc, chlorite, carbonate and quartz may have occurred during the Triassic (Tr) and/or Jurassic (J). Time and temperature constraints are presented by Dallmeyer and others (1986). Temperature is in Centigrade.

PHASES

A	Antigorite
B	Brucite
C	Chrysotile
Cl	Clinochlore
F	Forsterite
L	Lizardite
T	Talc
W	Water

METAMORPHIC REGIMES

A   Retrograde $F + W \rightarrow A$
B   Retrograde $F (+ E) + W \rightarrow L$ ($PH_2O < Pg$)
C   Prograde $L \rightarrow C \pm Cl$
D   Prograde $L \rightarrow A + F + Cl + W$ ($PH_2O = Pg$)
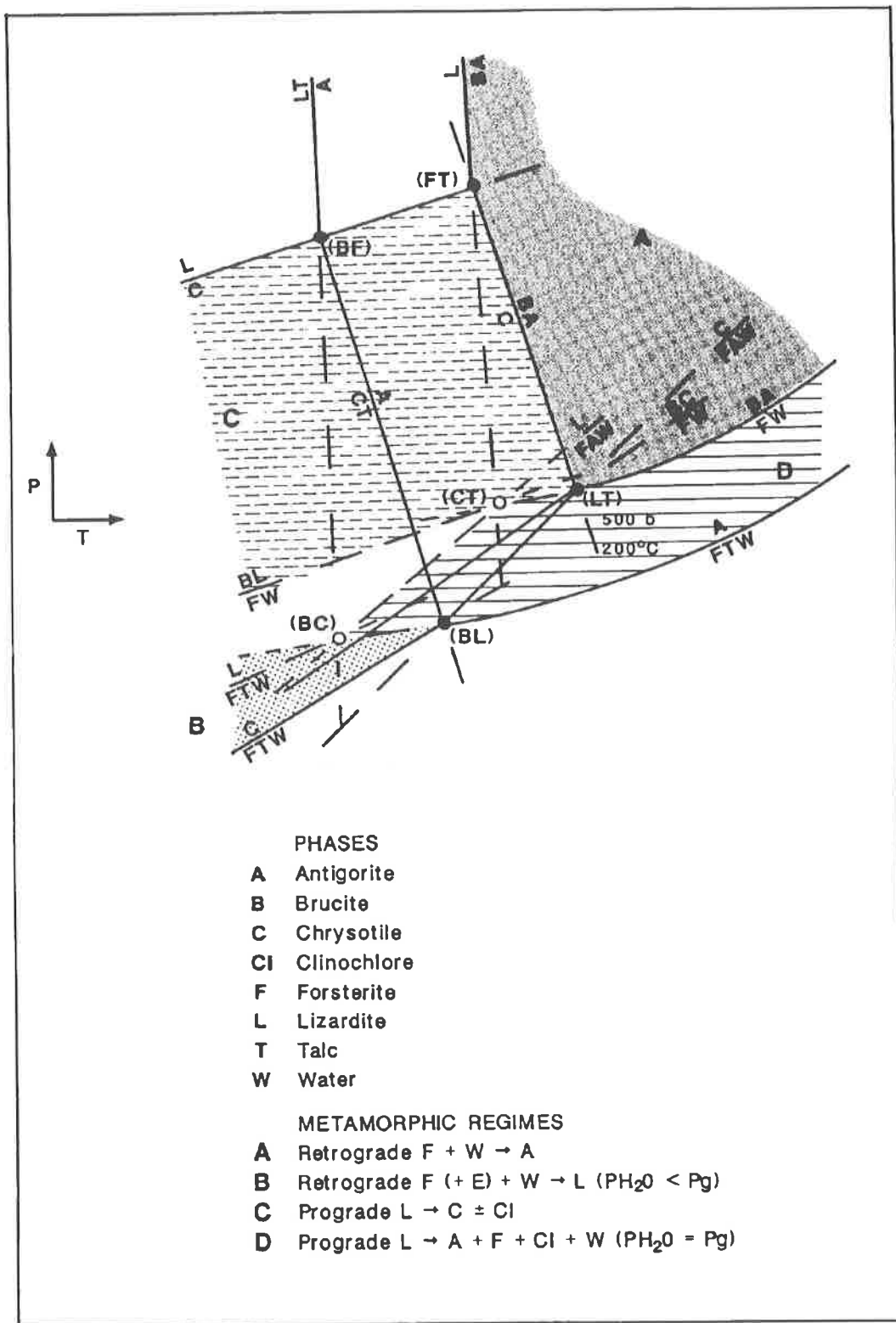
Figure 65. P-T phase diagram for MSH system. This is a schematic phase diagram illustrating the relative reactions and metamorphic regimes (after Wicks and O'Hanley, 1988). Retrograde metamorphism under most conditions should result in the formation of lizardite in regime B. The retrograde formation of antigorite is rare (only 1 or 2 occurrences are documented).
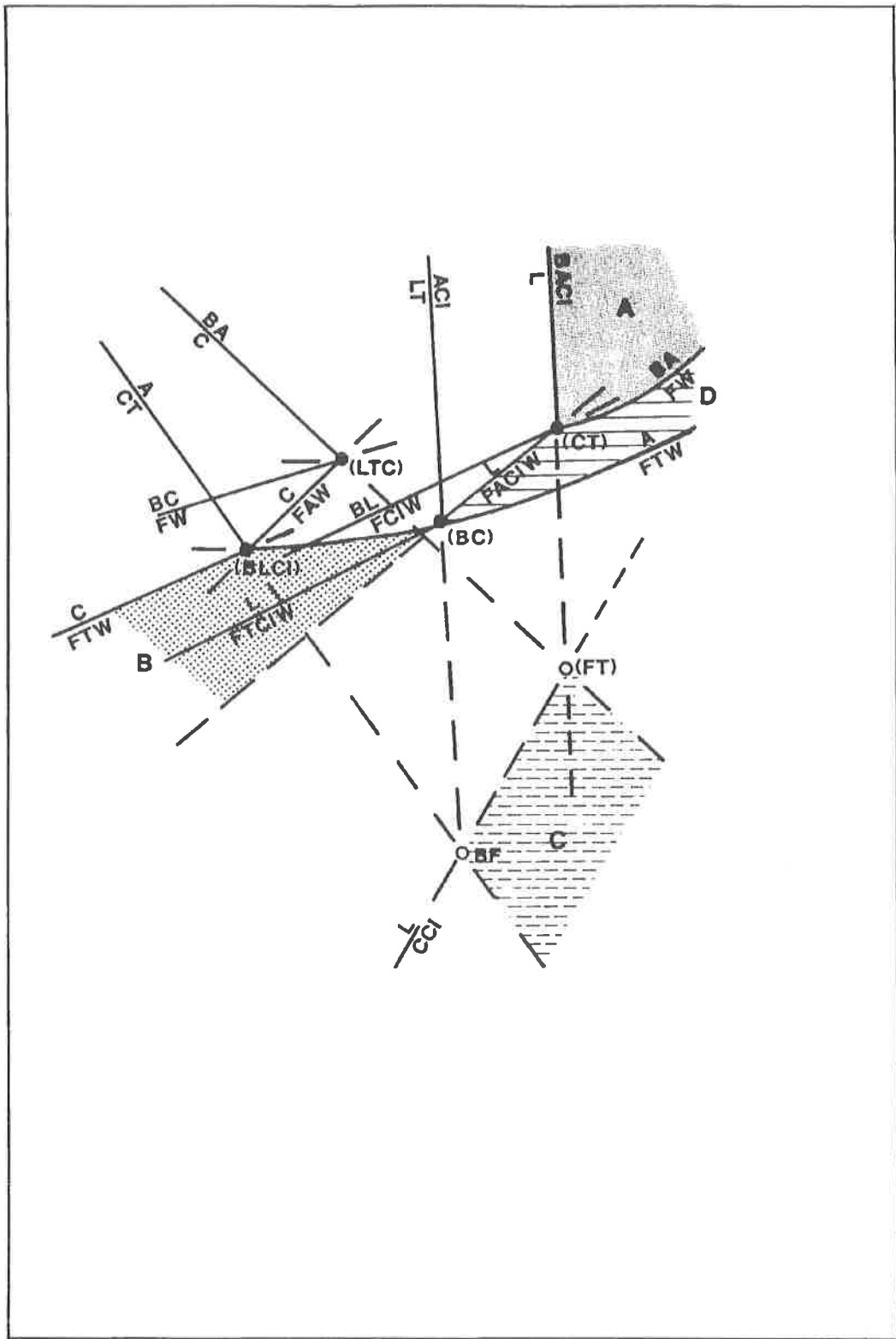
Figure 66. P-T phase diagram for MASH system. This is a schematic phase diagram illustrating the relative reactions and metamorphic regimes (after Wicks and O'Hanley, 1988).

intersection to 550°C and 5 kb for a(H_2O)=1 (Wicks and O'Hanley, 1988; Caruso and Chernosky, 1979). With an average Al_2O_3 content of less than 0.5 weight percent for the Burks Mountain serpentinites, this intersection should shift to still lower temperatures and pressures.

The reaction lizardite = chrysotile+/-clinochlore (Fig. 66) controls the P-T coordinates of the stability field of lizardite and is critical to the stability of lizardite during retrograde serpentinization. This reaction is displaced towards lower temperatures if the Al-content of lizardite increases. At pressures above those of invariant points [CT] and [BC], this reaction is stable, and lizardite is metastable during retrograde serpentinization. From these relations, low-Al, pseudomorphic lizardite is probably metastable (Wicks and O'Hanley, 1988).

During serpentinization, if water pressure, P(H_2O), is less than geostatic pressure, P(g), the system is under a hydrostatic head and depth becomes an important factor. With increasing depth, P(H_2O) will increase more rapidly than P(g) until they are equal. At any given depth, reactions with a positive slope will plot at a lower temperature and those with a negative slope will plot at a higher temperature if P(H_2O) < P(g) than if P(H_2O) = P(g) (Bruton and Helgeson, 1983). The geometry of the phase diagrams will remain unchanged, because a(H_2O)=1 (a is the activity of a component). If lizardite and chrysotile form at temperatures less than 250°C, and P(H_2O)<P(g) with thermal gradients of 30-100°C/km, fluid pressure would be 800 bars at 7.5 km or 300 bars at 2.5 km for a fluid density of 1 g/cm^3 (Bruton and Helgeson, 1983; Wicks and O'Hanley, 1988).

The Burks Mountain lizardite serpentinites can be placed within one of four major types or regimes of serpentinization (Wicks and O'Hanley, 1988). These regimes are defined by the relation of serpentine mineralogy and textures to reactions on the phase diagrams (Fig. 65 and 66). The Burks Mountain serpentinites developed in the retrograde regime B which involves the alteration of forsterite and enstatite to lizardite at low water pressure (P(H_2O)<P(g)) with production of pseudomorphic textures. This is probably a metastable reaction due to suppression of the forsterite to chrysotile reaction at low water pressures (Wicks and O'Hanley, 1988). The other regimes involve: A) the retrograde hydration of olivine to produce antigorite with decreasing temperature with P(H_2O)=P(g); C) the prograde reaction lizardite = chrysotile +/- clinochlore characteristic of chrysotile asbestos deposits; and D) the prograde reaction lizardite = antigorite + forsterite + clinochlore + water at higher temperatures and pressures with P(H_2O)=P(g) (Wicks and O'Hanley, 1988).

Maximum temperature of formation for lizardite serpentine is generally believed to occur below 200-250°C and may be as low as 100°C (Wenner and Taylor, 1971). Serpentinization at temperatures near 100°C may be possible by a non-equilibrium process of dissolution of olivine and pyroxene and the precipitation of brucite, serpentine and talc (Nesbitt and Bricker, 1978).

The age of serpentinization can not be determined directly, but within the context of a metamorphic-structural model developed for the Kiokee belt certain constraints may be placed on the timing of serpentinization. Using the time-temperature curve (Fig. 64) of Dallmeyer and others (1986), the first time that the metaharzburgites would cool from a higher temperature regime into a temperature range of 200-250°C for retrograde formation of lizardite, would be approximately 285 Ma. This Early Permian age is a maximum age of serpentinite formation.

Oxygen and hydrogen isotopic investigations of serpentinized oceanic and continental ophiolites indicate that most of the lizardite-chrysotile in continental ophiolites probably formed from hot, exchanged meteoric ground waters, mixed meteoric-magmatic waters, or mixed meteoric-connate waters instead of ocean or connate waters (Wenner and Taylor, 1973). The presence of lizardite in the Burks Mountain complex suggests but does not prove that meteoric waters were involved in formation of the Burks Mountain serpentinite.

PHYSICAL CONDITIONS DURING SERPENTINITE ALTERATION

Two distinctly different types of alteration affected the serpentinite: 1) talc + carbonate + chlorite alteration, and 2) silicification. Type 1 alteration is commonly developed as a sequence of relatively simple, essentially monomineralic zones.
The origin of these zones has been investigated in detail as a chemical mass transport process (Chidester, 1962; Jahns, 1967; and Sanford, 1982) and as a process related to the mineralogic stability relations (Hemley and others, 1977). Silicification of the Burks Mountain serpentinite involved the near total replacement of the serpentinite by quartz and certainly involved extraordinary amounts of chemical mass transport.

Origin of type 1 alteration by chemical mass transport involves movement of significant volumes of oxides between the country rock and ultramafic rock. The free energy or chemical potential differences between the country rock and ultramafite act as driving forces for diffusion of chemical components. Chemi-

cal potential differences calculated from compositional variations and equilibria among components indicate directions of mass transfer (Sanford, 1982). Some studies suggest that mass transfer involved the introduction of Si, Fe and CO_2 into the ultramafic body accompanied by the loss of H_2O and Mg (Sanford, 1982). During low-grade metamorphism Ca and CO_2 are transferred in, but at higher grades, they are removed from the ultramafic body and Na introduced. Generally, Na and K migrate into the country rock in front of the advancing chlorite zone (Sanford, 1982). Other studies suggest that Al moves outward in front of the outward growing talc zone. This conclusion is based on evidence that talc has replaced the chlorite (Jahns, 1967) but is opposite to Sanford's (1982) observations.

Although Cr_2O_3 and TiO_2 are considered immobile by Sanford (1982), magnetite-titanite intergrowths which replaced ilmenite and titanite which replaced rutile at lower greenschist facies metamorphism are petrographic evidence of the mobility of TiO_2. Numerous occurrences in New England, Virginia, North Carolina and Georgia of secondary titanite associated with chloritic alteration correlate with geochemical patterns that indicate TiO_2, is in fact, highly mobile in this environment. Significant enrichment of TiO_2 in chloritic fractures within the Burks Mountain serpentinite also demonstrate considerable mobility of TiO_2. Sanford (1982) attributes smaller Cr concentrations in the talc, talc-carbonate and actinolite-chlorite zones than in the original rock to a net volume increase. A similar decrease of Cr in the talc and chlorite zones in the Burks Mountain serpentinite is attributed in the present study to leaching of Cr from these rocks by the altering solutions. Similar modal concentrations of magnetite in the talc and chlorite zones in the Burks Mountain serpentinite suggest that volumes did not increase significantly.

An increase in silica activity or a decrease in temperature during metamorphism can also effect the observed zonation (Fig. 67). In ultramafites, talc can form from serpentine, olivine, enstatite, or amphibole (anthophyllite) with an increase in the activity of SiO_2 or a decrease in temperature. Calculated silica-activity diagrams (Fig. 67) indicate that talc could form from serpentine (antigorite) at temperatures down to at least 100°C. Because lizardite is the stable phase below 200-250°C, talc probably formed at or below that temperature. An increase in SiO_2 activity can result from an influx of SiO_2-saturated fluids, removal of MgO, or an increase in the Si/Mg ratio of the silicate fraction of the rock due to the conversion of Mg-silicate to Mg-carbonate. Influx of CO_2 to form $MgCO_3$ (Fig. 68) from serpentine releases silica which increases the activity of silica. The frequent association of carbonates and

talc in steatized serpentine favors this mechanism as the most common mode of steatization.

The stabilities of chlorites with different compositions enables estimations to be made concerning the physical conditions during chlorite formation. Chlorite is stable and will form under a broad range of metamorphic conditions from the prehnite-pumpellyite facies into the amphibolite facies. The upper limits of chlorite are defined by its breakdown to form forsterite + enstatite + green spinel + H_2O in the sillimanite zone of the amphibolite facies. The development of chlorite in a metamorphosed ultramafite requires a source of Al_2O_3.

In low-Al ultramafites like the Burks Mountain serpentinites, the most common sources of Al_2O_3 are spinels and the adjacent country rocks. The source for the Al_2O_3 in the chlorite which formed adjacent to the spinels was probably the spinels themselves. The amount of chlorite thus formed is minor compared to the large amounts of coarse-grained chlorite found in fractures in the serpentinite and in the matrix of the multilithic breccia. The formation of the coarse-grained chlorite requires an influx of solutions bearing Al_2O_3 and may require removal of SiO_2 or addition of MgO +/- FeO which is facilitated by fractures and breccias open to exchange with the surrounding rocks.

If the system is open to Al, the amount of Al substituting for Si and Mg will principally depend on the stability of the chlorite of that particular composition (Bailey, 1988b). The Al_2O_3 content of chlorites obtained from whole-rock and microprobe chemical analyses of chlorites demonstrate a strong correlation with metamorphic grade.

Within contact metamorphosed peridotite and blackwall rock, chlorite becomes more Al-rich with increasing metamorphic grade (decreasing distance) toward the heat source (Fig. 69). In the Blue River Peridotite, Cassiar, B.C., the Al_2O_3 content of chlorite increases from 1.1 weight percent 4 km (2.5 miles) away to over 19 weight percent adjacent to the batholith/peridotite contact (Pinsent and Hirst, 1977). Chlorites in thermally metamorphosed blackwall at Paddy-Go-Easy Pass in the central Cascades, Washington increase in Al_2O_3 from 12.1 weight percent in a forsterite-talc assemblage (equivalent to lower amphibolite facies) to over 20 weight percent in a chlorite-forsterite-enstatite-spinel assemblage (equivalent to upper amphibolite facies) near the batholith/ peridotite contact (Frost, 1975). The estimated maximum temperatures near the contacts are 700-750°C (Pinsent and Hirst, 1977) and greater than 700°C at 2 to 3 kb pressure (Frost, 1975).

Chlorites in ultramafic rocks subjected to regional metamorphism show a similar increase in Al_2O_3 con-
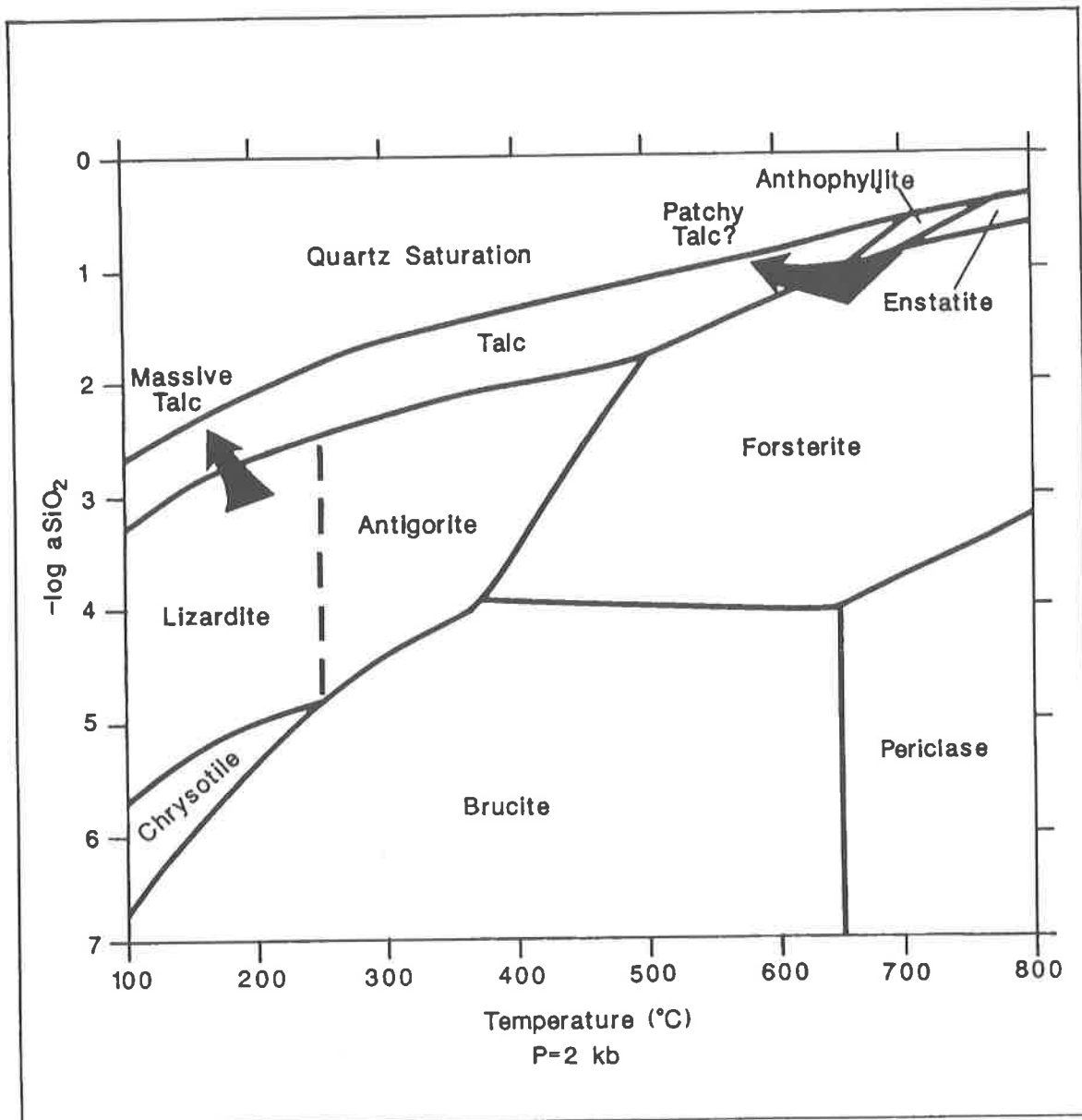
Figure 67. Silica activity versus temperature phase diagram for the MSH system. This diagram illustrates the relation of the talc stability field to those of lizardite, enstatite, forsterite (olivine). The disseminated patchy talc is anticipated to have formed at high temperatures during the retrograde alteration of enstatite +/- forsterite +/- anthophyllite. The principal mechanism for the formation of this talc is probably a decrease in temperature. The formation of the massive talc resulted from the alteration principally of lizardite at low temperatures. Talc probably formed from an increase in silica activity resulting from carbonate alteration of lizardite. The lizardite field is inserted in the antigorite field shown by Evans and Guggenheim (1988) based on the phase diagrams by Wicks and O'Hanley (1988) and the temperature anticipated for lizardite formation (see text). The boundary between lizardite and antigorite is independent of temperature (see Fig. 65 and 66).
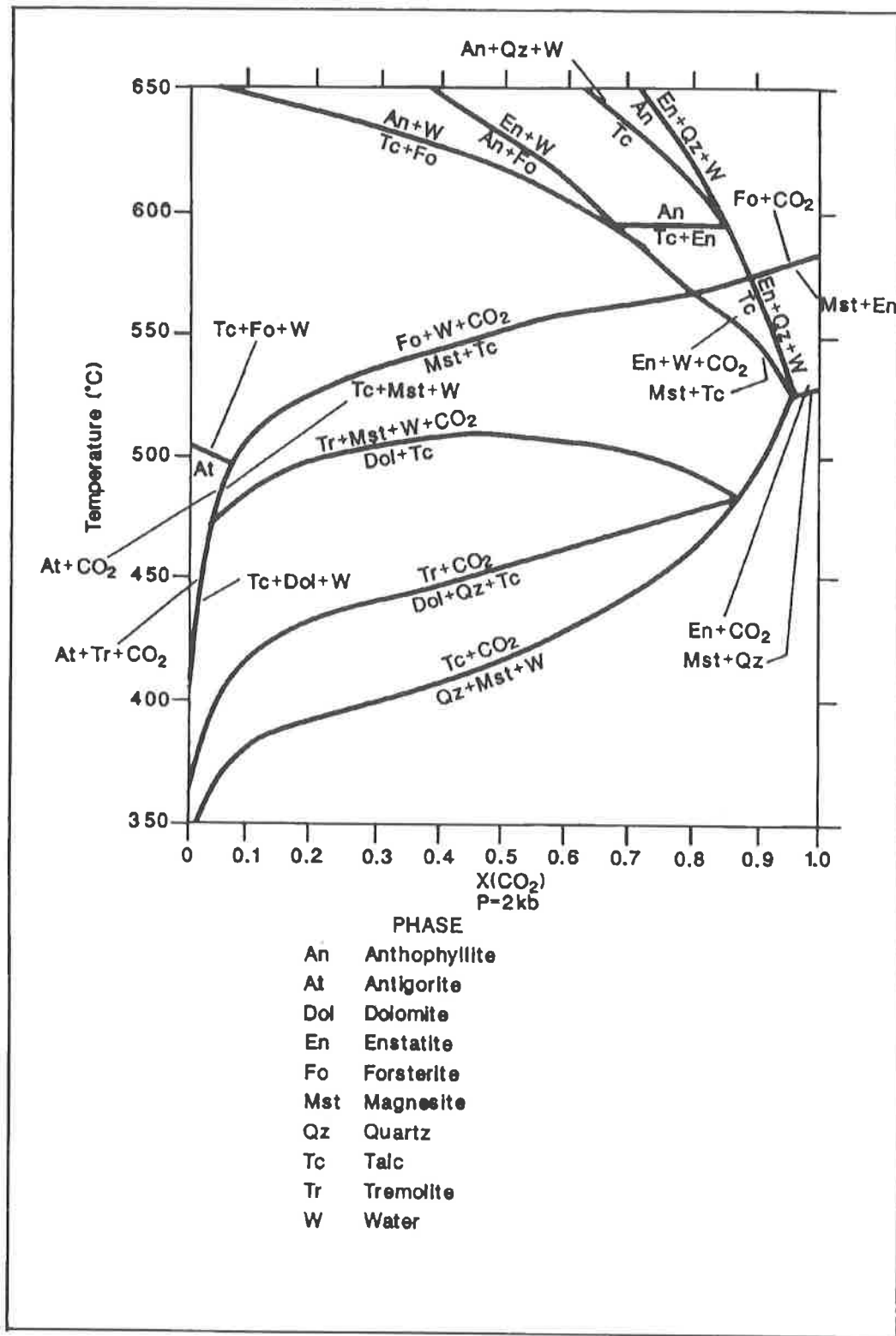
Figure 68. T-XCO$_2$ phase diagram. No similar diagrams have been constructed for lizardite at lower temperatures where lizardite would be stable. This phase diagram is constructed for antigorite with a minimum calculated temperature of 350°C. This diagram does illustrate the point that, with a slight increase in X(CO$_2$), antigorite (and probably lizardite) is unstable and will react, in general, to form talc plus magnesite, dolomite or calcite.

84
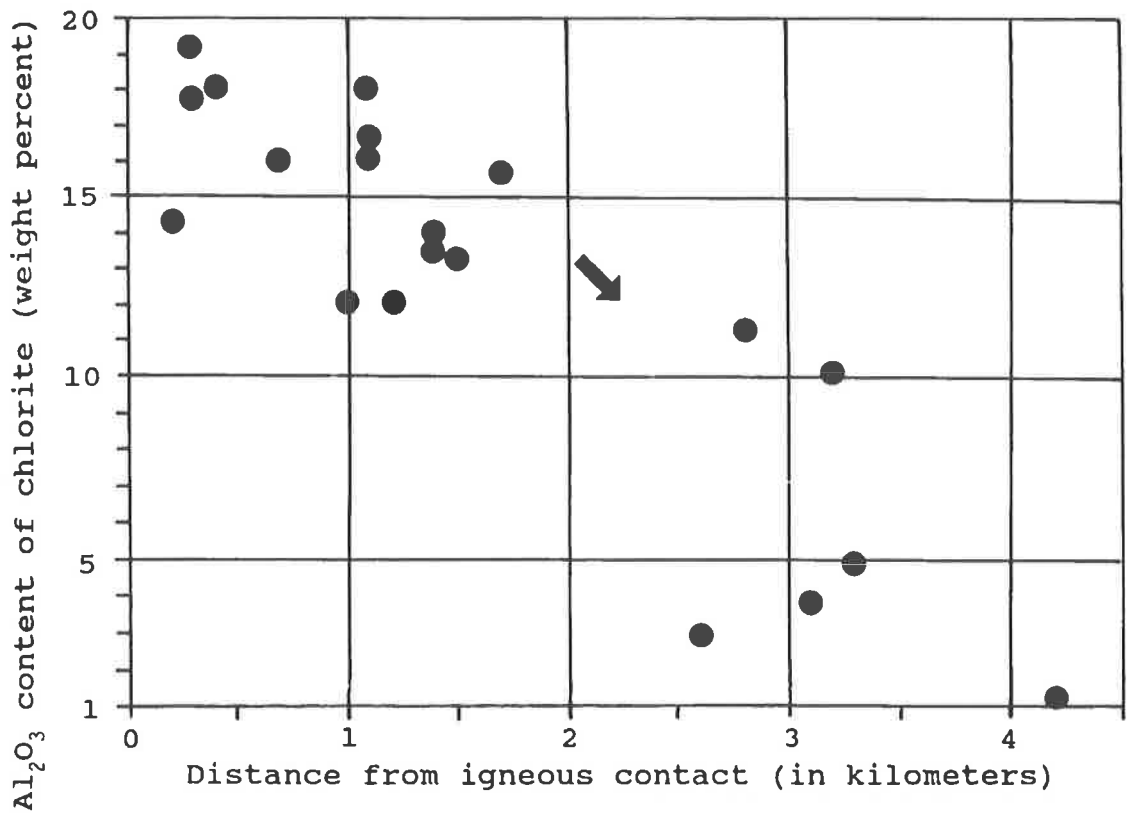
Figure 69. Chlorite Al$_2$O$_3$ content versus distance from igneous contact, WA. The intrusion of a younger batholith metamorphosed a peridotite and caused the growth of metamorphic chlorite in that peridotite. This diagram illustrates the dependence of the Al$_2$O$_3$ content of chlorite in that peridotite on temperature as reflected by the distance from the contact with the batholith. Chlorite formed at a higher temperature (and metamorphic grade) has a distinctly higher Al$_2$O$_3$ content than chlorite formed at a lower temperature (and metamorphic grade). Data is from Pinson and Hirst (1977).

tent with increasing grade. When plotted with chlorites from thermally and regionally metamorphosed ultramafites (Fig. 70), the coarse-grained chlorites from the Burks Mountain complex with low Al_2O_3 (average 7.85 weight percent) are in the range of the greenschist facies. This is compatible with the formation of lizardite under greenschist facies conditions.

Based on the evidence presented in this investigation, the conditions prevailing during the formation of lizardite and its alteration to talc, carbonate and chlorite include low temperatures, <200-250°C, and low pressures, <2.5 kb, and low $P(H_2O)$, <300 bars. Alteration of the lizardite to carbonate, talc and chlorite probably resulted from fracturing and brecciation leading to or resulting from a decrease in pressure plus the introduction of CO_2, SiO_2 and Al_2O_3. These conditions contrast with the suggested development of metasomatic reaction rims around the lizardite serpentinite bodies during amphibolite facies metamorphism (Sacks and others, 1989). The lizardite should have re-equilibrated to antigorite during upper greenschist to epidote amphibolite facies, and subsequently antigorite should break down to form olivine, enstatite and amphibole in the amphibolite facies. The second type of alteration, silicification, involves significant addition of silica and removal of most of the other oxides (see discussion under petrochemistry). The intimate association of multistage quartz veining with the silicification of Burks Mountain serpentinites is similar to other occurrences of extensive silicification and quartz veining commonly documented as hydrothermal in origin. The source of the hydrothermal silica-bearing solutions is presently unknown, but constraints on the conditions at the time of silicification can be estimated.

Sacks and others (1989) suggest that silicification occurred prior to or during amphibolite facies metamorphism; however, petrographic and field relations demonstrate silicification occurred after steatization and at low temperatures and pressures. Phase relations in the system serpentine + quartz also suggest that conditions of silicification were under relatively low temperatures. The assemblage serpentine + quartz reacts to form talc above 310°C at 1 kb. This assemblage is slightly more stable at higher pressures where the reaction takes place at 350°C at about 6.5 kb. Pressures were probably low (<3 kb) as suggested by the widespread association of open-space quartz veins with the silicification. These estimated temperature and pressure conditions plus the petrographic and field relations indicate conditions during or after silicification were well below the minimum 600°C of the amphibolite facies.

PARAGENESIS AND ORIGIN

PARAGENESIS

The paragenesis of the Burks Mountain ultramafites, detailed in Fig. 71, is inferred from petrographic, petrochemical and field relations to be:

1) intrusion and crystallization of an ultramafic/mafic magma or magmas;
2) emplacement of the Burks Mountain ultramafites into the Kiokee belt rocks;
3) prograde metamorphism of a harzburgite ultramafite to an upper amphibolite grade-assemblage of enstatite + chlorite +/-tremolite +/- anthophyllite + ferritchromite or Cr-magnetite with primary or recrystallized olivine + orthopyroxene stable;
4) retrograde metamorphism of olivine, enstatite, anthophyllite and tremolite to lizardite serpentine plus secondary magnetite;
5) fracturing/brecciation of the serpentinite and enclosing Kiokee rocks possibly by low-angle, small-scale thrusting;
6) influx of CO_2, which may be accompanied by SiO_2 and/or loss of MgO through a fracture system resulting in alteration of lizardite to carbonate + talc; CO_2 addition may extend beyond #7;
7) influx of Al_2O_3 along fractures and breccias to form coarse-grained chlorite from talc and lizardite; this may accompany or overlap #5; chloritization, albitization and biotitization of the country rocks immediately adjacent to the serpentinites also occurred at this time;
8) localized fracturing of the serpentinite with numerous periods of quartz +/- chalcedony deposition in veins and by pervasive silicification replacement of talc, serpentine, amphibole and chlorite;
9) further fracturing of serpentinite and Kiokee gneisses during Late Jurassic extensional tectonics(?) with little or no accompanying alteation.

GEOCHRONOLOGY OF METAMORPHISM AND ALTERATION

The age of the metamorphism and alteration that affected the metaharzburgites of the Burks Mountain complex is not known because of the lack of datable minerals in the metamorphic and alteration assemblages. However, certain events can be used to bracket the metamorphism and alteration of the Burks Mountain complex. The suggested model for the Burks Mountain complex is that it was emplaced into its present

Figure 70. Chlorite Al₂O₃ content versus metamorphic grade. A compilation of chlorite analyses from ultramafic rocks with documented metamorphic grades indicates a progressive increase in the Al_2O_3 content with increasing metamorphic grade. The metamorphic facies equivalents are summarized in Table 1. Data from Chidester (1962), Cocker (this report), Frost (1975), Pinsent and Hirst (1977), and Tracy and others (1984).

The chart shows Al₂O₃ content of chlorite (weight percent) on the x-axis and Metamorphic Rank on the y-axis, with the following explanation:

EXPLANATION

Metamorphic Rank	Primary Phases
1	Chrysotile
2	Lizardite
3	Antigorite
4	Forsterite - Talc
5	Forsterite - Anthophyllite
6	Forsterite - Enstatite
7	Biotite
8	Garnet
9	Kyanite
10	Sillimanite
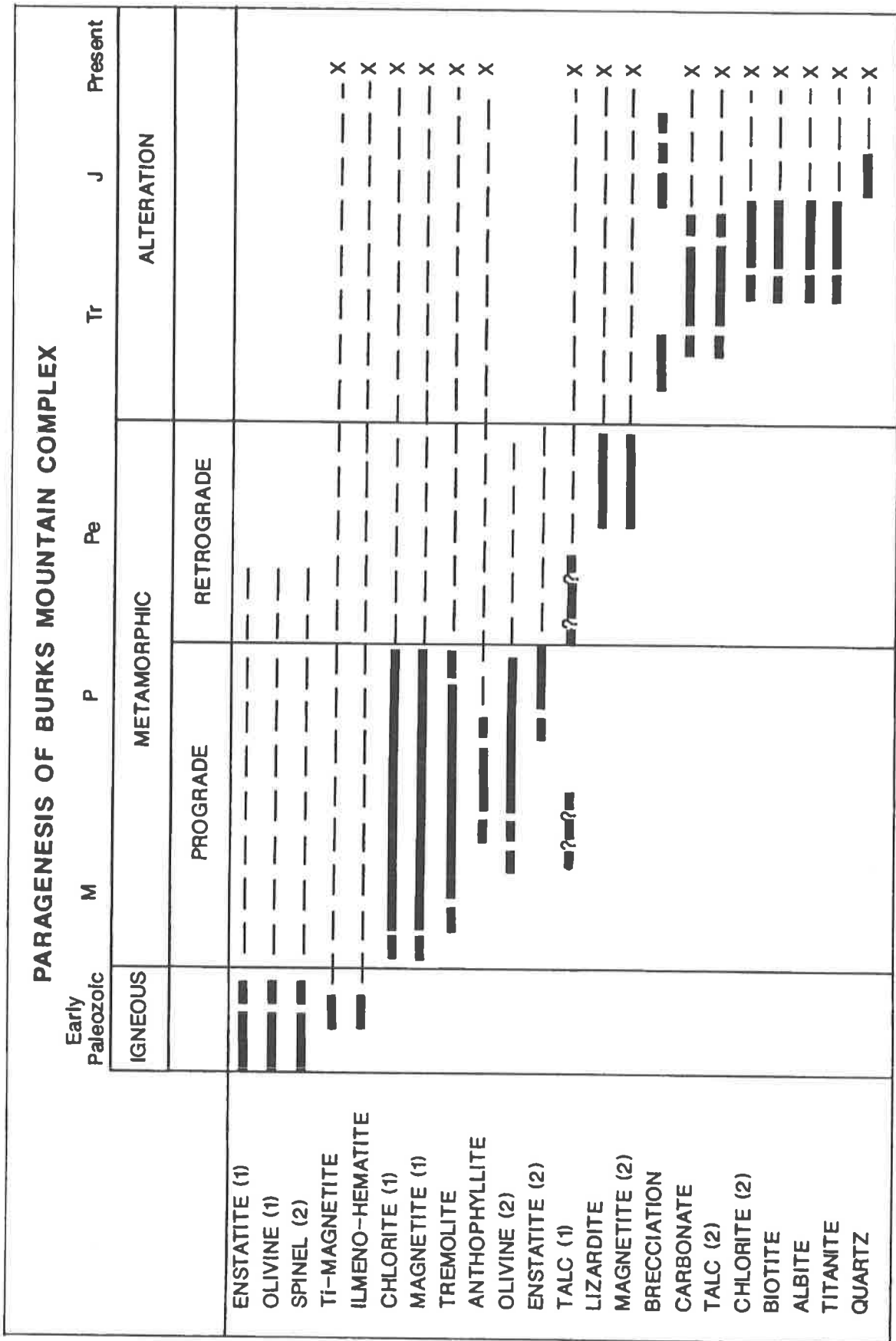
Figure 71. Paragenesis of Burks Mountain complex. The development of each mineral (or event) is illustrated by a thick solid or dashed bar. The thin dashed lines illustrate probable preservation of that phase during that time. The large X's indicate the mineral is presently preserved. Time symbols are the same as in Fig. 64. The numbers after the mineral phase refer to the relative temporal position of each phase when more than one of the same phase may have developed.

position within the Kiokee belt at some point during the Alleghanian orogeny. It was probably not emplaced prior to the Alleghanian orogeny as little evidence exists of penetrative deformation which affected the Kiokee rocks in this area during the Alleghanian orogeny.

The preserved mineral assemblages suggest that the Burks Mountain complex was subjected to middle to upper amphibolite facies prograde metamorphism. Because penetrative deformation that would accompany emplacement is absent in the metamorphic silicates, this metamorphism appears to have occurred after emplacement of the ultramafites. It is suggested that the age of peak metamorphism of the Burks Mountain complex is thus similar to the age of prograde Alleghanian metamorphism which has been established as 295 to 315 Ma in rocks from the northwest limb of the Kiokee antiform (Dallmeyer and others, 1986).

A period of rapid cooling from above approximately $500^{\circ}C$ to below approximately $300^{\circ}C$ as defined by retention of Ar in hornblende and biotite apparently occurred between 295 and 285 Ma (Dallmeyer, and others, 1986). This was followed by slower cooling through about $100\text{-}125^{\circ}C$ at 130-150 Ma as defined by apatite fission ages (Zimmerman, 1979; Naeser and Cebula, 1978; Dallmeyer and others, 1986). Rapid cooling followed by slower cooling is interpreted as recording a period of rapid uplift from mid-crustal depths followed by erosion in the latest Carboniferous and Early Permian.

It is probable that the retrograde formation of lizardite serpentine occurred at some time following the period of rapid cooling. The maximum age of serpentinization may be constrained by the last cooling of the metaharzburgites through a temperature of approximately $250^{\circ}C$. The intersection of the slope of the time-temperature curve for the Kiokee belt rocks (Dallmeyer and others, 1986) with a temperature of approximately $250^{\circ}C$ suggests a maximum age of about 270-280 Ma.

The youngest event which can be directly correlated is the chloritization in the multilithic breccia, the serpentinite, and in the immediately adjacent Kiokee rocks. This event includes the extensive development of coarse grained chlorite in fractures and breccias in the serpentinite and along the contact between the serpentinite and the country rock, and the chloritization, albitization, biotitization and TiO_2 remobilization of the country rock immediately adjacent to the serpentinite. Dating of this event does not presently exist, but the abundant secondary titanite and biotite formed at this time present an opportunity to constrain what may be the waning stages of Alleghanian metamorphism.

Silicification appears unrelated, chemically and structurally, with any previous metamorphism or alteration events and may be related to the initial stages of extensional tectonics associated with Jurassic-Triassic rifting.

ORIGIN OF THE BURKS MOUNTAIN ULTRAMAFIC ROCKS

The Burks Mountain complex contains an assemblage of serpentinite, amphibolite and metagabbro interpreted as harzburgites, basalts and gabbros (Sacks and others, 1989; Cocker, 1989a and 1989c). The complex may be part of a cumulate mafic and ultramafic intrusive and extrusive complex formed within or below the Carolina slate belt or tectonically incorporated from an exotic terrane (Sacks and others, 1989). The gneisses and schists of the Kiokee belt have been interpreted as part of an accretionary complex containing fragments (Burks Mountain complex) of the Iapetus oceanic crust (Higgins and others, 1988; Sacks and others, 1989).

Clusters of ultramafic and mafic rocks near the Inner Piedmont-Kings Mountain belt boundary, and in the Raleigh and Kiokee belts (the Burks Mountain complex) are interpreted to be a regionally distinct group of ophiolitic complexes or ophiolitic melanges (Butler, 1989). Other ultramafites in South Carolina and North Carolina are interpreted as Alpine-type or island-arc intrusive complexes (Butler, 1989). Zoned mafic-ultramafic intrusions in the Kings Mountain belt are suggested to indicate a period of intra-arc rifting during development of the Carolina terrane (Dennis and Shervais, 1988).

Ophiolites are considered to be oceanic lithosphere which may occur in midocean ridges, back-arc basins and island arcs. Ophiolites may be incorporated into continental rocks during thrusting associated with collisions involving continents or continents and arcs.

Harzburgite tectonites are a common component of the lower part of ophiolites found incorporated into continental rocks. Evidence for a tectonized harzburgite in rocks studied in this part of the Burks Mountain complex was not found in any of the core drilling and in surface outcrops examined in this investigation. A relic fabric, defined by flattened chromite grains in the serpentinized harzburgite, which would indicate that the protolith is a harzburgite tectonite is described by Sacks and others (1989). Some of the large Cr-magnetites disseminated in the serpentinite might appear to be flattened. Detailed petrographic studies in this study indicate extensive resorption and/or metamorphic reaction has deeply embayed the Cr-magnetites re-

sulting in a wide variety of shapes. Most of the shapes of these spinels are rather ornately developed and probably would not have survived penetrative deformation. Where observed in thin-sections, olivine and pyroxene pseudomorphs are not deformed. However, the high-grade metamorphism and the complete serpentinization of the harzburgite could have obscured any metamorphic fabric that might have developed in the olivine and pyroxene textures.

Current evidence does not indicate the mode of emplacement of the Burks Mountain complex. Ultramafites can be emplaced originally as ultramafic melts or as solid masses of serpentinite. As solid masses they may be squeezed into their final sites during the last stages of folding or as brecciated masses along post-orogenic faults (Chidester, 1962; Jahns, 1967; Chidester and Cady, 1972). High-temperature contact aureoles indicate that some large ultramafic masses are emplaced as melts that differentiated and cooled in place (Challis, 1965; Green, 1964a and 1964b). The relative ease of serpentinite remobilization commonly separates the ultramafic bodies from their former contact aureoles. Subsequent metamorphism may also obscure contact relations. The behavior of serpentinites as competent, relatively strong masses may obscure more extensive tectonism.

The lack of penetrative metamorphic textures, the preservation of delicate prograde metamorphic textures (Cocker, 1989a), and the preservation of a probable igneous differentiation sequence (Cocker, 1989c) strongly suggest that the ultramafite has undergone little internal tectonic deformation since it was emplaced as a melt or solid mass and subsequently metamorphosed.

The Burks Mountain complex has similarities to ophiolite complexes such as the Marum ophiolite complex in Northern Papua New Guinea (Jaques, 1981) and to layered mafic complexes such as the Stillwater in Montana and the Bushveld in South Africa. The overall poor exposure and intense weathering, in addition to the high grade metamorphism and subsequent serpentinization, steatization and silicification severely limit a more rigorous mineralogical and petrological comparison. In general, the ultramafic/mafic rock suite of the Burks Mountain complex is more similar to that of ophiolitic complexes.

Whole rock analyses suggest that the composition of the parental magma that produced the harzburgite might have been very low in TiO_2, Na_2O, K_2O, Al_2O_3 and REE's. The $100 Mg/(Mg + Fe^{+2})$ ratio was probably 80 +/- 2 (Fig. 72) which is similar to that of the Marum ophiolite parent magma (Jaques, 1981). The magma must have been Cr- and Ni-rich with 2250-2350 ppm Ni and 2000-2950 ppm Cr in the stratigraphically lowermost harzburgites.

Differentiation of a single magma probably produced the observed SiO_2-enrichment trend manifested as an increase in normative enstatite and a decrease in normative olivine with increasing stratigraphic height. The rather sudden appearance of fine-scale, rhythmic igneous layering followed by separation of an immiscible liquid which formed TiO_2-V-P-REE-rich massive magnetite segregations (Cocker, 1989c), is best interpreted as an influx of a new, more differentiated magma or magmas. The extreme enrichment in Ti-V-P-REE in an Fe-rich liquid is commonly developed within layered mafic intrusions and is not known to be associated with ophiolitic complexes.

The present investigation suggests that the Burks Mountain complex was emplaced into a more mature, differentiated, calc-alkaline suite of rocks than has previously been assigned to the Kiokee belt. The petrochemical results obtained from fresh core samples indicate that the gneisses and amphibolites enclosing the Burks Mountain serpentinites are not geochemically similar to the Carolina Slate belt volcanics which have been proposed as correlative rocks. The Na_2O-rich, Carolina Slate belt volcanics are interpreted as a primitive volcanic arc (Whitney and others, 1978). The Kiokee belt rocks are considerably higher in K_2O and may represent a more mature island arc or continental setting. The amphibolites are enriched in REE's compared with mafic volcanics commonly associated with ophiolitic complexes (Snoke and others, 1981) suggesting they are part of the Kiokee belt suite described above. The unusual enrichment of REE, Ti and V in certain layered rocks of the Burks Mountain complex suggests a subsequent intrusion of a magma enriched in those elements. Concentration of those elements may have been cause by contamination from country rocks enriched in these elements, extreme differentiation of a parent magma, or dynamic partial melting of crustal material.
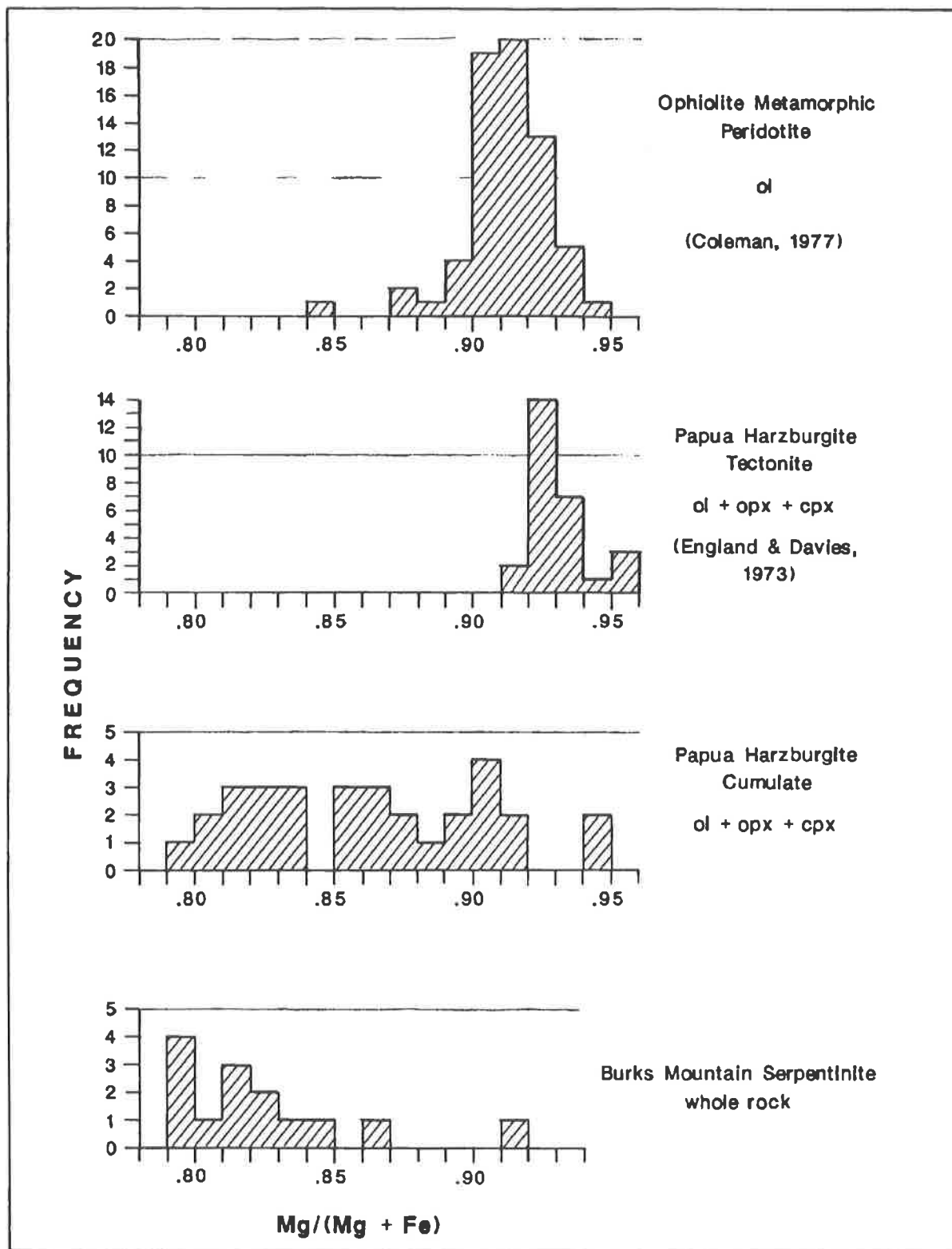
Figure 72. Frequency versus Mg/(Mg+Fe) in selected ultramafites. The high MgO content and narrow concentration of analyses distinguish residual metamorphic peridotite/harzburgite tectonite from the lower MgO content and broader range in composition of harzburgite cumulates. The distribution of analyses of Burks Mountain serpentinites is similar to that of the harzburgite cumulates.

91

REFERENCES CITED

Akpanika, O.I., Ukpong, E.E., and Olade, M.A., 1987, Mineralogy and geochemical dispersion in tropical residual soils overlying a talc deposit in southwestern Nigeria: Chemical Geology, v. 63, p. 109-119.

Armstrong, R.L., and Dick, H.J.B., 1974, A model for development of thin overthrust sheets of crystalline rock: Geology, v. 2, p. 35-40.

Bailey, S.W., 1969, Polytypism of trioctahedral 1:1 layer silicates: Clays and Clay Minerals, v. 17, p. 355-371.

Bailey, S.W., 1988, Chlorites: structures and crystal chemistry: in Bailey, S.W., ed., Hydrous Phyllosilicates (exclusive of micas): Mineralogical Society of America Reviews in Mineralogy, v. 19, p. 347-404.

Bliss, N.W. and MacLean, W.H., 1975, The paragenesis of zoned chromite from central Manitoba: Geochimica et Cosmochimica Acta, v. 39, p. 973-990.

Blount, A.M. and Vassiliou, A.H., 1980, The mineralogy and origin of the talc deposits near Winterboro, Alabama: Economic Geology, v. 75, p. 107-116.

Breiner, S., 1980, Applications for portable magnetometers: in Van Blaricom, R., ed., Practical Geophysics for the Exploration Geologist, N.W. Mining Association, Spokane, WA, p. 153-164.

Bruton, C.J. and Helgeson, H.C., 1983, Calculation of the chemical and the thermodynamic consequences of differences between fluid and geostatic pressure in hydrothermal systems: American Journal of Science, v. 283-A, p. 540-588.

Burfoot, J.D., 1930, The origin of the talc and soapstone deposits of Virginia: Economic Geology, v. 25, p. 805-826.

Butler, J.R., 1989, Review and classification of ultramafic rocks in the Piedmont of the Carolinas: in Mittwede, S.K. and Stoddard, E.F., eds., Ultramafic Rocks of the Appalachian Piedmont: Geological Society of America Special Paper 231, p.19-31.

Caruso, L. and Chernosky, J.V., Jr., 1979, The stability of lizardite: Canadian Mineralogist, v. 17, p. 757-769.

Challis, G.A., 1965, The origin of the New Zealand ultramafic intrusions: Journal of Petrology, v. 6, p. 322-364.

Chidester, A.H., 1962, Petrology and geochemistry of selected talc-bearing ultramafic rocks and adjacent country rocks in north-central Vermont: U.S. Geological Survey Professional Paper 345, 207 pp.

Chidester, A.H. and Cady, W.M., 1972, Origin and emplacement of Alpine-type ultramafic rocks: Nature Physical Science, v. 240, p. 27-31.

Cocker, M.D., 1989a, Metamorphism and deformation of the Burks Mountain ultramafic complex, Columbia County, Georgia: Geological Society of America Abstracts with Programs, v. 21, no. 3, p. 8.

Cocker, M.D., 1989b, Talc alteration of a serpentinite in the Burks Mountain ultramafic complex, Columbia County, Georgia: Geological Society of America Abstracts with Programs, v. 21, no. 3, p. 8.

Cocker, M.D., 1989c, Geochemistry of a vertically zoned, metamorphosed and serpentinized harzburgite: implications for the tectonic evolution of the southern Appalachian Piedmont: Geological Society of America Abstracts with Programs, v. 21, no. 7, p. 106.

Cocker, M.D., 1990, Mineralogy, geochemistry and genesis of REE-Ti-V enriched iron oxides in the Burks Mountain Complex, Columbia County, Georgia: Geological Society of America Abstracts with Programs, v. 22, no. 4, p. 8.

Cocker, M.D., in press (a), Geology and origin of a talc prospect in the Burks Mountain Complex, Columbia County, Georgia: in Pickering, Jr., S., Proceedings of the Symposium on the Economic Geology of Southeastern Industrial Minerals: Georgia Geologic Survey Bulletin 120, p.

Cocker, M.D., in press (b), Economic geology of altered serpentinites in the Burks Mountain complex, Columbia County, Georgia: Georgia Geological Survey Bulletin 123, pp.

Coleman, R.G., 1971, Petrologic and geophysical nature of serpentinites: Geological Society of America Bulletin, v. 82, p. 897-918.

Coleman, R.G., 1977, Ophiolites: ancient oceanic litho-

sphere?: Springer-Verlag, New York, 229 pp.

Coleman, R.G. and Keith, T.E., 1971, A chemical study of serpentinization - Burro Mountain, California: Journal of Petrology, v. 12, p. 311-328.

Cook, F.A., Albaugh, D.S., Brown, L.D., Kaufman, S., Oliver, J.E., and Hatcher, R.D., Jr., 1979, Thin-skinned tectonics in the crystalline southern Appalachians: COCORP seismic reflection profiling of the Blue Ridge and Piedmont: Geology, v. 7, p. 563-567.

Crickmay, G.W., 1952, Geology of the crystalline rocks of Georgia: Georgia Geologic Survey Bulletin 43, p. 54.

Dallmeyer, R.D., Wright, J.E., Secor, D.T., Jr., Snoke, A.W., 1986, Character of the Alleghanian orogeny in the southern Appalachians: Part II. Geochronological constraints on the tectonothermal evolution of the eastern Piedmont in South Carolina: Geological Society of America Bulletin, v. 97, p. 1329-1344.

Daniels, D.L., 1974, Geologic interpretations of geophysical maps, central Savannah River area, South Carolina and Georgia: U.S. Geological Survey Geophysical Investigations Map GP-893.

Dennis, A.J., and Shervais, J.W., 1988, Field relationships and geochemistry of arc-related mafic-ultramafic intrusives in the southern Kings Mountain belt: Geological Society of America Abstracts with Programs, v. 20, no. 4, p. 260.

Eargle, D.H., 1955, Stratigraphy of the outcropping Cretaceous rocks of Georgia: U.S. Geological Survey Bulletin 1014, 101 pp.

Ehlers, E.G., and Blatt, H., 1982, Petrology: Igneous, Sedimentary and Metamorphic: W.H. Freeman and Co., San Francisco, 732 pp.

England, R.N., and Davies, H.L., 1973, Mineralogy of ultramafic cumulates and tectonites from eastern Papua: Earth and Planetary Science Letters, v. 17, p. 416-425.

Evans, B.W. and Frost, B.R., 1975, Chrome-spinel in progressive metamorphism - a preliminary analysis: Geochimica et Cosmochimica Acta, v. 39, p. 959-972.

Evans, B.W. and Guggenheim, S., 1988, Talc, pyrophyllite and related minerals: in Bailey, S.W., ed., Hydrous Phyllosilicates (exclusive of micas): Mineralogical Society of America Reviews in Mineralogy, v. 19, p. 225-294.

Feiss, P.G., 1982, Geochemistry and tectonic setting of the volcanics of the Carolina slate belt: Economic Geology, v. 77, p. 273-293.

Frazier, W.J., and Schwimmer, D.R., 1987, Regional Stratigraphy of North America: Plenum Press, New York, 719 pp.

Frost, B.R., 1975, Contact metamorphism of serpentinite, chlorite blackwall and rodingite at Paddy-Go-Easy Pass, Central Cascades, Washington: Journal of Petrology, v. 16, p. 272-313.

Golding, H.G., and Bayliss, P., 1968, Altered chrome ores from the Coolac serpentine belt, New South Wales, Australia: American Mineralogist, v. 53, p. 162-183.

Green, D.H., 1964a, Petrogenesis of the high-temperature peridotite intrusion in the Lizard area, Cornwall: Journal of Petrology, v. 5, p. 131-188.

Green, D.H., 1964b, The metamorphic aureole of the peridotite at the Lizard, Cornwall: Journal of Geology, v. 72, p. 543-563.

Helz, R.T., 1985, Compositions of fine-grained mafic rocks, from sills and dikes associated with the Stillwater Complex, in Czamanske, G.K. and Zientek, eds., The Stillwater Complex, Montana: Geology and Guide: Montana Bureau of Mines and Geology Special Publication 92, p. 97-117.

Hemley, J.J., Shaw, D.R., and Luce, R.W., 1977, Mineral equilibria in the $MgO-SiO_2-H_2O$ system: II. Talc-antigorite-forsterite-enstatite stability relations and geologic implications in the system: American Journal of Science, v. 277, p. 353-383.

Higgins, M.W., Atkins, R.L., Crawford, T.J., Crawford, R.F., III, Brooks, R., Cook, R.B., 1988, The structure, stratigraphy, tectonostratigraphy, and evolution of the southernmost part of the Appalachian orogen: U.S. Geological Survey Professional Paper 1475, 173 pp.

Hopkins, O.B., 1914, Asbestos, talc, and soapstone

deposits of Georgia: Georgia Geologic Survey Bulletin 29, 319 pp.

Howell, D.E. and Pirkle, W.A., 1976, Geologic section across the Modoc fault zone, Modoc, South Carolina: in Chowns, T.M., ed., Stratigraphy, structure, and seismicity in Slate Belt rocks along the Savannah River, Georgia Geologic Survey/Georgia Geological Society Field Trip Guide, p. 16-20.

Hurst, V.J., Crawford, T.J., and Sandy, J., 1966, Mineral resources of the Central Savannah River area: U.S. Dept. of Commerce publication, 467 pp.

Jahns, R.H., 1967, Serpentinites in the Roxbury district, Vermont: in Wyllie, P.J., ed., Ultramafic and Related Rocks: New York, John Wiley and Sons, p. 137-160.

Jaques, A.L., 1981, Petrology and petrogenesis of cumulate peridotites and gabbros from the Marum ophiolite Complex, northern Papua New Guinea: Journal of Petrology, v. 22, p. 1-40.

Kish, S.A., Butler, J.R., and Fullagar, P.D., 1979, The timing of metamorphism and deformation in the central and eastern Piedmont of North Carolina: Geological Society of America Abstracts with Programs, v. 11, p. 184-185.

Leake, B. E., 1964, The chemical distinction between ortho- and para-amphibolites: Journal of Petrology, v. 5, Part 2, p. 238-254.

LeGrand, H.E., and Furcron, A.S., 1956, Geology and ground-water resources of central-east Georgia: Georgia Geologic Survey Bulletin 64, p. 174.

Lipin, B.R., 1984, Chromite from the Blue Ridge Province of North Carolina: American Journal of Science, v. 284, p.507-529.

Long, L.T., 1987, Analysis of gravity data over a talc deposit: Pollards Corner, GA: unpublished consulting report for the Georgia Geologic Survey, 26 pp.

MacDonald, A.H., 1984, Water diffusion rates through serpentinized peridotites. Implications for reaction induced and chemical effects in ultramafic rocks: University of Western Ontario, unpublished Ph.D. Dissertation, 226 pp.

Maher, H.D., Jr., 1978, Stratigraphy and structure of the Belair and Kiokee belts near Augusta, Georgia: in Snoke, A.W., ed., Geological investigations of the eastern Piedmont, southern Appalachians: South Carolina Geological Survey, Carolina Geological Society Guidebook for 1978, p. 47-54.

Maher, H.D., Jr., 1987, Kinematic history of mylonitic rocks from the Augusta Fault Zone, South Carolina and Georgia: American Journal of Science, v. 287, p. 795-816.

McLemore, W.H., 1965, Geology of the Pollard's Corner Area, Columbia County, Georgia, unpublished M.S. thesis, University of Georgia, 49 pp.

Moody, J.B., 1976b, An experimental study on the serpentinization of iron-bearing olivines: Canadian Mineralogist, v. 14, p. 462-478.

Naeser, C.W., and Cebula, G.T., 1978, Fission-track dating of apatite and zircon: an interlaboratory comparison: U.S. Geological Survey Open-File Report 78-104, 14 pp.

Nesbitt, H.W. and Bricker, O.P., 1978, Low temperature alteration processes affecting ultramafic bodies: Geochimica et Cosmochimica Acta, v. 42, p. 403-409.

O'Connor, B.J. and Prowell, D.C., 1976, The geology of the Belair Fault Zone and basement rocks of the Augusta, Georgia area: in Chowns, T.M., ed., Stratigraphy, structure, and seismicity in Slate Belt rocks along the Savannah River, Georgia Geologic Survey/ Georgia Geological Society Field Trip Guide, p. 16-20.

Onyeagocha, A.C., 1974, Alteration of chromite from the Twin Sisters dunite, Washington: American Mineralogist, v. 59, p. 608-612.

Parker, A., 1970, An index of weathering for silicate rocks: Geology Magazine, v. 107, p. 501-504.

Peacock, M.A., 1931, Classification of igneous rock series: Journal of Geology, v. 39, p. 54-67.

Pinsent, R.H., and Hirst, 1977, The metamorphism of the Blue River ultramafic body, Cassiar, British Columbia, Canada: Journal of Petrology, v. 18, p. 567-594.

Reynolds, I.M., 1985, Contrasted mineralogy and textural relationships in the uppermost titaniferous

magnetite layers of the Bushveld Complex in the Bierkraal area north of Rustenburg: Economic Geology, v. 80, p. 1027-1048.

Rogers, J.J.W., 1982, Criteria for recognizing environments of formation of volcanic suites; Application of these criteria to volcanic suites in the Carolina slate belt, in Bearce, D.N., Black, W.W., Kish, S.A., and Tull, J.F., eds., Tectonic studies in the Talladega and Carolina slate belts, southern Appalachian orogen: Geological Society of America Special Paper 191, p. 99-   107.

Sacks, P.E., and Dennis, A.J., 1987, The Modoc Zone - D2 (Early Alleghanian) in the Eastern Appalachian Piedmont, South Carolina and Georgia: in Snoke, A.W., ed., Geological investigations of the eastern Piedmont, southern Appalachians: Columbia, South Carolina Geological Survey, Carolina Geological Society Guidebook for 1978, p. 19-34.

Sacks, P.E., Maher, H.D., Jr., and Secor, D.T., 1987, The Burks Mtn. belt of ultramafic rocks in the Kiokee belt, southern Appalachian Piedmont: Geological Society of America Abstracts with Programs, v. 19, p. 127.

Sacks, P.E., Maher, H.D., Secor, D.T., Shervais, J.W., 1989, The Burks Mountain complex, Kiokee belt, southern Appalachian Piedmont of South Carolina and Georgia: in Mittwede, S.K. and Stoddar, E.F., eds., Ultramafic Rocks of the Appalachian Piedmont: Geological Society of America Special Paper 231, p.   75-86.

Sanford, R.F., 1982, Growth of ultramafic reaction zones in greenschist to amphibolite facies metamorphism: American Journal of Science, v. 282, p. 543-616.

Savin, S.M. and Lee, M., 1988, Isotopic studies of phyllosilicates: in Bailey, S.W., ed., Hydrous Phyllosilicates (exclusive of micas): Mineralogical Society of America Reviews in Mineralogy, v. 19, p. 189-224.

Secor, D.T., Jr., 1987, Regional Overview: in Secor, D.T., Jr. (ed.) Anatomy of the Alleghanian orogeny as seen from the Piedmont of South Carolina and Georgia: Carolina Geological Society Field Trip Guidebook, p. 1-18.

Secor, D.T., Jr., Samson, S.L., Snoke, A.W., and Palmer, A.R., 1983, Confirmation of the Carolina slate belt as an exotic terrane: Science, v. 221, p. 649-650.

Secor, D.T., Jr., Snoke, A.W., Bramlett, K.W., Costello, O.P., and Kimbrell, O.P., 1986a, Character of the Alleghanian orogeny in the southern Appalachians: Part I. Alleghanian deformation in the eastern Piedmont of South Carolina: Geological Society of America Bulletin, v. 97, p. 1319-1328.

Secor, D.T., Jr., Snoke, A.W., and Dallmeyer, R.D., 1986b, Character of the Alleghanian orogeny in the southern Appalachians: Part III. Regional tectonic relations: Geological Society of America Bulletin, v. 97, p. 1345-1353.

Shelley, S.A., Shervais, J.W., and Secor, D.T., Jr., 1988, Geochemical characterization of metavolcanic rocks of the Carolina slate belt, central South Carolina: Geological Society of America Abstracts with Programs, v. 20, no. 4, p. 314.

Shteinberg, D.S., 1960, Novye dannye o serpentinizatsii dunitov Urala [New data concerning the serpentinization of dunites and peridotites of the Urals]: Rep. 21st Int. Geol. Cong. Doklady Sovet. Geol. Prob., v.13, p. 250-260.

Snoke, A.W., Quick, J.E., Bowman, H.R., 1981, Bear Mountain igneous complex, Klamath Mountains, California: an ultrabasic to silicic calc-alkaline suite: Journal of Petrology, v. 22, p. 501-55.

Snoke, Arthur, W., and Frost, B. Ronald, 1988, High pressure pelitic schist from the Lake Murray Spillway, South Carolina Piedmont: Geological Society of America Abstracts with Programs, v. 20, no. 4, p. 316.

Springer, R.K., 1974, Contact metamorphosed ultramafic rocks in the western Sierra Nevada foothills, California: Journal of Petrology, v. 15, p. 160-195.

Telford, W.M., Geldart, L.P., Sheriff, R.E., and Keys, D.A., 1976, Applied Geophysics, Cambridge University Press, New York, N.Y., 860 pp.

Tracy, R.J., Robinson, P., and Wolff, R.A., 1984, Metamorphosed ultramafic rocks in the Bronson Hill anticlinorium, Central Massachusetts: American Journal of Science, v. 284, p. 530-558.

Tschudy, R.H., and Patterson, S.H., 1975, Palynological evidence for Late Cretaceous, Paleocene and

Early and Middle Eocene ages for strata in the kaolin belt, central Georgia: U.S. Geological Survey, Journal of Research, v. 3, p. 437-445.

Tull, J.F., 1978, Structural development of the Alabama Piedmont northwest of the Brevard Zone: American Journal of Science, v. 278, p. 442-460.

Van der Plas, L. and Tobi, A.C., 1965, A chart for judging the reliability of point counting results: American Journal of Science, v. 263, p. 87-90.

Vick, H.K., Channell, J.E.T., and Opdyke, N.D., 1987, Ordovician docking of the Carolina slate belt: Paleomagnetic data: Tectonics, v. 6, p. 573-583.

Vincent, H.R., McConnell, K.I., and Perley, P.C., 1990, Geology of selected mafic and ultramafic rocks of Georgia: a review: Georgia Geologic Survey Information Circular 82, 59 pp.

Wenner, D.B. and Taylor, H.P., 1971, Temperatures of serpentinization of ultramafic rocks based on O^{18}/O^{16} fractionation between co-existing serpentine and magnetite: Contributions to Mineralogy and Petrology, v. 32, p. 165-185.

Wenner, D.B., and Taylor, H.P., 1973, Oxygen and hydrogen isotope studies of the serpentinization of ultramafic rocks in oceanic environments and continental oceanic environments and continental ophiolite complexes: American Journal of Science, v. 273, p. 207-239.

Wharton, C.H., 1978, The Natural Environments of Georgia: Georgia Geological Survey Miscellaneous Publication, 227 pp.

Whitney, J.A., Paris, R.H., Carpenter, R.H., and Hartley, M.E., III, 1978, Volcanic evolution of the southern slate belt of Georgia and South Carolina - A primitive volcanic arc: Journal of Geology, v. 86, p. 173-192.

Whitney, James A., Herz, Norman, and Leagato, Jeff M., 1987, Allochthonous mafic and ultramafic lithologies from near the Russell Reservoir, eastern Georgia: evidence for Late Paleozoic thrust emplacement of a dismembered ophiolite: Geological Society of America Abstracts with Programs, v. 19, no. 2, p. 136.

Wicks, F.J. and O'Hanley, D.S., 1988, Serpentine minerals: structures and petrology: in Bailey, S.W., ed.,

Hydrous Phyllosilicates (exclusive of micas): Mineralogical Society of America Reviews in Mineralogy, v. 19, p. 91-164.

Williams, H., and Hatcher, R.D., 1982, Suspect terranes and accretionary history of the Appalachian orogen: Geology, v. 10, p. 530-536.

Worthington, J.E., 1964, An exploration program for nickel in the southeastern United States: Economic Geology, v. 59, p. 97-109.

Yoder, H.S., Jr., 1968, Albite-anorthite-quartz-water at 5 Kb.: Carnegie Institute of Washington Year Book, v.67, p. 477-478.

Zimmerman, R.A., 1979, Apatite fission track evidence of post-Triassic uplift in the central and southern Appalachians: Geological Society of America Abstracts with Programs, v. 11, p. 219.

APPENDICES

APPENDIX I.

Whole Rock Chemistry - Mafic and Felsic Rocks
(values are in weight percent, except for V, Co and Ba which are in ppm)

	A	B	C	D	E	F	G	H	I	J
SiO_2	46.1	43.9	50.7	47.9	65.5	70.0	50.6	76.1	75.3	74.0
Al_2O_3	19.6	17.2	16.0	16.6	14.8	14.5	16.3	14.1	0.9	14.0
Fe_2O_3	9.40	7.2	5.3	7.2	3.6	0.73	6.2	0.4	10.2	0.01
FeO	2.0	4.0	3.8	5.8	1.5	3.3	5.1	0.26	2.7	0.85
MgO	0.45	8.3	7.0	5.2	2.3	1.2	4.9	0.11	6.3	0.56
CaO	19.0	14.5	4.3	6.9	3.1	3.0	7.5	1.5	1.2	1.2
Na_2O	0.74	1.6	3.2	4.0	4.0	3.5	3.5	4.2	0.03	4.0
K_2O	0.2	0.37	1.2	0.77	1.6	2.5	1.2	4.1	0.02	4.5
LOI	1.4	0.9	7.1	2.8	1.9	0.4	2.8	0.3	1.2	0.07
TiO_2	1.1	1.1	1.3	1.9	0.77	0.54	2.1	0.05	0.01	0.08
P_2O_5	0.23	0.22	0.24	0.27	0.14	0.1	0.56	0.01	0.14	0.03
MnO	0.17	0.18	0.18	0.21	0.11	0.13	0.25	0.029	0.17	0.09
SrO		0.14	0.053	0.001		0.03				0.007
Rb_2O		0.001	0.006	0.001		0.008				0.0005
Ni	0.0002					0.0015				0.001
Cr	0.0295					0.0145				0.003
V	285.0					200.0			25.0	15.0
Co										
Ba	90.0					280.0			20.0	150.0
TOTAL	100.418	99.611	100.379	99.552	99.32	99.938	100.019	101.159	98.17	99.331

	K	L	M	N	O	P	Q	R	S
SiO_2	72.1	71.3	76.7	62.5	70.5	58.0	65.6	70.0	64.4
Al_2O_3	15.0	14.7	12.7	15.6	14.4	16.1	18.9	16.8	15.0
Fe_2O_3	0.94	1.3	0.65	5.0	1.2	5.3	3.6	2.4	3.6
FeO	1.8	1.3	0.81	0.3	1.5	2.4	0.23	0.26	0.83
MgO	0.64	0.56	0.39	2.7	0.68	3.6	0.31	0.33	2.6
CaO	2.3	2.0	1.1	1.7	1.8	5.8	0.032	0.019	3.2
Na_2O	3.9	3.5	4.2	2.2	3.3	3.8	0.08	0.15	4.0
K_2O	4.5	4.2	3.2	1.9	4.7	1.6	1.4	3.0	3.2
LOI	0.5	0.5	0.4	6.4	1.0	1.9	7.9	6.0	1.7
TiO_2	0.36	0.34	0.18	0.62	0.33	1.2	0.35	0.28	0.78
P_2O_5	0.11	0.09	0.03	0.02	0.11	0.32	0.01	0.01	0.29
MnO	0.038	0.042	0.036	0.072	0.048	0.16	0.029	0.038	0.058
SrO	0.034		0.016						
Rb_2O	0.015	0.009							
Ni									
Cr									
V				55.0	30.0	155.0	35.0	25.0	80.0
Co									
Ba				51.0	105.0	33.0	20.0	41.0	105.0
TOTAL	102.237	99.832	100.421	99.012	99.568	100.18	99.441	99.287	99.331

Sample		Location		
A	PC 88-2, 60'	DDH 88-2	60	feet
B	S1-43	DDH 87-1	43	feet
C	S1-175	DDH 87-1	175	feet
D	S4-225	DDH 87-4	225	feet
E	S2-81	DDH 87-2	81	feet
F	S1-231	DDH 87-1	231	feet
G	PC88-2, 61'	DDH 88-2	61	feet
H	S2-88	DDH 87-2	88	feet
I	E900-S500	surface		
J	PC88-2, 222'	DDH 88-2	222	feet
K	S1-282	DDH 87-1	282	feet
L	S2-43	DDH 87-2	43	feet
M	S1-208	DDH 87-1	208	feet
N	D230-240	surface		
O	E300-N00	surface		
P	E50-S2275	surface		
Q	E50-N70	surface		
R	E50-N310	surface		
S	E50-S2410	surface		

Surface samples are located in Figure 73.

APPENDIX II.

Whole Rock Chemistry - Ultramafic Rocks
(values are in weight %, except for V, Co and Ba which are in ppm)

	A	B	C	D	E	F	G	H	I	J	K
SiO_2	41.6	40.6	40.8	40.8	38.6	35.1	36.2	33.4	36.9	37.0	40.1
Al_2O_3	0.34	0.47	0.46	0.37	0.32	0.34	0.40	0.35	0.38	0.46	0.42
Fe_2O_3	6.4	5.3	6.5	2.5	6.2	7.2	5.1	5.9	5.386	7.655	6.658
FeO	0.73	0.78	0.39	0.89	0.30	1.4	0.41	2.30	2.10	0.75	0.81
MgO	36.80	35.90	36.10	36.70	35.00	37.10	37.50	36.90	35.10	35.60	36.20
CaO	0.076	0.08	1.10	0.60	2.90	2.00	0.48	0.84	0.45	1.70	0.69
Na_2O	0.03	0.03	0.01	0.01	0.02	0.02	0.04	0.04	0.005	0.005	0.005
K_2O	0.03	0.02	0.01	0.02	0.02	0.01	0.01	0.02	0.024	0.011	0.012
LOI	13.4	15.2	13.2	12.4	16.0	16.0	17.3	18.5	15.2	17.6	13.4
TiO_2	0.01	0.01	0.01	0.01	0.01	0.01	0.01	0.01	0.01	0.01	0.01
P_2O_5	0.01	0.01	0.01	0.01	0.01	0.01	0.01	0.01	0.01	0.02	0.01
MnO	0.17	0.085	0.067	0.056	0.12	0.12	0.11	0.12	0.12	0.09	0.10
SrO	0.001	0.001	0.001	0.001	0.004	0.006	0.001	0.002			
Rb_2O	0.001	0.001	0.001	0.001	0.001	0.001	0.001	0.001			
Ni	0.230	0.170	0.225	0.245	0.230	0.225	0.235	0.220	0.210	0.235	0.205
Cr	0.310	0.310	0.445	0.280	0.200	0.285	0.175	0.295	0.099	0.110	0.077
V									5.0	15.0	5.0
Co		70.0	90.0	85.0		90.0	95.0	105.0			
TOTAL	100.138	98.967	99.329	94.893	99.935	99.827	97.982	98.908	95.994	101.246	98.697

	L	M	N	O	P	Q	R	S	T	U
SiO_2	61.0	55.5	42.1	31.5	41.2	39.7	37.6	43.7	37.9	52.9
Al_2O_3	0.37	1.0	0.62	0.35	3.8	7.8	10.4	5.9	12.3	6.9
Fe_2O_3	1.1	3.4	4.8	2.9	1.9	9.4	6.0	3.9	5.9	12.3
FeO	1.5	1.3	1.1	1.5	0.96	0.89	0.41	0.6	1.7	2.2
MgO	30.1	30.2	24.1	28.5	36.9	26.2	25.5	31.0	24.1	22.6
CaO	0.022	0.82	8.4	7.0	0.23	0.03	0.04	0.71	2.3	0.51
Na_2O	0.01	0.04	0.04	0.04	0.05	0.07	0.01	0.28	0.25	0.23
K_2O	0.02	0.02	0.036	0.024	0.03	0.03	0.05	0.15	0.75	0.18
LOI	5.00	6.40	15.40	24.10	13.80	14.70	18.10	14.10	12.10	7.80
TiO_2	0.01	0.01	0.01	0.01	0.09	0.12	0.30	0.16	0.51	0.21
P_2O_5	0.01	0.01	0.01	0.01	0.01	0.01	0.01	0.01	0.43	0.04
MnO	0.033	0.047	0.37	0.13	0.024	0.07	0.074	0.085	0.22	0.23
SrO	0.001									
Rb_2O	0.001									
Ni			0.130	0.195	0.070	0.410	0.140	0.093	0.110	0.120
Cr			0.210	0.220	0.020	0.170	0.120	0.120	0.105	0.113
V			20.0	5.0						
Co										
TOTAL	99.266	98.747	97.326	96.479	99.084	99.600	98.754	100.808	98.675	99.633

APPENDIX II. (cont.)

	V	W	X	Y	Z	AA	AB	AC	AD
SiO_2	41.8	89.0	89.2	90.4	85.8	75.1	15.0	43.9	46.1
Al_2O_3	11.1	0.12	0.43	0.21	0.45	0.21	11.2	17.2	19.6
Fe_2O_3	24.7	5.8	6.7	5.4	4.3	2.1	38.2	7.2	9.398
FeO	0.38	0.30	0.43	0.43	0.26	0.65	2.7	4.0	2.0
MgO	9.70	2.30	1.80	2.00	7.70	10.80	15.80	8.30	0.45
CaO	0.031	0.091	0.021	0.022	0.017	4.20	0.10	14.50	19.00
Na_2O	0.04	0.0	0.03	0.01	0.03	0.02	0.02	1.60	0.74
K_2O	0.06	0.024	0.02	0.04	0.02	0.02	0.05	0.37	0.20
LOI	9.90	1.4	1.6	1.3	1.9	7.6	6.4	0.9	1.4
TiO_2	0.26	0.01	0.01	0.01	0.01	0.01	9.20	1.10	1.10
P_2O_5	0.19	0.01	0.02	0.05	0.02	0.01	0.34	0.22	0.23
MnO	0.042	0.066	0.060	0.025	0.069	0.110	0.300	0.180	0.170
SrO						0.059		0.140	
Rb_2O						0.125		0.001	
Ni	0.195	0.165	0.165	0.110	0.094			0.021	0.0
Cr	0.460	0.260	0.220	0.180	0.125			0.01	0.030
V	100.0	5.0	5.0	5.0	5.0		750.0		285.0
Co			35.0			15.0			
TOTAL	98.858	99.546	100.706	100.187	100.795	101.014	99.341	99.611	100.418

Sample		Location	Sample		Location
A	S1-74	DDH 87-1 74 feet	B	S4-90	DDH 87-4 90 feet
C	S4-140	DDH 87-4 140 feet	D	S5-158.5	DDH 87-4 158.5 feet
E	S1-160	DDH 87-1 160 feet	F	S4-196	DDH 87-4 196 feet
G	S5-205	DDH 87-5 205 feet	H	S5-236	DDH 87-5 236 feet
I	PC88-2, 115'	DDH 88-2 115 feet	J	PC88-2, 151'	DDH 88-2 151 feet
K	PC88-2, 176'	DDH 88-2 176 feet	L	S1-132	DDH 87-1 132 feet
M	S5-163	DDH 87-5 163 feet	N	PC88-2, 203'	DDH 88-2 203 feet
O	PC88-2, 128'	DDH 88-2 128 feet	P	S5-177	DDH 87-5 177 feet
Q	S4-23	DDH 87-4 23 feet	R	S4-47	DDH 87-4 47 feet
S	S4-170	DDH 87-4 170 feet	T	PC1-173	DDH 87-1 173 feet
U	PC88-2, 104'	DDH 88-2 104 feet	V	D-139	surface
W	PC88-3, 18'	DDH 88-3 18 feet	X	BM-1	surface
Y	PC104-1	surface	Z	B-825	surface
AA	S5-103	DDH 87-5 103 feet	AB	B-850	surface
AC	S1-43	DDH 87-1 43 feet	AD	PC88-2, 60'	DDH 88-2 60 feet

Surface samples are located in Figure 73.

Norms - Mafic and Felsic Rocks

	A	B	C	D	E	F	G	H
Corundum	2.298	0.0	1.221	0.798	0.0	0.052	0.0	0.985
Quartz	8.686	0.637	27.132	30.052	5.166	32.295	25.364	29.821
Orthoclase	7.603	4.703	9.706	14.842	7.221	24.023	26.139	24.987
Albite	29.028	29.028	34.982	34.742	29.752	30.148	35.235	32.436
Anorthite	21.341	25.917	14.848	14.377	25.69	7.313	9.968	9.397
Diopside	0.0	6.040	0.0	0.0	6.707	0.0	0.526	0.0
Hy(En)	18.690	10.910	5.879	3.000	9.570	0.270	1.450	1.400
Hy(Fs)	0.840	1.650	0.0	4.830	0.970	0.120	1.820	0.840
Magnetite	8.238	10.790	3.040	1.063	9.142	0.575	1.340	1.897
Chromite	0.0	0.0	0.0	0.0	0.022	0.0	0.0	0.0
Hematite	0.0	0.0	1.599	0.0	0.0	0.0	0.0	0.0
Ilmenite	2.647	3.730	1.501	1.030	4.061	0.094	0.672	0.650
Apatite	0.596	0.646	0.333	0.233	1.321	0.023	0.250	0.210

	A	B	C	D	E	F	G	H
Anorthite	40.930	41.120	28.720	31.290	44.540	16.360	22.460	22.900
Albite	59.070	58.880	71.280	68.710	55.460	83.640	77.540	77.100
Di(En)	0.0	44.850	0.0	0.0	46.420	0.0	25.540	0.0
Di(Fs)	0.0	5.150	0.0	0.0	3.580	0.0	24.460	0.0
Di(Wo)	0.0	50.0	0.0	0.0	50.0	0.0	50.0	0.0
Hy(En)	96.680	89.690	100.0	44.960	92.840	75.270	51.090	68.830
Hy(Fs)	3.320	10.310	0.0	55.040	7.160	24.730	48.910	31.170
Di+En+Fo	18.690	16.950	5.879	3.00	16.277	0.270	1.976	1.400
Di	0.0	35.634	0.0	0.0	41.205	0.0	26.619	0.0
En	100.0	64.366	100.0	100.0	58.795	100.0	73.381	100.0

	I	J	K	L	M	N	O	P	Q
Corundum	0.386	0.891	0.0	0.0	19.020	14.254	7.431	0.0	0.0
Quartz	36.814	28.570	14.098	19.465	65.470	61.252	37.595	66.084	0.0
Orthoclase	18.906	28.177	9.621	19.307	9.136	19.005	12.126	0.124	2.215
Albite	35.531	28.329	32.721	34.548	0.745	1.362	20.104	0.262	13.159
Anorthite	5.303	8.327	22.543	13.815	0.102	0.027	8.964	2.331	38.429
Nepheline	0.0	0.0	0.0	0.0	0.0	0.0	0.0	0.0	0.301
Diopside	0.0	0.0	3.587	0.358	0.0	0.0	0.0	2.231	26.087
Hy (En)	0.970	3.046	7.459	6.443	0.852	0.882	7.259	15.145	0.0
Hy (Fs)	0.720	0.0	0.0	0.0	0.0	0.0	0.0	0.0	0.0
Fo (Ol)	0.0	0.0	0.0	0.0	0.0	0.0	0.0	0.0	6.761
Fa (Ol)	0.0	0.0	0.0	0.0	0.0	0.0	0.0	0.0	0.0
Magnetite	0.942	1.765	4.863	0.615	0.0	0.164	0.0	9.514	8.238
Chromite	0.0	0.0	0.0	0.0	0.0	0.0	0.0	0.0	0.0
Hematite	0.0	0.0	2.039	3.251	3.976	2.460	3.24	3.957	0.0
Ilmenite	0.342	0.636	2.319	1.512	0.605	0.570	0.851	0.019	2.647
Apatite	0.070	0.259	0.755	0.686	0.025	0.025	0.051	0.334	0.0
Rutile	0.0	0.0	0.0	0.0	0.069	0.0	0.221	0.0	0.0

	I	J	K	L	M	N	O	P	Q
Anorthite	12.33	21.70	39.37	27.37	11.42	1.86	29.59	89.34	73.35
Albite	87.67	78.30	60.63	72.63	88.58	98.14	70.41	10.66	26.65
Di (En)	0.0	0.0	50.0	50.0	0.0	0.0	0.0	50.0	48.55
Di (Fs)	0.0	0.0	0.0	0.0	0.0	0.0	0.0	0.0	1.45
Di (Wo)	0.0	0.0	50.0	50.0	0.0	0.0	0.0	50.0	50.0
Forsterite	0.0	0.0	0.0	0.0	0.0	0.0	0.0	0.0	97.09
Fayalite	0.0	0.0	0.0	0.0	0.0	0.0	0.0	0.0	2.91
Hy (En)	63.930	62.980	100.0	100.0	100.0	100.0	100.0	100.0	0.0
Hy (Fs)	36.070	37.020	0.0	0.0	0.0	0.0	0.0	0.0	0.0
Di+En+Fo	0.970	3.046	11.046	6.081	0.852	0.882	7.259	17.376	32.848
Di	0.0	0.0	32.473	5.264	0.0	0.0	0.0	12.840	79.417
En	100.0	100.0	67.527	94.736	100.0	100.0	100.0	87.160	0.0
Fo	0.0	0.0	0.0	0.0	0.0	0.0	0.0	0.0	20.583

Sample		Location
A	S1-175	DDH 87-1 175 feet
B	S4-225	DDH 87-4 225 feet
C	S2-81	DDH 87-2 81 feet
D	S1-231	DDH 87-1 231 feet
E	PC88-2, 61'	DDH 88-2 61 feet
F	S2-88	DDH 87-2 88 feet
G	S1-282	DDH 87-1 282 feet
H	S2-43	DDH 87-2 43 feet
I	S1-208	DDH 87-1 208 feet
J	E300-N00	surface
K	E50-S2275	surface
L	E50-S2410	surface
M	E50-N70	surface
N	E50-N310	surface
O	D230-240	surface
P	E900-S500	surface
Q	PC1-43	DDH 87-1 43 feet

Surface samples are located in Figure 73.

Norms - Ultramafic Rocks

	A	B	C	D	E	F	G	H	I	J	K
Corundum	0.165	0.330	0.0	0.0	0.0	0.0	0.0	0.0	0.0	0.0	0.0
Quartz	0.0	0.0	0.0	0.0	0.0	0.0	0.0	0.0	0.0	0.0	0.0
Orthoclase	0.204	0.141	0.069	0.143	0.141	0.070	0.073	0.147	0.177	0.077	0.083
Albite	0.293	0.303	0.098	0.102	0.201	0.201	0.420	0.421	0.051	0.051	0.051
Anorthite	0.361	0.399	1.371	1.098	0.863	0.965	1.094	0.892	1.167	1.436	1.274
Diopside	0.0	0.0	3.809	1.895	12.621	8.418	1.385	3.283	1.182	6.613	2.074
Hy (En)	52.991	53.673	46.283	49.733	30.281	16.004	29.570	17.40	40.620	30.288	46.400
Hy (Fs)											
Fo (Ol)	36.907	37.180	39.476	42.172	47.451	63.287	59.941	66.827	46.970	50.90	40.87
Fa (Ol)											
Magnetite	3.569	3.274	1.56	3.025	2.134	6.117	2.713	9.932	9.446	3.878	4.015
Chromite	0.769	0.796	1.112	0.730	0.513	0.732	0.467	0.789	0.181	0.194	0.133
Hematite	4.917	4.069	6.471	0.944	5.915	4.370	4.450	0.488	0.151	6.476	5.036
Ilmenite	0.022	0.023	0.022	0.023	0.023	0.023	0.023	0.024	0.023	0.023	0.023
Apatite	0.027	0.028	0.027	0.028	0.028	0.028	0.029	0.029	0.028	0.056	0.028
Anorthite	53.76	55.41	92.94	91.00	80.16	81.87	71.07	66.65	95.59	96.38	95.95
Albite	46.24	44.59	7.06	9.0	19.84	18.13	28.93	33.35	4.41	3.62	4.05
Di (En)			50.0	50.0	50.0	50.0	50.0	50.0	50.0	50.0	50.0
Di (Fs)											
Di (Wo)			50.0	50.0	50.0	50.0	50.0	50.0	50.0	50.0	50.0
Forsterite	100.0	100.0	100.0	100.0	100.0	100.0	100.0	100.0	100.0	100.0	100.0
Fayalite											
Hy (En)	100.0	100.0	100.0	100.0	100.0	100.0	100.0	100.0	100.0	100.0	100.0
Hy (Fs)											
Di+En+Fo	89.898	90.853	89.568	93.80	90.353	87.709	90.896	87.510	88.772	87.801	89.344
Diopside	0.0	0.0	4.253	2.02	13.969	9.598	1.524	3.752	1.332	7.532	2.321
Enstatite	58.946	59.077	51.674	53.020	33.514	18.247	32.532	19.883	45.758	34.496	51.934
Forsterite	41.054	40.923	44.074	44.959	52.517	72.156	65.945	76.365	52.911	57.972	45.745

	L	M	N	O	P	Q	R	S	T
Corundum	9.039	12.788	4.637	3.863	0.234	12.78	0.373	0.410	12.635
Quartz	0.133	0.0	0.0	0.0	88.481	31.804	87.804	74.964	0.0
Orthoclase	0.210	0.368	1.025	0.208	0.236	0.396	0.118	0.118	0.319
Albite	0.702	0.105	2.739	0.497	0.0	0.0	0.204	0.167	0.0
Anorthite	0.100	0.166	3.996	1.263	0.0	0.0	0.048	2.697	0.0
Diopside	0.0	0.0	0.0	0.0	0.0	0.0	0.0	0.0	0.0
Hy (En)	77.38	76.040	65.310	50.22	5.038	27.155	4.522	19.39	18.507
Hy (Fs)	0.0	0.0	0.0	0.05	0.0	0.0	0.0	0.0	0.0
Fo (Ol)	2.07	16.780	0.0	40.39	0.0	0.0	0.0	0.0	16.698
Fa (Ol)	0.0	0.0	0.0	0.04	0.0	0.0	0.0	0.0	0.0
Magnetite	3.260	0.862	2.02	3.324	1.521	0.575	1.745	1.15	0.0
Chromite	0.0	0.0	0.0	0.0	0.0	0.761	0.327	0.186	0.016
Hematite	8.899	6.868	3.115	0.0	0.0	27.155	5.556	3.555	41.101
Ilmenite	0.270	0.709	0.351	0.201	0.019	0.555	0.002	0.019	6.862
Apatite	0.027	0.029	0.027	0.027	0.118	0.496	0.046	0.046	0.848
Na-carbonate	0.0	0.0	0.0	0.0	0.085	4.66	0.010	0.018	0.706
Rutile	0.0	0.0	0.0	0.0	0.0	0.0	0.0	0.0	6.286

	L	M	N	O	P	Q	R	S	T
Anorthite	11.79	59.88	57.90	70.55	0.0	0.0	0.0	0.0	0.0
Albite	88.21	40.12	42.10	29.45	100.0	100.0	100.0	100.0	0.0
Di (En)	0.0	0.0	0.0	0.0	0.0	0.0	0.0	0.0	0.0
Di (Fs)	0.0	0.0	0.0	0.0	0.0	0.0	0.0	0.0	0.0
Di (Wo)	0.0	0.0	0.0	0.0	0.0	0.0	0.0	0.0	0.0
Forsterite	100.0	100.0	100.0	99.93	0.0	0.0	0.0	0.0	100.0
Fayalite	0.0	0.0	0.0	0.07	0.0	0.0	0.0	0.0	0.0
Hy (En)	100.0	100.0	100.0	99.93	100.0	100.0	100.0	100.0	100.0
Hy (Fs)	0.0	0.0	0.0	0.07	0.0	0.0	0.0	0.0	0.0
Di+En+Fo	77.38	78.11	82.09	90.61	5.038	27.155	4.522	19.32	35.205
Diopside	0.0	0.0	0.0	0.0	0.0	0.0	0.0	0.0	0.0
Enstatite	100.0	97.35	79.559	55.42	100.0	100.0	100.0	100.0	52.569
Forsterite	0.0	2.65	20.441	44.58	0.0	0.0	0.0	0.0	47.431

Sample		Location		
A	S1-74	DDH 87-1	74	feet
B	S4-90	DDH 87-4	90	feet
C	S4-140	DDH 87-4	140	feet
D	S5-158.5	DDH 87-4	158.5	feet
E	S1-160	DDH 87-1	160	feet
F	S4-196	DDH 87-4	196	feet
G	S5-205	DDH 87-5	205	feet
H	S5-236	DDH 87-5	236	feet
I	PC88-2, 115'	DDH 88-2	115	feet
J	PC88-2, 151'	DDH 88-2	151	feet
K	PC88-2, 176'	DDH 88-2	176	feet
L	S4-23	DDH 87-4	23	feet
M	S4-47	DDH 87-4	47	feet
N	S4-170	DDH 87-4	170	feet
O	S5-177	DDH 87-5	177	feet
P	PC104-1	surface		
Q	D-139	surface		
R	BM-1	surface		
S	B-825	surface		
T	B-850	surface		

Surface samples are located in Figure 73.

Note: Hy (En) = enstatite component of hypersthene;
       Hy (Fs) = ferrosalite component of hypersthene;
       Di (En) = enstatite component of diopside;
       Di (Fs) = ferrosalite component of diopside;
       Di (Wo) = wollastonite component of diopside;
       Fo = forstersite component of olivine;
       Fa = fayalite component of olivine.

Modal Analyses - Mafic and Felsic Rocks

	A	B	C	D	E	F	G	H
Hornblende	50.6	0.0	32.55	1.55	0.0	0.0	0.0	43.45
Epidote	25.45	0.0	0.0	0.0	0.65	0.0	0.0	0.0
Plagioclase	18.26	0.0	0.0	0.0	0.33	0.0	0.0	2.24
Magnetite	5.09	0.0	0.0	0.0	0.33	0.0	0.0	2.24
Apatite	0.3	0.0	0.26	0.0	0.0	0.0	0.0	1.28
Zircon	0.3	0.0	0.0	0.0	0.0	0.0	0.0	0.0
Quartz	0.0	33.22	3.15	23.6	30.94	29.77	36.16	0.0
Plagioclase	0.0	44.63	43.57	40.37	28.99	23.41	26.71	46.96
Microcline	0.0	19.22	0.0	26.71	29.64	0.0	33.88	0.0
Biotite	0.0	2.28	8.4	5.9	7.82	24.75	2.93	6.07
Zircon	0.0	0.33	0.0	0.0	0.0	0.67	0.0	0.0
Opague	0.0	0.33	3.67	0.0	0.0	0.0	0.33	0.0
Biotite(sec)	0.0	0.0	8.4	0.0	0.0	0.0	0.0	0.0
Muscovite	0.0	0.0	0.0	1.86	1.30	0.0	0.0	0.0
Titanite	0.0	0.0	0.0	0.0	0.0	0.67	0.0	0.0
Orthoclase	0.0	0.0	0.0	0.0	0.0	20.74	0.0	0.0
TOTAL	100.0	100.0	100.0	100.0	100.0	100.0	100.0	100.0

Note: Biotite (sec) is biotite formed during chloritic and albitic alteration.

Sample		Location	
A	PC1-43	DDH 87-1	43 feet
B	PC1-208	DDH 87-1	208 feet
C	PC1-175	DDH 87-1	175 feet
D	PC1-282	DDH 87-1	282 feet
E	PC2-43	DDH 87-2	43 feet
F	PC2-81	DDH 87-2	81 feet
G	PC2-88	DDH 87-2	88 feet
H	PC4-225	DDH 87-4	225 feet

APPENDIX VI.

Modal Analyses - Ultramafic Rocks

	A	B	C	D	E	F	G	H	I	J	K	L
Lizardite	84.89	79.63	76.42	70.10	67.97	67.17	65.31	62.88	48.05	42.26	42.12	40.91
Talc	0.64	13.27	12.26	17.36	25.82	16.41	0.94	22.71	10.71	37.10	27.58	14.55
Carbonate	9.65	3.4	0.0	3.54	0.0	5.17	26.25	0.0	29.55	8.06	18.48	35.45
Chlorite(b)	0.0	0.31	2.52	0.64	1.96	1.82	0.0	10.48	8.44	9.35	3.64	0.3
Chlorite(gy)	0.0	0.0	0.31	0.0	0.0	0.0	0.0	0.0	0.0	0.0	0.0	0.0
Chlorite(tot)	0.0	0.31	2.83	0.64	1.96	1.82	0.0	10.48	8.44	9.35	3.64	0.3
Tremolite	2.57	0.0	0.0	0.0	0.0	0.0	0.94	0.0	0.65	0.0	0.0	0.0
Anthophyllite	0.0	0.0	0.0	0.0	0.0	0.0	0.0	0.0	0.0	0.0	0.0	0.0
Magnetite	2.25	3.4	8.49	8.36	4.25	9.42	6.56	3.93	2.6	3.23	8.18	8.79
Picotite	0.0	0.0	0.0	0.0	0.0	0.0	0.0	0.0	0.0	0.0	0.0	0.0
Quartz	0.0	0.0	0.0	0.0	0.0	0.0	0.0	0.0	0.0	0.0	0.0	0.0
Chalcedony	0.0	0.0	0.0	0.0	0.0	0.0	0.0	0.0	0.0	0.0	0.0	0.0
Garnierite	0.0	0.0	0.0	0.0	0.0	0.0	0.0	43.23	0.0	0.0	0.0	0.0
Zoisite	0.0	0.0	0.0	0.0	0.0	0.0	0.0	0.0	0.0	0.0	0.0	0.0
TOTAL	100.0	100.0	100.0	100.0	100.0	100.0	100.0	100.0	100.0	100.0	100.0	100.0

	M	N	O	P	Q	R	S	T	U	V	W	X
Lizardite	37.05	35.74	27.72	12.58	6.29	5.14	1.27	0.0	0.0	0.0	0.0	0.0
Talc	24.26	22.95	59.41	75.48	57.86	93.57	36.62	21.12	22.57	45.37	53.4	17.1
Carbonate	33.77	35.74	0.66	0.97	6.29	0.0	10.51	20.5	0.0	0.0	22.22	0.0
Chlorite(b)	3.93	2.95	6.60	3.23	25.47	0.0	46.82	47.2	0.31	0.31	0.62	0.0
Chlorite(gy)	0.0	0.0	0.0	0.0	0.0	0.0	0.0	0.0	0.0	0.0	0.0	0.0
Chlorite(tot)	3.93	2.95	6.60	3.23	25.47	0.0	46.82	47.2	0.31	0.31	0.62	0.0
Tremolite	0.0	0.66	0.0	0.0	0.0	0.0	0.0	0.0	0.0	0.0	0.0	0.0
Anthophyllite	0.0	0.0	0.0	0.0	0.0	0.0	0.0	0.0	0.0	0.0	0.0	0.0
Magnetite	0.98	1.97	4.29	7.74	4.09	1.29	4.78	1.55	0.31	2.16	5.86	4.84
Picotite	0.0	0.0	0.0	0.0	0.0	0.0	0.0	0.0	0.0	0.0	0.0	0.0
Quartz	0.0	0.0	1.32	0.0	0.0	0.0	0.0	9.63	68.03	46.91	17.90	78.06
Chalcedony	0.0	0.0	0.0	0.0	0.0	0.0	0.0	0.0	8.78	5.25	0.0	0.0
Garnierite	0.0	0.0	0.0	0.0	0.0	0.0	0.0	0.0	0.0	0.0	0.0	0.0
Zoisite	0.0	0.0	0.0	0.0	0.0	0.0	0.0	0.0	0.0	0.0	0.0	0.0
TOTAL	100.0	100.0	100.0	100.0	100.0	100.0	100.0	100.0	100.0	100.0	100.0	100.0

	Y	Z	AA	AB	AC	AD	AE	AF	AG
Lizardite	0.0	0.0	0.0	0.0	0.0	0.0	0.0	0.0	0.0
Talc	1.0	16.61	15.41	39.2	0.0	79.0	0.0	0.65	56.86
Carbonate	0.0	0.0	0.0	0.0	0.0	0.0	0.0	0.0	0.0
Chlorite(b)	20.6	13.74	0.0	0.31	0.0	2.82	0.0	0.0	0.33
Chlorite(gy)	0.0	64.54	0.0	0.0	87.5	0.0	59.59	67.1	0.0
Chlorite(tot)	20.6	78.27	0.0	0.31	87.5	2.82	59.59	67.1	0.33
Tremolite	0.0	0.0	0.0	0.0	0.0	0.0	0.0	0.0	0.0
Anthophyllite	0.33	0.0	0.0	0.0	0.0	16.3	30.81	31.94	39.54
Magnetite	4.32	5.11	5.66	5.86	12.5	1.88	6.69	0.32	3.27
Picotite	0.0	0.0	0.0	0.0	0.0	0.0	2.91	0.0	0.0
Quartz	73.75	0.0	78.93	54.63	0.0	0.0	0.0	0.0	0.0
Chalcedony	0.0	0.0	0.0	0.0	0.0	0.0	0.0	0.0	0.0
Garnierite	0.0	0.0	0.0	0.0	0.0	0.0	0.0	0.0	0.0
Zoisite	0.0	0.0	0.0	0.0	0.0	0.0	1.74	0.0	0.0
TOTAL	100.0	100.0	100.0	100.0	100.0	100.0	100.0	100.0	100.0

Note: (b) = blue birefringent chlorite;
(gy) = gray birefringent chlorite;
(tot) = total chlorite.

Sample		Location		Sample		Location	
A	PC1-78	DDH 87-1	78 feet	B	PC4-140	DDH 87-4	140 feet
C	EV 5	surface		D	PC4-185	DDH 87-4	185 feet
E	PC1-88	DDH 87-1	88 feet	F	PC5-156	DDH 87-5	156 feet
G	PC4-196	DDH 87-4	196 feet	H	EV 11	surface	
I	PC5-195	DDH 87-5	195 feet	J	PC4-210	DDH 87-4	210 feet
K	PC4-90	DDH 87-4	90 feet	L	PC5-236	DDH 87-5	236 feet
M	PC5-219	DDH 87-5	219 feet	N	PC5-209	DDH 87-5	209 feet
O	PC4-67	DDH 87-4	67 feet	P	PC4-73	DDH 87-4	73 feet
Q	PC5-158	DDH 87-5	158 feet	R	PC1-132	DDH 87-1	132 feet
S	PC1-144	DDH 87-1	144 feet	T	PC5-103	DDH 87-5	103 feet
U	PC5-122	DDH 87-5	122 feet	V	PC5-147	DDH 87-5	147 feet
W	PC5-149	DDH 87-5	159 feet	X	AP 5	surface	
Y	AP 2	surface		Z	AP 3	surface	
AA	AP 1	surface		AB	AP 1A	surface	
AC	EV 1A	surface		AD	EV 7	surface	
AE	EV 4	surface		AF	EV 9	surface	
AG	EV 5	surface					

Surface samples are located in Figure 73.

EXPLANATION

Sample Site	Sample Number		Sample Site	Sample Number
1	D230-240		13	EV 1A
2	E300-N00		14	EV 4
3	E50-S2275		15	EV 5
4	E50-N70		16	EV 7
5	E50-N310		17	EV 9
6	E900-S500		18	EV 11
7	E50-S2410		19	AP 1
8	D-139		20	AP 1A
9	BM-1		21	AP 2
10	PC104-1		22	AP 3
11	B-825		23	AP 4
12	B-850			

Figure 73. Sample Location Maps. Maps are portions of the northwestern corner of the Evans 7.5 Minute and northeastern corner of the Appling 7.5 Minute Quadrangle Maps of the United States Geological Survey. Samples include those collected during this investigation and some which were collected by Vincent and others (1990). The EV and AP series were collected by Vincent and others (1990).

APPLING QUADRANGLE
GEORGIA—COLUMBIA CO.
7.5 MINUTE SERIES (TOPOGRAPHIC)
SE/4 APPLING 15' QUADRANGLE
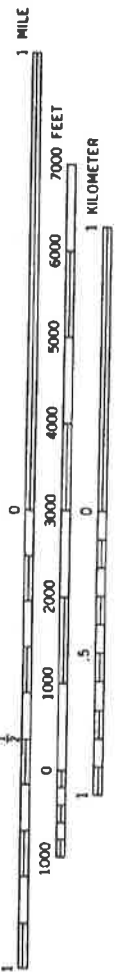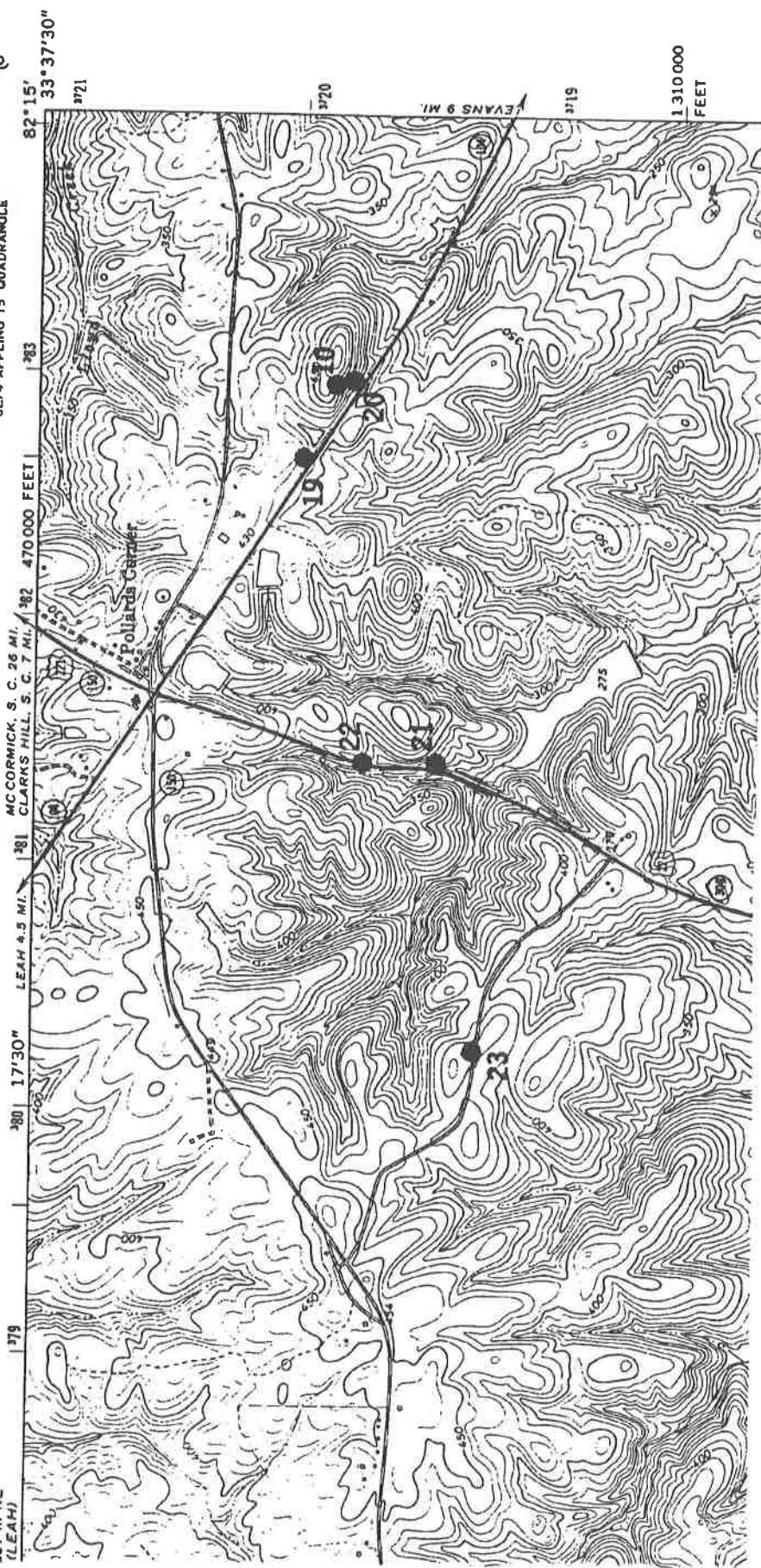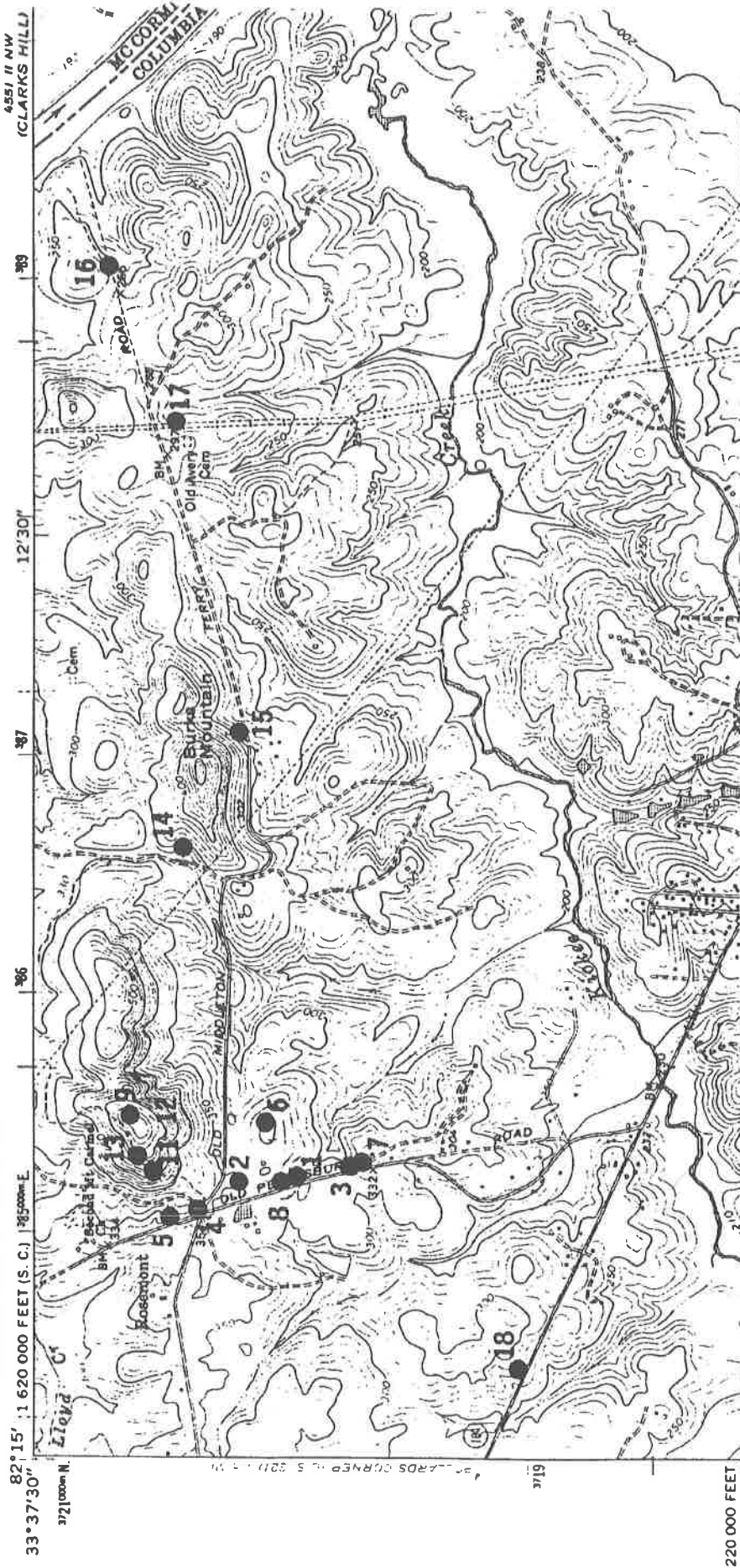
CONTOUR INTERVAL 10 FEET
DATUM IS MEAN SEA LEVEL
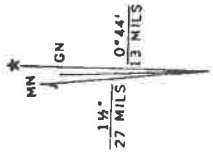
UTM GRID AND 1971 MAGNETIC NORTH
DECLINATION AT CENTER OF SHEET

UNITED STATES
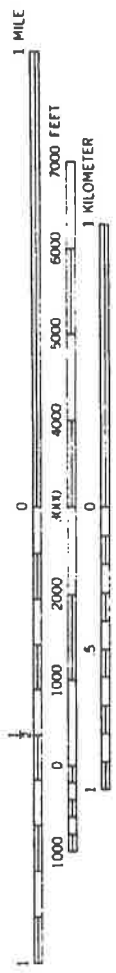DEPARTMENT OF THE INTERIOR
GEOLOGICAL SURVEY

EVANS QUADRANGLE
GEORGIA–SOUTH CAROLINA
7.5 MINUTE SERIES (TOPOGRAPHIC)

CONTOUR INTERVAL 10 FEET
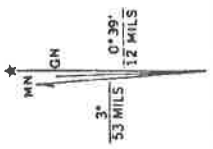NATIONAL GEODETIC VERTICAL DATUM OF 1929

UTM GRID AND 1980 MAGNETIC NORTH
DECLINATION AT CENTER OF SHEET

112

For convenience in selecting our reports from your bookshelves, they are color-keyed across the spine by subject as follows:

Red	Valley and Ridge mapping and structural geology
Dk. Purple	Piedmont and Blue Ridge mapping and structural geology
Maroon	Coastal Plain mapping and stratigraphy
Lt. Green	Paleontology
Lt. Blue	Coastal Zone studies
Dk. Green	Geochemical and geophysical studies
Dk. Blue	Hydrology
Olive	Economic geology
	Mining directory
Yellow	Environmental studies
	Engineering studies
Dk. Orange	Bibliographies and lists of publications
Brown	Petroleum and natural gas
Black	Field trip guidebooks
Dk. Brown	Collections of papers

Colors have been selected at random, and will be augmented as new subjects are published.

$3404/500